

UNIVERSITÀ DEGLI STUDI DELL'INSUBRIA
Dipartimento di Scienza e Alta Tecnologia

PHYSICAL AND PROJECTED
PAIRS OF QUASARS

A Thesis submitted for the degree of Doctor of Philosophy

Emanuele Paolo Farina

supervisor: A. Treves
co-supervisor: R. Falomo

November 2012

There is a theory which states that if ever anyone discovers exactly what the Universe is for and why it is here, it will instantly disappear and be replaced by something even more bizarre and inexplicable.

There is another theory which states that this has already happened.

D. Adams

Contents

Outline	1
Introduction	3
I Quasars probing quasars: unveiling the cool gas halo of quasars	7
1 Quasar absorption systems	9
1.1 Absorption systems associated to inactive galaxies	10
1.2 Absorption systems associated to quasars	11
2 The VLT sample	13
2.1 Sample selection	13
2.2 Analysis of VLT spectroscopic data	16
2.2.1 Observations and data reduction	16
2.2.2 Fits of quasar spectra	16
2.2.3 Search for absorption lines	16
2.3 Absorption systems associated to quasars	23
2.3.1 Transverse absorption systems	23
2.3.2 Line-of-sight absorption systems	26
2.4 The EW–host galaxy mass relation	26
2.5 Effects of the quasar radiation	31
2.6 Origin of the absorption systems	32
2.7 Conclusions	32
3 The SDSS sample	35
3.1 The OSIRIS–GTC sample	35
3.2 Analysis of SDSS spectra	37
3.2.1 MgII absorption systems associated to quasars	37
3.2.2 CIV absorption systems associated to quasars	41
3.3 Conclusions	43
II Physical systems of multiple quasars	51
4 The study of physical systems of multiple quasars	53
5 Six physical pairs of quasars	55
5.1 Sample selection	55

5.2	Systemic velocity differences from [OIII] lines	57
5.3	The virial mass of quasar pairs	58
5.4	The galactic environment of quasar pairs	61
5.4.1	SDSS images analysis	61
5.4.2	Expected mass of the clusters	62
5.4.3	Limits on the mass-to-light ratio	64
5.5	Conclusions	64
6	One (new) physical triplet of quasars	67
6.1	Sample selection	67
6.2	Observations and data reduction	69
6.2.1	Long-slit spectroscopy	69
6.2.2	Broad band photometry	70
6.3	The origin of the triplet	71
6.3.1	Gravitational lens	71
6.3.2	Chance superposition	75
6.4	The galactic environment of the triplet	75
6.5	Conclusions	78
7	Conclusions and Future Perspective	79
A	On the catalogues of quasars	81
A.1	The SDSS catalogues	81
A.1.1	The spectroscopic quasar catalogue	81
A.1.2	Quasars photometric selection	85
A.2	The Véron-Cetty and Véron catalogue	85
B	Notes on individual projected quasar pairs	89
C	List of publications	91

Outline

Quasars are the most luminous type of active galactic nuclei and their study is fundamental to shed light on the high redshift Universe. In this work we take advantage of the rare cases of close projected and physical quasar pairs to detect the presence of the cool enriched gas and of the dark mass that surround quasars.

This Thesis consists of two parts. In the first one we present optical spectroscopy of projected quasar pairs (i.e., two quasars that are close in the sky but have discordant redshifts) that represents a powerful tool to investigate the metal absorption lines imprinted on the spectrum of the background quasar by the gaseous halo surrounding the foreground one (Chapter 1). In the last decades, this technique has been extensively used to detect the haloes of non-active galaxies, but to date no systematic study has been performed in the case of quasars. We selected a sample of 46 projected pairs, with separations ranging from ~ 50 kpc to ~ 200 kpc, aimed to assess the presence of Mg II and CIV absorptions systems associated to foreground quasars. In Chapter 2 we show the first outcomes of our programme, based on the spectra of 13 pairs partially collected by me at the ESO Very Large Telescope (VLT). These data reveal a high covering fraction for the Mg II absorbers and a non isotropical distribution of the gas. Our results are compared to those of similar works performed on non-active galaxies available in the literature. We propose that the cool gaseous haloes of quasars and of normal galaxies are similar, once the stellar mass of the systems is taken into account. Observations of the remaining 33 pairs are ongoing at the Gran Telescopio Canarias (GTC). The preparatory analysis of the SDSS spectra of these systems show that a 10 m class telescope is mandatory for this kind of studies (Chapter 3).

The second part of the Thesis addresses with physical systems of quasars (i.e., two or more quasars that have small projected and redshift separations) that are an expected outcome of the current hierarchical framework of galaxy formation and evolution (Chapter 4). In Chapter 5 we accurately study the dynamics of six low redshift quasar pairs and we found that the dynamical mass required for this systems to be gravitationally bound is larger of than the stellar masses of the host galaxies. This suggests that these pairs are hosted by galaxies with massive dark haloes or that they reside in a group/cluster of galaxies. In Chapter 6, we present our discovery of the second physical quasar triplet known to date. We estimate that these systems are extremely rare in terms of simple accidental superposition of the three quasars, suggesting a possible common origin for their ignition. Finally, conclusions and future perspectives of this study are presented in Chapter 7.

The present work principally deals with the analysis and studies presented in Farina et al. (2012b, on the gaseous haloes of quasars), in Farina et al. (2011, on the dynamical study of low redshift quasar pairs), and in Farina et al. (2012c, on the discovery of a new quasar triplet). A complete list of works published during my PhD is provided in Appendix C.

Introduction

Thanks to their high luminosities, quasars play a fundamental role in our understanding of the processes that have built the galaxies, especially at high redshift (the highest redshift quasar known to date is ULASJ112001.48+064124.3 at $z = 7.085$, Mortlock et al. 2011). Soon after their discovery (3C 273, Schmidt 1963) it was clear that the huge emission and the short time scale variability of quasars require an intense gas accretion onto a super massive black hole (SMBH) at the centre of galaxies (e.g., Salpeter 1964; Zel'dovich & Novikov 1964; Lynden-Bell 1969). This scenario is now widely accepted, but the mechanism responsible for the gas inflow is still matter of debate. Some theoretical models suggest that gas-rich galaxy mergers provide an efficient way to channel the gas down to the circumnuclear regions and possibly to activate the star formation and the quasar activity of the host galaxies (e.g., Hernquist 1989; Di Matteo et al. 2005; Kauffmann & Haehnelt 2000; Callegari et al. 2011). From the observative point of view, this scenario is supported by the detection of features associated to recent or on-going mergers reported in the host galaxy of quasars (e.g., Canalizo et al. 2007; Bennert et al. 2008). Moreover, the analysis of quasar field with deep broad band images and the study of the galaxy-quasar correlation function suggest that quasars prefer to reside in galactic environment richer than average (e.g., Wold et al. 2001; Söchting et al. 2002, 2004; Serber et al. 2006; Hutchings et al. 2009). This is confirmed also by hydrodynamic simulations of the quasar evolutions, that show that quasars are more often located in group of galaxies, where major mergers of $\sim L^*$ galaxies are more likely to occur (e.g., Hopkins et al. 2008). More pieces of evidence are given by the discovery of an excess of small separation quasar pairs ($\lesssim 150$ kpc) relative to the simple extrapolations of the larger scale two-point correlation function. This can be understood if mergers trigger the quasar activity (e.g., Djorgovski 1991; Hennawi et al. 2006b; Myers et al. 2007b; Kayo & Oguri 2012).

The presence of the SMBH have a substantial effect on its host galaxy. In the last decades, many evidences have emerged suggesting that most, if not all, nearby massive elliptical galaxies host a SMBH in their centre (e.g., Kormendy & Richstone 1995; Richstone et al. 1998) and that SMBH and their host galaxies share a common history throughout the Cosmic Time. For instance the evolution of the quasar luminosity function (e.g., Dunlop & Peacock 1990; Fontanot et al. 2007; Croom et al. 2009) closely matches the density of star-formation through Cosmic ages (Madau et al. 1998; Lapi et al. 2006). Moreover, in the local Universe, the black hole mass (M_{BH}) is tightly correlated with the large scale properties of the host galaxy such as: luminosity (e.g., Kormendy & Richstone 1995; Magorrian et al. 1998; Marconi & Hunt 2003; Bennert et al. 2010); velocity dispersion (e.g., Ferrarese & Merritt 2000; Gebhardt et al. 2000; Salviander & Shields 2012); Sérsic index (Graham & Driver 2007); and stellar mass (M_{host} ; e.g., McLure et al. 2006; Peng et al. 2006b,a; Decarli et al. 2010b,c). These correlations suggest that the formation and evolution of SMBHs and of their host galax-

ies are closely linked, however the origin of these scaling relations remains unclear. For instance the nuclear activity could affect the large scale properties of the host galaxy (e.g., Silk & Rees 1998; Di Matteo et al. 2005; Springel & Hernquist 2005) and/or the activation of gas accretion onto the black hole could be triggered by the same processes (e.g., dynamical instabilities caused by secular evolution or by gravitational interactions or merger events) regulating the properties of the host galaxy (e.g., Knapen 2005; Peng 2007; Hopkins et al. 2006).

In the context of the joint evolution black holes and host galaxies, over the last several years, our research group have performed an extensive study of the black hole masses (e.g., Decarli et al. 2010b, 2011; Farina et al. 2012a) and of the luminosities/masses of the host galaxies ($L_{\text{host}}/M_{\text{host}}$; e.g., Kotilainen et al. 1998, 2006, 2009; Falomo et al. 2001, 2004, 2005, 2006; Hyvönen et al. 2007) in a wide range of redshifts. This large sample has allowed to probe the evolution of the $M_{\text{BH}}/M_{\text{host}}$ ratio from redshift $z \sim 3$ to the present age: given a quasar host galaxy, its central black hole at high redshift is *more massive* with respect to its low redshift counter parts (e.g., Decarli et al. 2010c, 2012; Portinari et al. 2012). This Thesis fits into this research line. It has the purposes of **(i)** exploring the relations between the host galaxy of quasars and their surrounding cool gas haloes and of **(ii)** measuring the mass of the dark haloes through the virial theorem applied to quasar pairs.

In the first part of the Thesis we present the first results of our spectroscopic programme aimed to reveal the presence of Mg II and C IV absorbers associated to quasars. We take advantage of projected quasars pairs that are ideal observational tools for this purpose, since they are composed of a very bright source in the background ($z \equiv z_{\text{B}}$) which enlightens the gas halos of the foreground object ($z \equiv z_{\text{F}} < z_{\text{B}}$). It is worth noting that this technique was extensively used to detect metal absorbers around galaxies (e.g., Bahcall & Spitzer 1969; Steidel & Sargent 1992; Steidel et al. 1994; Churchill et al. 1999; Chen et al. 2001, 2010a; Kacprzak et al. 2011; Bowen & Chelouche 2011), however has not yet been considered in the context of quasars, mainly because close projected quasar pairs are extremely rare. Our whole sample consists of 46 targets (33 of which was already observed with the optical spectrographs FORS2 at ESO-VLT and OSIRIS at GTC) aimed to detect Mg II and C IV absorption systems in the proximity of quasars (i.e., within a projected separation of ~ 200 kpc). This large sample will represent a breakthrough in our knowledge of the amount of enriched cool gas that surround quasars, in fact the only similar study published to date deals with only 4 targets (Bowen et al. 2006).

The second part of the Thesis concerns physical systems of quasars, their dark mass, and their galactic environment. Recent studies have led to the discovery of many physical pairs (Myers et al. 2008; Hennawi et al. 2006b, 2010) but only few of them have a precise redshift measurement. Indeed, it is well known that redshifts derived from broad emission lines of ions of various species can differ by as much as thousands km/s (e.g., Bonning et al. 2007). We thus select a small sample of low redshift quasar pairs, for which the velocity differences could be derived from [O III] narrow emission lines, that are optimal tracers of the systemic redshift of these objects (e.g. Hewett & Wild 2010). The frequency of these pairs in terms of simple accidental superposition is rather low, supporting the idea that these are true physical association of quasars. We can thus

accurately estimate the dynamical mass of these systems through the virial theorem. A comparison of these values with the stellar masses of the host galaxies and with the galactic environment allows us to estimate lower limits to the mass-to-light ratio for these systems.

Until now the search for physical grouping of quasar has focused only on binary systems, and little is known for systems composed by more than two quasars. We have thus started a systematic search for physical triple quasars taking advantage of the large amount of photometric data made publicly available thanks to the Sloan Digital Sky Survey. This study has driven to the discovery of QQQ J1519+0627 the second triplet of quasar known to date (after QQQ J1432-0106, Djorgovski et al. 2007). The discovery of this new class of physical quasar systems strongly support the merger driven scenario for the ignition of the quasar activity.

The results presented here are largely based on article published or submitted during my PhD. In particular the study of the enriched cool gaseous haloes of quasars deals with ESO-VLT optical spectra gathered, reduced and analysed by me. These will appear in Farina et al. (2012b). The search in quasar archives for quasar pairs and triplets and the investigation of the galactic environment of the systems found are presented in Farina et al. (2011) and in Farina et al. (2012c, submitted to MNRAS). In my last year of PhD, I have joined the MAGIC collaboration. I have covered the observing shift P116 (May–June 2012) at the Roque de los Muchachos Observatory and I have presented two articles concerning the analysis of optical spectra and broad band images of the blazars PKS 1222+216 (Farina et al. 2012a, on the long term optical variability of the source) and PKS 0447-439 (Fumagalli et al. 2012, on the controversial redshift of this object) that have recently showed strong flares in the Very High Energy domain (VHE, i.e., $E > 100 \text{ GeV}$).

Throughout this Thesis we consider a concordance cosmology with $H_0 = 70 \text{ km/s Mpc}^{-1}$, $\Omega_m = 0.3$, and $\Omega_\Lambda = 0.7$. All the quoted magnitude are expressed in the AB standard photometric system (Oke 1974).

Part I

Quasars probing quasars: unveiling the cool gas halo of quasars

1 Quasar absorption systems

Absorption features in quasar spectra provide a unique tool for probing the gas and dust content of foreground galaxies and of the intergalactic medium with a sensitivity that is almost independent of redshift. The possibility that cool clouds of neutral hydrogen and of other species could cause pronounced absorption lines in the spectra of distant source was proposed by Bahcall & Salpeter (1965) and Bahcall & Salpeter (1966) shortly before their first detections (3C 191, Burbidge et al. 1966; Stockton & Lynds 1966)¹. Since then a number of absorption lines have been observed in the spectra of several quasars (e.g., Sargent et al. 1988; Churchill et al. 1999; Curran et al. 2002; Ryabinkov et al. 2003; Nestor et al. 2005; Trump et al. 2006; Rao et al. 2006; Misawa et al. 2007; Vanden Berk et al. 2008). Three are the possible sources for this absorbing gas: (i) *intrinsic*, if it is produced by processes related to the SMBH itself; (ii) *associated*, if it is due to the quasar host galaxy or to its surrounding gas halos; (iii) *intervening* if the material is intercepted along the line-of-sight but it is not connected to the quasar. The broad absorption lines (called BAL if $\text{FWHM} \gtrsim 2000 \text{ km/s}$, or mini-BAL if $500 \text{ km/s} \lesssim \text{FWHM} \lesssim 2000 \text{ km/s}$), detected in $\sim 10 - 20\%$ of optically selected quasar (e.g., Weymann et al. 1991; Hewett & Foltz 2003; Reichard et al. 2003; Rodriguez Hidalgo et al. 2012), are thought to be intrinsic, since only the SMBH can feasibly generate the high-velocity outflows of gas responsible for the absorption (e.g., Crenshaw et al. 2003). It is worth noting that absorptions with velocity shift up to thousands of km/s from the quasar could be still intrinsic (e.g., Richards et al. 1999; Wild et al. 2008). The narrow absorption lines (NAL, $\text{FWHM} \lesssim 500 \text{ km/s}$) are instead expected to be most probably associated or intervening. However, some studies have noted a statistical excess of NALs close to the quasar emission lines (e.g., Weymann et al. 1979, 1981; Foltz et al. 1986; Wild et al. 2008; Tytler et al. 2009), suggesting that a fraction of these systems with redshift similar to that of the quasar could be intrinsic.

The topic of this Part of the Thesis will be the study of metal associated NALs (in particular Mg II and C IV) detected in projected quasar pairs. It is worth to recall that both Mg II and C IV are doublets and thus are easy to spot in quasar spectra. Moreover, these species have very different ionising potential ($E(\text{Mg II})=15.03 \text{ eV}$ and $E(\text{C IV})=64.50 \text{ eV}$), allowing to reveal the presence of gas at different temperature ($T \sim 30000 \text{ K}$ and $T \sim 30000 - 100000 \text{ K}$, respectively) around quasars.

¹Note that, however, Greenstein & Schmidt (1964) have already reported the presence of an unidentified sharp absorption line in the spectrum of 3C 48 and that also Sandage (1965) have observed an absorption feature superimposed to the 1550 \AA emission line of BSO 1.

1.1 Absorption systems associated to inactive galaxies

Since the works of Bahcall & Spitzer (1969) and Boksenberg & Sargent (1978) metal NALs are thought to be linked to large gaseous haloes around galaxies (metal enriched by past stars) extending up to 100 kpc (see Churchill et al. 2005, for a review). Despite a number of studies aimed to connect these features with galaxy properties (e.g., Young et al. 1982; Lanzetta et al. 1987; Bergeron & Boissé 1991; Steidel & Sargent 1992; Steidel et al. 1994; Churchill et al. 1999; Rigby et al. 2002; Nestor et al. 2005; Bergeron et al. 2011), the origin of the absorbing gas is still unclear. However, in the last decades, it is progressively emerging a scenario in which the stronger absorption lines (rest frame equivalent width $EW_r \gtrsim 1 \text{ \AA}$) are due to winds driven by the star formation activity, while the weaker one ($EW_r \lesssim 1 \text{ \AA}$) are associated with inflows of gas onto the host galaxies.

For instance, Zibetti et al. (2007), stacking SDSS images of 2800 Mg II absorbers with $0.37 < z < 1.00$, show that the stronger absorption systems reside preferentially in blue star-forming galaxies, while the weaker ones in red passive galaxies. This result was confirmed by Ménard et al. (2011) in a sample of 8500 Mg II absorption systems present in the SDSS quasar spectra. They discovered a strong correlation between the EW_r of the absorbers and the luminosity of the associated [O II] lines, considered as a tracer of the star formation rate (SFR) of galaxies. Prochter et al. (2006) investigated the evolution of the number density of ~ 7400 Mg II strong absorption systems and found rough correspondence with the evolution of the star formation rate at redshifts between $z = 0.5$ and 2, suggesting a link between the two phenomena. Recently Nestor et al. (2011) reported clear evidence that ultrastrong Mg II absorbers ($EW_r \gtrsim 3 \text{ \AA}$) reside in galaxies with very high SFRs. In addition to that, spectroscopic observations of highly star forming galaxies reveals the presence of blueshifted Mg II absorption features, further supporting the outflowing winds scenario (Tremonti et al. 2007; Weiner et al. 2009; Rubin et al. 2010; Martin et al. 2012).

The existence of a link between galaxy luminosity/halo mass and strength of absorption features, expected in the infalling scenario, is still debated. Chen et al. (2001) and Chen et al. (2010a) found that the EW_r and the extent of Mg II and C IV absorption systems are related to host galaxy luminosity. More directly, Chen et al. (2010b) search for absorption systems in a sample of 94 galaxies at redshifts between $z = 0.1$ and 0.5 within $pd \lesssim 85 \text{ kpc}$ from a quasar sight-line. The EW_r of the systems found (the great majority of which have $EW_r \lesssim 1 \text{ \AA}$) scale with the stellar mass and only little with the star formation rate of the host galaxies. These results are interpreted considering that Mg II absorption systems arise from infalling clouds to fuel star formation. Kacprzak et al. (2011) directly compared the relative Mg II halo gas and host galaxy kinematics for 13 L^* galaxies at $z \sim 0.1$. They found that these galaxies have low SFR and a kinematically quiescent interstellar medium containing no outflowing gas. Given that these galaxies live in isolated environment, they suggest a scenario in which the cool gas halo was infalling and providing a gas reservoir that could maintain the low levels of star formation within the host galaxies. Bowen & Chelouche (2011) investigate the absorption properties of Luminous Red Galaxy (LRG) like galaxies with redshifts $0.46 < z < 0.6$. They suggest that the low covering factor (k) for absorber with

$EW_r \gtrsim 0.6 \text{ \AA}$ and the lack of correlation between EW_r and impact parameter or r-band absolute magnitude, are due or to the rich environment of these objects that make their haloes too hot to maintain cool gas, or to the low rates of star formation that are not enough to fill their haloes of Mg II. Cross correlating Mg II absorption systems and the properties of LRGs Bouché et al. (2006) found at redshift $z \sim 0.5$ an anti-correlation between the halo mass and the EW_r of absorbers (most of which have $EW_r \gtrsim 1 \text{ \AA}$), which suggests that the Mg II absorption systems are not virialised within the haloes. These results were further confirmed in larger sample by Lundgren et al. (2009) and by Gauthier et al. (2009). Intriguingly, Rubin et al. (2012) detect inflow of gas into isolated star-forming galaxies at $z \sim 0.5$.

1.2 Absorption systems associated to quasars

In contrast to the large attention given to absorptions in normal galaxies, only few studies have been focused on the properties of the gaseous halo of galaxies hosting a quasars in their centre. The observation of projected quasar pairs allows to probe the properties of the foreground quasar (QSO_F, $z \equiv z_F$), through the study of absorption features imprinted on the background quasar spectra (QSO_B, $z \equiv z_B > z_F$). The standard model on the origin of quasar high luminosity requires an intense gas accretion on a supermassive black hole that dramatically increases its activity. Feasible mechanisms responsible for the gas infall are instabilities caused by strong gravitational interactions and galaxy mergers (e.g., Canalizo et al. 2007; Bennert et al. 2008; Green et al. 2010). The close (few hundreds kiloparsecs) environment of quasars is expected to be populated by tidal debris, streams, and diffuse cool gas clouds, as commonly observed in interacting galaxies (e.g., Sulentic et al. 2001; Cortese et al. 2006). Given their low surface brightness, most of the properties of these features could be investigated almost exclusively in absorption, especially at high redshift.

Some studies have been performed to analyse the distribution of neutral hydrogen around quasars. For instance Hennawi et al. (2006a), starting from a sample of 149 projected quasar pairs (projected distance: $30 \text{ kpc} \lesssim \text{pd} \lesssim 2.5 \text{ Mpc}$; redshift: $1.8 < z_F < 4.0$), found that the probability to have an absorber with $N_{\text{HI}} > 10^{19} \text{ cm}^{-2}$ coincident within 200 kpc with a QSO_F is high ($\sim 50\%$), and that the distribution of these absorbers is highly anisotropic (Hennawi et al. 2007, see also Kirkman & Tytler 2008 and Prochaska & Hennawi 2009). The study of projected quasar pairs gives also the possibility to investigate the so-called *transverse proximity effect*: i.e., the expected decrease of absorption systems in the Ly α forest of a QSO_B due to the ionising flux of a QSO_F. Intriguingly the many attempts to measure this effect, with perhaps one exception (Gallerani et al. 2008), have led to only marginal or no detection (e.g., Crofts 1989; Dobrzycki & Bechtold 1991; Liske & Williger 2001; Schirber et al. 2004). The presence of a transverse proximity effect for heavier elements is still unclear. For instance it was observed for He II by Worseck & Wisotzki (2006), but not for Mg II (Bowen et al. 2006) or for C IV (Tytler et al. 2009).

Up to now, only a few metal absorption systems associated or near to a quasar have been serendipitously discovered (e.g., Shaver et al. 1982; Shaver & Robertson 1983, 1985; Decarli et al. 2009a). This statistics is limited by the little number of known close

projected pairs. The only two systematic search for absorption lines was performed by Tytler et al. (2009) and Bowen et al. (2006).

Tytler et al. (2009) studied the distribution of metal absorption features (in most cases C IV) present in the spectra of 170 close ($z_B - z_F \lesssim 0.5$) projected quasar pairs with separations $100\text{kpc} \lesssim \text{pd} \lesssim 2.5\text{Mpc}$ in order to investigate their Mpc scale clustering properties around quasars and other absorbers. They found 16 absorbers within $\pm 500\text{ km/s}$ from the QSO_F, all with $\text{pd} > 400\text{ kpc}$, that cluster with an approximately isotropic distribution, with a hint of an excess for systems with redshift $z < z_F$.

Bowen et al. (2006) select from the sample of projected quasar systems of Hennawi et al. (2006b) 4 the pairs with $30\text{ kpc} \lesssim \text{pd} \lesssim 100\text{kpc}$ and $0.5 \lesssim z_F \lesssim 1.5$. In all these systems they detect Mg II absorption lines clearly associated to QSO_F (see Figure 2.1 in the next Chapter). Despite the small sample size, they speculate that the absence of corresponding absorption lines in the spectra of QSO_F involve a non isotropic distribution of the absorbing gas. On the basis of these data Chelouche et al. (2008) proposed that the gas in the outer region of quasars (i.e., at radius larger than $\sim 20\text{ kpc}$) is distributed in the same way of L^{*} galaxies, but their thermal and ionisation structure is highly influenced by the central black hole emission.

In this scenario we have started a programme aimed to systematic investigate the presence of Mg II and C IV absorbing gas associated to quasars. In order to detect absorption lines down to a sensitive limits (i.e., $\text{EW} \sim 0.5\text{ \AA}$) spectra with optimal signal-to-noise are mandatory. We have thus taken advantage of the large collecting area of the ESO Very Large Telescope (VLT, 8.2 m) and of the Gran Telescopio CANARIAS (GTC, 10.4 m) to observe a sample of 46 close quasar pairs ($\text{pd} \lesssim 200\text{ kpc}$ at the redshift of the foreground quasar). In Chapter 2 we will present our first results, based on the 13 spectra gathered with the FOcal Reducer and low dispersion Spectrograph (FORS2) mounted on the UT1 (Antu) VLT telescope (see Farina et al. 2012b). In Chapter 3 we will show the analysis of the SDSS spectra of projected pairs, that allow us to detect the presence of the stronger absorption features. This is the premise to the study of GTC spectra, which have been collected in the first semester of 2012 but not yet analysed.

2 The VLT sample

In this Chapter we present the first results of our ongoing spectroscopic survey of Mg II and CIV absorption features linked to quasars. We analyse the spectra of 13 quasar pairs collected at ESO–VLT in service mode in Period P85A and by E.P. Farina in visitor mode during Period P86A (Section 2.2). These data allows us to investigate the difference between the gas associated to quasars and to non–active galaxies (Section 2.4), and to comment on the effects of the quasar emission on the distribution of the absorbing gas (Section 2.5). Finally, we speculate on possible origins for the detected absorbers (Section 2.6). The results presented here are based principally on Farina et al. (2012b, see Appendix C).

2.1 Sample selection

We searched in the Véron-Cetty & Véron (2010) quasar catalogue (see Appendix A.2) for close projected pairs that satisfy the requirement:

- i) the angular separation is $\Delta\theta \lesssim 15''$.

This gave us a list systems that are suitable for the study of the absorption lines associated to the foreground quasar. However, to gathered data, we have to impose some other *observative* constraints:

- ii) the redshifts of fore– and back–ground quasars combine so that the CIV and Mg II emissions of the QSO_F fall within the wavelength range observed with FORS2 GRISM 1400V or GRISM 1200R, avoiding important sky features or narrow emission lines in the spectrum of the QSO_B;
- iii) the QSO_B is brighter than $m_V \sim 21$ in order to collect spectra with signal–to–noise $S/N \gtrsim 10$ in a reasonable amount of time;
- iv) targets have declination $< 15^\circ$, so that they are visible from the Paranal site.

The resulting sample consists of 19 close pairs, 13 of which were observed with FORS2 at ESO–VLT. Note that in the redshifts explored by our sample ($0.7 \lesssim z_F \lesssim 2.2$) the limit on the angular separation ($\Delta\theta \lesssim 15''$) allows us to study scales typical of the gaseous halos observed around galaxies ($pd \lesssim 120$ kpc).

In Table 2.1 and in Figure 2.1 we present the general properties of the 13 observed pairs. These are radio quiet quasars, with an average angular separation of $11''.4$ that corresponds to an average projected distance of ~ 90 kpc. It is worth noting that in the definition of the sample we have not taken into account the presence of absorption features *a priori*, thus it seems suitable to estimate the unbiased frequency of absorption systems.

Table 2.1: Properties of the observed quasar pairs. (01) most common name of the foreground quasar, (02) our identification label of the pair, (03,04) redshift from broad emission line, (05,06) absolute V-band magnitude of the quasar, (07) angular and (08) projected separation, (09) bolometric luminosity of the foreground quasar (see text for details), (10) black hole mass of the foreground quasar (see text for details), (11) average seeing during observations, and (12,13) average signal-to-noise ratio per pixel on the continuum close to the expected position of the absorption lines. The label F and B refer to the foreground and to the background quasar, respectively.

QSO _F	ID	$z_{\text{bl,F}}$	$z_{\text{bl,B}}$	V_{F}	V_{B}	$\Delta\theta$	pd	$L_{\text{bol,F}}$	$M_{\text{BH,F}}$	See.	S/N_{F}	S/N_{B}
(01)	(02)	(03)	(04)	(05)	(06)	[arcsec] (07)	[kpc] (08)	[10^{46} erg/s] (09)	[$10^8 M_{\odot}$] (10)	[arcsec] (11)	(12)	(13)
SDSSJ00022-0053B	QQ01	1.542	2.205	-24.83	-26.66	7.8	66	0.89 ± 0.04	12.3	0.71	12	13
2QZJ003954-2725C	QQ02	1.262	2.100	-24.29	-23.96	11.1	93	0.56 ± 0.01	6.2	0.84	20	10
2QZJ004344-3000B	QQ03	1.346	1.554	-22.67	-24.71	11.3	95	0.27 ± 0.03	4.6	0.88	10	14
SDSSJ00541-0946B	QQ04	2.113	2.113	-25.59	-28.05	14.1	117	1.89 ± 0.02	13.7	1.41	49	20
Q0059-2702B	QQ05	0.941	1.963	-24.96	-23.95	10.7	84	2.23 ± 0.06	10.4	1.35	41	22
2QZJ011050-2719	QQ06	1.332	2.254	-23.59	-24.86	10.0	84	0.60 ± 0.02	6.8	1.36	23	10
2QZJ101636-0234A	QQ07	1.518	3.448	-25.65	-26.64	10.1	86	2.11 ± 0.13	9.9	0.75	15	15
2QZJ102425+0013A	QQ08	1.138	2.350	-23.99	-26.13	10.1	83	0.21 ± 0.05	0.9	1.18	6	9
SDSSJ11318-0222A	QQ09	2.198	2.353	-25.65	-26.95	10.8	89	0.54 ± 0.11	6.5	2.35	5	5
SDSSJ22028+1236A	QQ10	2.063	2.504	-26.80	-26.35	11.8	99	4.09 ± 0.11	24.4	0.89	31	16
SDSSJ22067-0039A	QQ11	1.230	1.516	-25.32	-25.60	13.1	109	1.41 ± 0.09	10.3	0.71	16	11
2QZJ222446-3200	QQ12	0.689	0.731	-23.32	-22.99	17.0	120	0.34 ± 0.03	1.3	0.79	29	18
Q2225-4023B	QQ13	0.931	2.398	-23.51	-26.24	9.9	78	0.26 ± 0.02	3.5	0.99	20	22

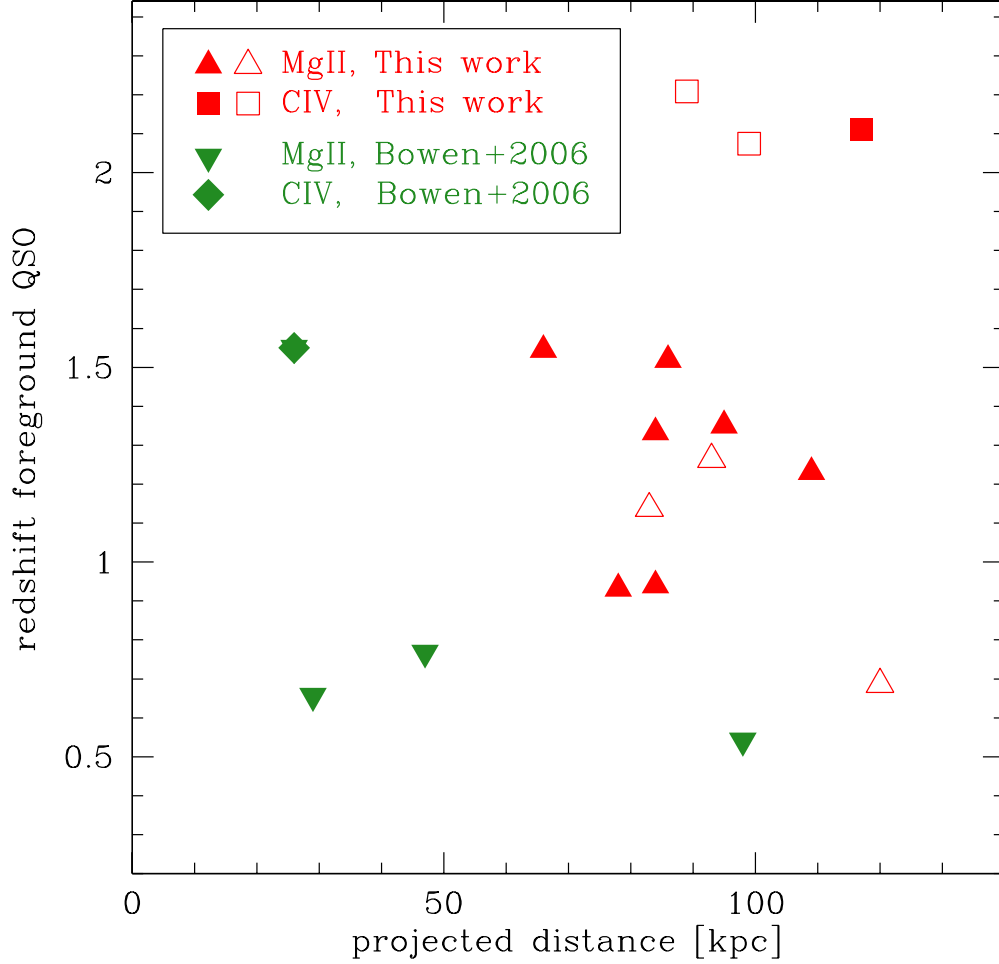


Figure 2.1: Distribution of close projected pairs in the $pd-z_F$ plane. Triangles are objects in which we investigate for the Mg II absorption features, while squares for the CIV. The systems showing an line in the QSO_B spectra associated to the QSO_F are marked with filled points, otherwise with empty ones. Red and green points are from our sample and from that of Bowen et al. (2006), respectively.

2.2 Analysis of VLT spectroscopic data

2.2.1 Observations and data reduction

Spectra of the projected quasar pairs were collected with the VLT Antu telescope at the ESO Paranal observatory. Observations were performed with the grisms 1200R and 1400V on FORS2 (Appenzeller et al. 1998), yielding a spectral resolution of $R(1200R)=2900$ and $R(1400V)=2800$ (with the $1''$ slit). The slit used was long enough to collect the spectra of the two quasars at the same time (see Figure 2.2). Typical exposure times were ~ 4000 seconds (~ 6000 seconds for fainter objects). The only exceptions were QQ08 and QQ09, for which the poor weather condition did not allow exposures longer than 2600 seconds. A summary of the observations is in Table 2.2.

The data reduction was carried adopting standard IRAF¹ tools for long-slit spectroscopy. The `ccdred` package was employed to perform bias subtraction, flat field correction, image alignment and combination. Usually, two sets of three exposures of the same pair were collected, this allowed to get rid of cosmic rays applying the `crreject` algorithm. The spectra extraction, the background subtraction, and the calibrations both in wavelength and in flux were performed with the `twodspec` and `onedspec` packages. The typical accuracy in the wavelength calibration is $\sim 0.1 \text{ \AA}$. Galactic extinction was accounted for according to Schlegel et al. (1998), assuming $R_V = 3.1$. The spectra obtained are presented in Figure 2.3.

2.2.2 Fits of quasar spectra

For the analysis of the quasar spectra we followed the procedure presented in Decarli et al. (2010b) and De Rosa et al. (2011). Namely, data are first inspected by eyes and regions showing apparent absorption features are masked. Then, we designed the continuum with the superposition of:

- a) the non thermal power-law-like component;
- b) the host galaxy star light (assuming the elliptical galaxy template of Mannucci et al. 2001);
- c) the contribution from blended Fe II multiplets (modelled in the UV band with the template of Vestergaard & Wilkes 2001 and in the optical band with our original spectrum of IZw001).

Finally, we have fitted broad emission lines with two Gaussian curves with the same central wavelength (see Decarli et al. 2008). Uncertainties on derived quantities are estimated from the 1σ errors in both continuum and line fits.

2.2.3 Search for absorption lines

We here present our own set of automated software routines we have developed for absorption feature finding and for measuring the line positions and equivalent widths

¹IRAF is distributed by the National Optical Astronomy Observatories, which are operated by the Association of Universities for Research in Astronomy, Inc., under cooperative agreement with the National Science Foundation.

2.2 Analysis of VLT spectroscopic data

Table 2.2: Journal of observations. (01) our identification label of the quasar, (02) modified julian date of the observations, (03) grism and filter, (04) slit width, (05) total exposure time, and (06) ESO–VLT period. P85A data was collected in service mode, while P86A spectra was collected by E.P. Farina in visitor mode.

ID	MJD	grism+filter	slit [arcsec]	expt [sec]	period
(01)	(02)	(03)	(04)	(05)	(06)
QQ01F	55399.31944402	1200R+GG435	1.0	6750	P85A
QQ01B	55399.31944402	1200R+GG435	1.0	6750	P85A
QQ02F	55382.33696889	1400V	1.0	4200	P85A
QQ02B	55382.33696889	1400V	1.0	4200	P85A
QQ03F	55356.38363239 – 55360.35942113	1200R+GG435	1.0	4200	P85A
QQ03B	55359.34166952 – 55360.39519774	1200R+GG435	1.0	4500	P85A
QQ04F	55399.38365588 – 55416.25082569	1400V	1.0	4200	P85A
QQ04B	55399.38365588 – 55416.25082569	1400V	1.0	4200	P85A
QQ05F	55355.38966632 – 55382.39798717	1200R+GG435	1.0	4500	P85A
QQ05B	55355.38966632 – 55382.39798717	1200R+GG435	1.0	4500	P85A
QQ06F	55443.30961396 – 55446.29311134	1400V	1.0	4500	P85A
QQ06B	55443.30961396 – 55446.29311134	1400V	1.0	4500	P85A
QQ07F	55397.37089712 – 55416.32383463	1400V	1.0	4200	P85A
QQ07B	55397.37089712 – 55416.32383463	1400V	1.0	4200	P85A
QQ08F	55416.28800169 – 55446.37322529	1200R+GG435	1.0	4200	P85A
QQ08B	55416.28800169 – 55446.37322529	1200R+GG435	1.0	4200	P85A
QQ09F	55616.03381408	1200R+GG435	1.0	5850	P86A
QQ09B	55616.03381408	1200R+GG435	1.0	5850	P86A
QQ10F	55617.03753243	1200R+GG435	1.0	1300	P86A
QQ10B	55617.03753243	1200R+GG435	1.0	1300	P86A
QQ11F	55616.35010138	1400V	1.6	2600	P86A
QQ11B	55616.35010138	1400V	1.6	2600	P86A
QQ12F	55356.34630667 – 55359.30550907	1400V	1.0	4200	P85A
QQ12B	55356.34630667 – 55359.30550907	1400V	1.0	4200	P85A
QQ13F	55357.28668640	1200R+GG435	1.0	4200	P85A
QQ13B	55357.28668640	1200R+GG435	1.0	4200	P85A
QQ14F	55326.38341641 – 55353.36298430	1400V	1.0	4200	P85A
QQ14B	55326.38341641 – 55353.36298430	1400V	1.0	4200	P85A
QQ15F	55324.39594935 – 55325.34747037	1400V	1.0	4200	P85A
QQ15B	55324.39594935 – 55325.34747037	1400V	1.0	4200	P85A

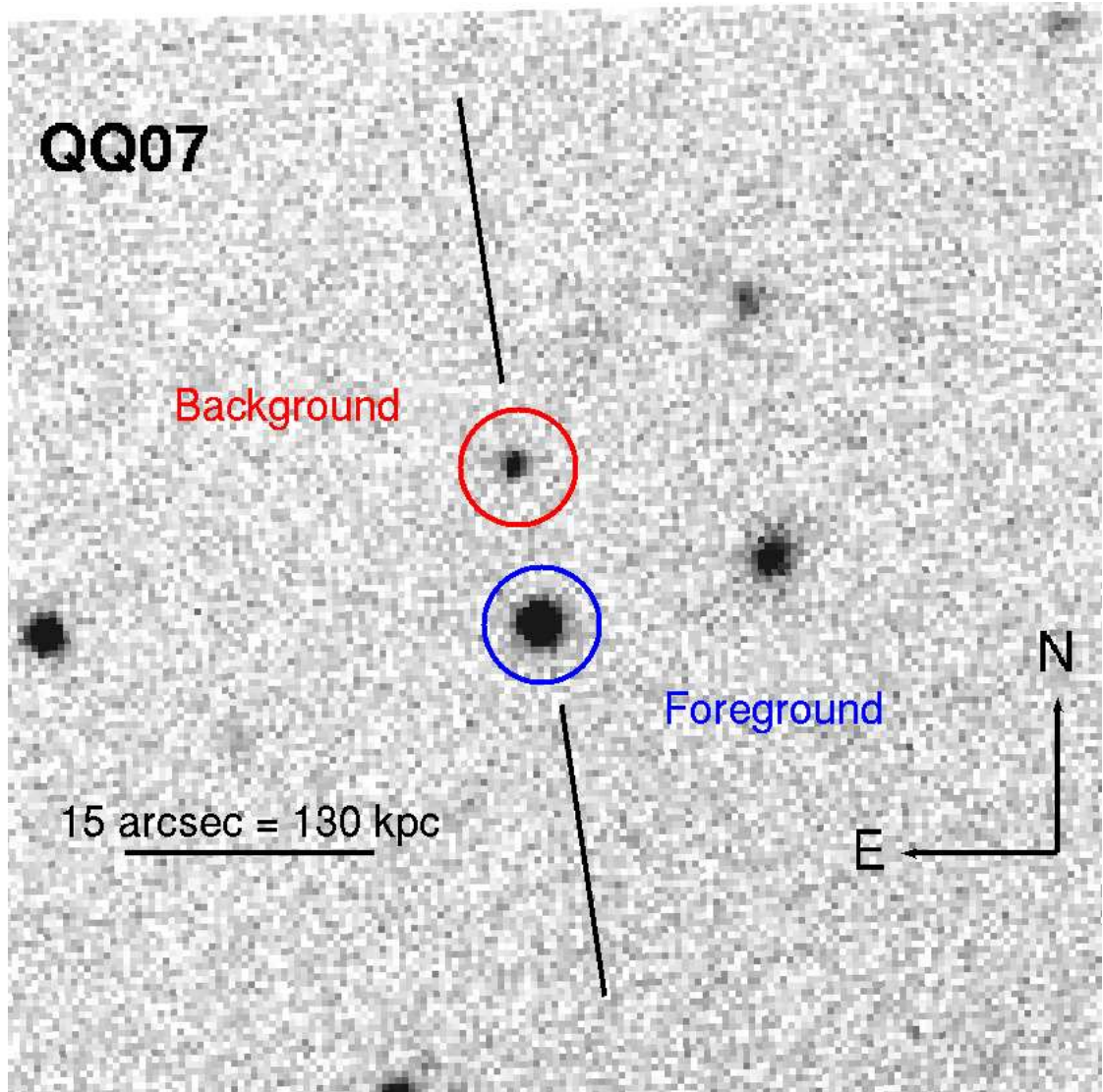


Figure 2.2: The field of the quasar pair QQ07 as imaged in SDSS i-band. The angular separation between the two sources is $\Delta\theta = 10''.1$. This allow to orientate the slit so that both the spectra could be acquired at the same time.

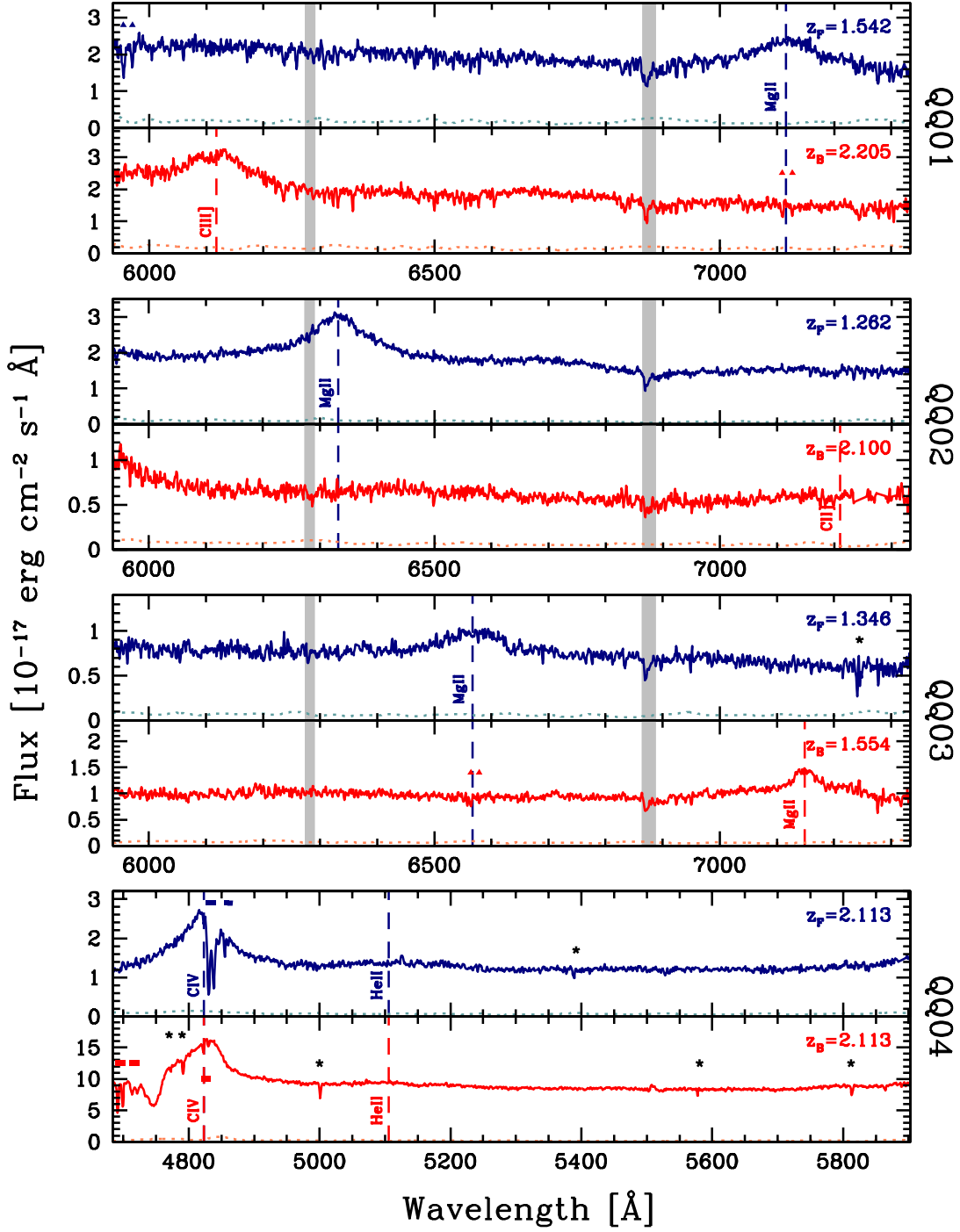


Figure 2.3: Spectra of the projected quasar pairs corrected for Galactic extinction. The blue solid lines refer to QSO_F and the red ones to QSO_B. The corresponding 1σ error spectrum is shown at the bottom of each panel. Triangles and squares point to all the MgII and CIV absorptions identified, respectively, while stars to other lines detected above a 3σ threshold (see Appendix B). Main quasar emission lines are labelled and the gray regions mask regions with prominent telluric features.

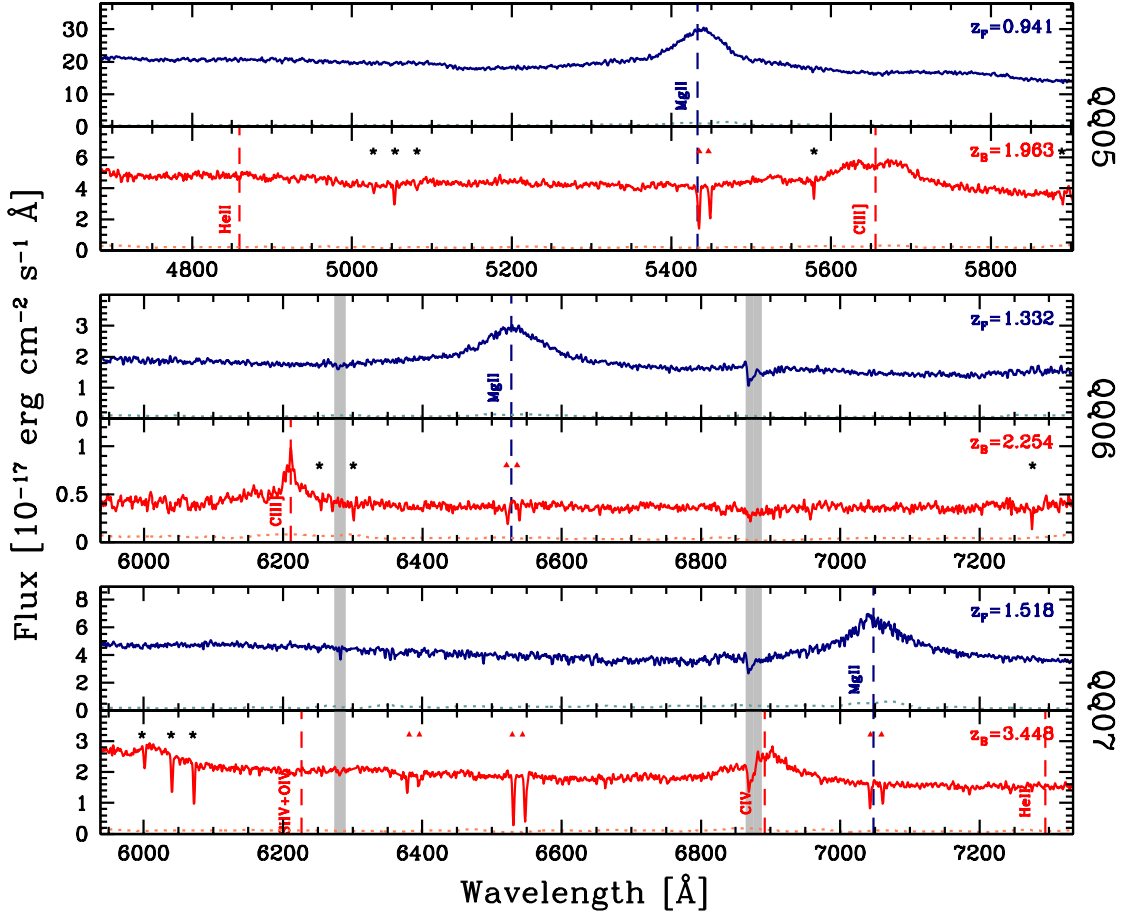


Figure 2.3: continued.

(EW). Most of our algorithms are based upon those described by Schneider et al. (1993) and Churchill et al. (2000), which are optimal in the case of not resolved lines (in the sense that their typical widths are smaller than the instrumental profile). Our procedure takes place in three steps:

1) Modelling the quasar emission. The *continuum*² fitting strongly depends on the signal-to-noise ratio of the spectra and give a substantial contribution to the uncertainties associated to the measures of the lines. We split the spectrum of quasars (after masking for the most apparent absorption features) in intervals of fixed size (i.e., 20 Å, see for a similar approach Sbarufatti et al. 2005), and we modelled the continuum (I_c) and the sigma of the spectrum (σ_I) by interpolating the median values in each bin of the flux and of the associated standard deviations with a cubic spline function.

2) Absorption lines finding. Each pixel in the spectrum is searched for the presence of an absorption feature. We first model the Instrumental Spread Function (ISF) with

²Note that in this Section we will refer to *continuum* as the whole emission of the quasars.

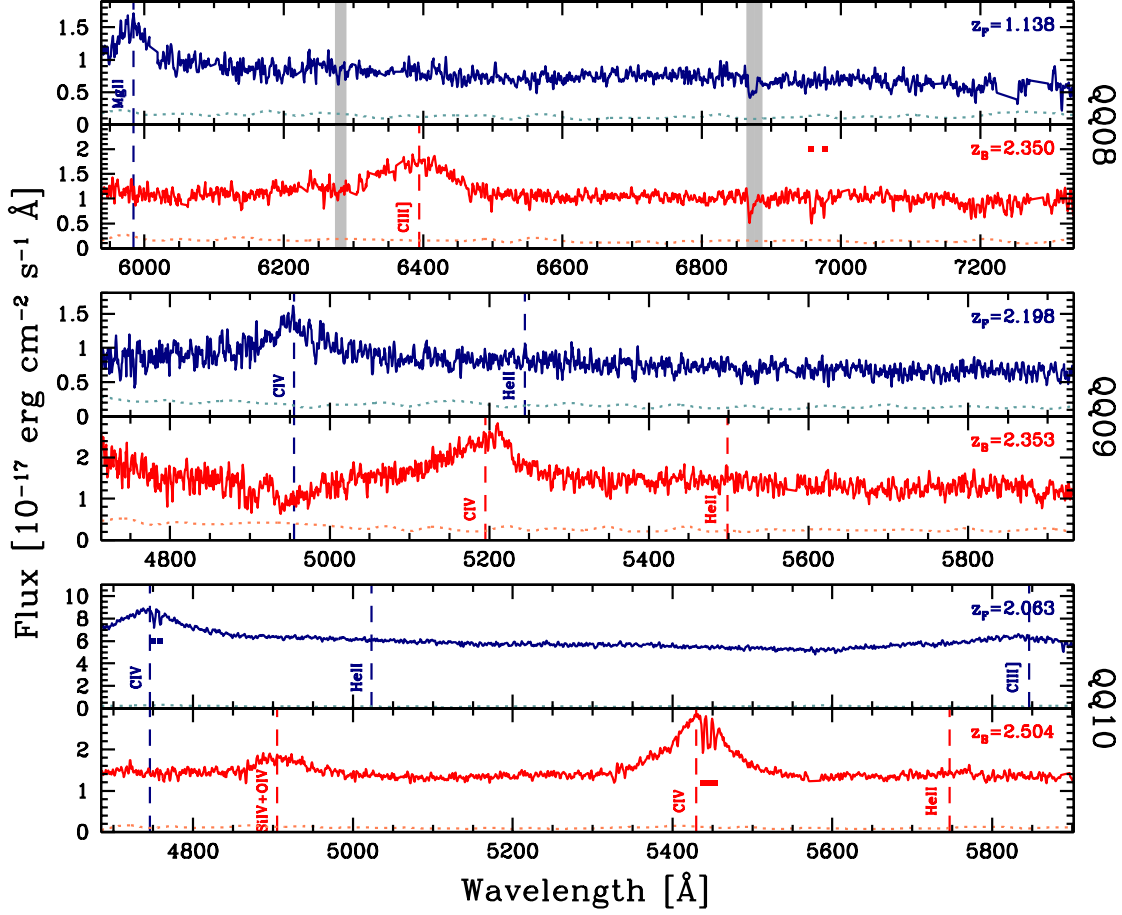


Figure 2.3: continued.

a Gaussian (P_i) centred on the pixel i with FWHM equal to the spectral resolution:

$$P_i(\lambda_j) = (2\pi\sigma_{\text{ISF}}^2)^{-\frac{1}{2}} e^{-\frac{1}{2}\left(\frac{\lambda_j - \lambda_i}{\sigma_{\text{ISF}}}\right)^2} \quad (2.1)$$

$$\sigma_{\text{ISF}}^2 = \frac{\text{FWHM}_{\text{ISF}}^2}{8 \ln 2}. \quad (2.2)$$

Then, the equivalent width of an unresolved features (EW_u) centred in the pixel i is calculate computing:

$$\text{EW}_u(\lambda_i) = \Delta\lambda_i \frac{\sum_{j=j_i}^{j_f} P_i(\lambda_j) [1 - I_n(\lambda_j)]}{\sum_{j=j_i}^{j_f} P_i^2(\lambda_j)} \quad (2.3)$$

where $I_n(\lambda_j) = I(\lambda_j)/I_c(\lambda_j)$ is the normalised flux, $I(\lambda_j)$ is the measured quasar emission at the pixel λ_j , $\Delta\lambda_i = \frac{1}{2}(\lambda_{i+1} - \lambda_{i-1})$ is the wavelength interval spanned by one pixel, j_i

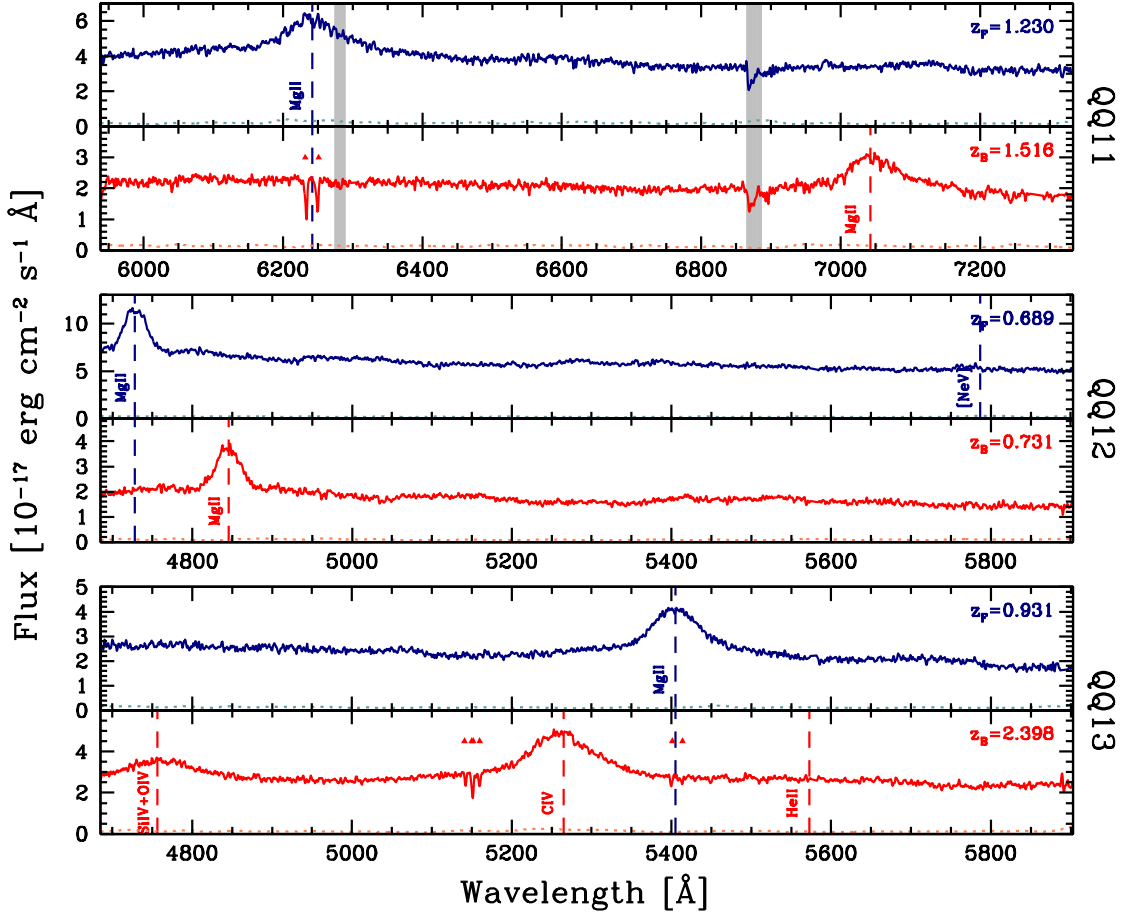


Figure 2.3: continued.

and j_f are the minimum and the maximum points in the ISF model³. Note that, with this definition, absorption features have positive equivalent width. The uncertainty in $EW_u(\lambda_i)$ is given by:

$$\sigma_u(\lambda_i) = \Delta\lambda_i \frac{\sqrt{\sum_{j=j_i}^{j_f} P_i^2(\lambda_j) \sigma_n(\lambda_j)}}{\sum_{j=j_i}^{j_f} P_i^2(\lambda_j)} \quad (2.4)$$

where $\sigma_n(\lambda_j) = \sigma_I(\lambda_j)/I_c(\lambda_j)$. These uncertainties serves as 1σ observed equivalent width detection threshold. An unresolved absorption line at the pixel i is detected when $EW_u(\lambda_i) > N_{SL}\sigma_u(\lambda_i)$, where N_{SL} is an arbitrarily defined number that give the significance level of the detection. Since we are not performing a blind search, but we know the expected location of MgII and CIV lines in our spectra (see Section 2.3), a $N_{SL} = 3$ detection limits on MgII($\lambda 2796$) and CIV($\lambda 1548$) lines seems adequate to identify the absorption systems.

³We choose j_i and j_f in order to completely cover the resolution element of the spectra, i.e., $\lambda_{j_f} - \lambda_{j_i} = 6\sigma_{ISF}$ that sample more than 99.9% of the Gaussian.

3) Estimating the equivalent widths. The EWs and the centroid positions are measured by fitting a single Gaussian function (e.g., Churchill et al. 2000) to the detected absorption lines with a χ^2 minimisation procedure. The 1σ uncertainties are based upon standard error propagation and assuming that largest source of errors is given by the continuum placement.

2.3 Absorption systems associated to quasars

We estimate the covering factor (k) of cool gas around quasars basing on the detection of absorbers close to the redshift of the QSO_F. It is well known that the redshifts derived from broad emission lines can differ from the systemic redshift by also hundreds km/s (e.g., Tytler & Fan 1992; Bonning et al. 2007, see also Section 5.2), and that absorbers within up to thousands km/s from a quasar are still connected with the quasar itself (e.g., Wild et al. 2008). Thus, as an operational definition, we consider an absorption system as associated to a quasar if its velocity difference with the the broad line redshift is smaller than ± 1000 km/s. Henceforth, we will refer to *transverse* or to *LOS* absorption features associated to QSO_F depending on whether they are observed in the the spectrum of QSO_B or of QSO_F, respectively.

We can not discriminate between absorbers associated to the QSO_F and absorbers that occur by chance coincidence. However, the small separations in both projected distances and relative velocities suggest that we are probing the cool gas strictly related to the quasar. As zeroth order test in support if this hypothesis, we calculate that the probability of finding a Mg II chance absorber with $0.5 \text{ \AA} < EW_r < 1.5 \text{ \AA}$ enclosed between ± 1000 km/s from a quasar is rather low: $\lesssim 1\%$ (Nestor et al. 2005). However, this estimate could be increased taking into account the clustering properties of absorbers (e.g., Quashnock & vanden Berk 1998; Quashnock & Stein 1999; Tytler et al. 2009).

The properties of the detected absorption systems associated to the QSO_F are listed in Tables 2.3 and 2.4. Notes on single objects are in Appendix B.

2.3.1 Transverse absorption systems

Mg II transverse absorption features are present in 7 out of 10 pairs (see Figure 2.4). Excluding QQ08, for which our data do not allow to state stringent upper limit to EW_r , we estimate a covering fraction of $k(\text{Mg II}) \sim 75\%$ for systems with $EW_r \gtrsim 0.3 \text{ \AA}$ and $pd \leq 120$ kpc. This value is lower than (but consistent within poissonian errors) the 100% found by Bowen et al. (2006) in a sample of 4 quasar pairs. Combining the two results we obtain $k(\text{Mg II}) \sim 75\%$ for $EW_r(\text{Mg II}) \gtrsim 0.3 \text{ \AA}$. It is worth noting that, at higher redshift, Hennawi et al. (2006a) found a similar high covering fraction for HI asborbers ($k(\text{HI}) \sim 75\%$) in quasar pairs with projected separations $pd \lesssim 150$ kpc. The quasar Mg II covering factor seems to be larger than that observed in non active galaxies, although for these objects it spans a wide range of values, depending on impact parameter and galaxy properties: i.e., from $k(\text{Mg II}) \sim 10\%–15\%$ (Bowen & Chelouche 2011), to 25% (Bechtold & Ellingson 1992), to $\sim 50\%$ (Tripp & Bowen 2005; Kacprzak et al. 2008), up to $\sim 70\%$ (Chen et al. 2010a).

2 *The VLT sample*

Table 2.3: Properties of Mg II absorption features associated to QSO_F. (01) our identification label of the quasar, (02,04) observed wavelength, (03,05) rest frame equivalent width, (06) doublet ratio, and (07) redshift of the absorption. If no absorption system is present, the 2σ upper limit for the EW_r is quoted. The label F and B refer to absorption systems observed on the spectra of the foreground and of the background quasar, respectively.

Mg II						
ID	$\lambda 2796$		$\lambda 2803$		DR	z_{abs}
	λ_{abs} [Å]	EW_r [Å]	λ_{abs} [Å]	EW_r [Å]		
(01)	(02)	(03)	(04)	(05)	(06)	(07)
QQ01F	...	< 0.28	...	< 0.28
QQ01B	7109.0	0.48±0.17	7126.6	0.37±0.14	1.30±0.35	1.5421±0.0003
QQ02F	...	< 0.20	...	< 0.20
QQ02B	...	< 0.31	...	< 0.31
QQ03F	...	< 0.28	...	< 0.28
QQ03B	6564.1	0.46±0.12	6578.7	0.25±0.14	1.86±0.71	1.3470±0.0003
QQ05F	...	< 0.14	...	< 0.14
QQ05B	5434.5	1.21±0.09	5448.6	0.77±0.09	1.57±0.03	0.9434±0.0001
QQ06F	...	< 0.19	...	< 0.19
QQ06B	6522.8	0.91±0.17	6539.7	0.56±0.10	1.63±0.11	1.3326±0.0003
QQ07F	...	< 0.23	...	< 0.23
QQ07B	7043.0	0.58±0.07	7060.9	0.47±0.09	1.23±0.06	1.5186±0.0001
QQ08F	...	< 0.41	...	< 0.41
QQ08B	...	< 0.37	...	< 0.37
QQ11F	...	< 0.22	...	< 0.22
QQ11B	6233.4	1.36±0.16	6249.5	0.95±0.15	1.44±0.05	1.2291±0.0003
QQ12F	...	< 0.15	...	< 0.15
QQ12B	...	< 0.20	...	< 0.20
QQ13F	...	< 0.19	...	< 0.19
QQ13B	5399.6	0.24±0.07	5413.7	0.16±0.05	1.51±0.28	0.9310±0.0002

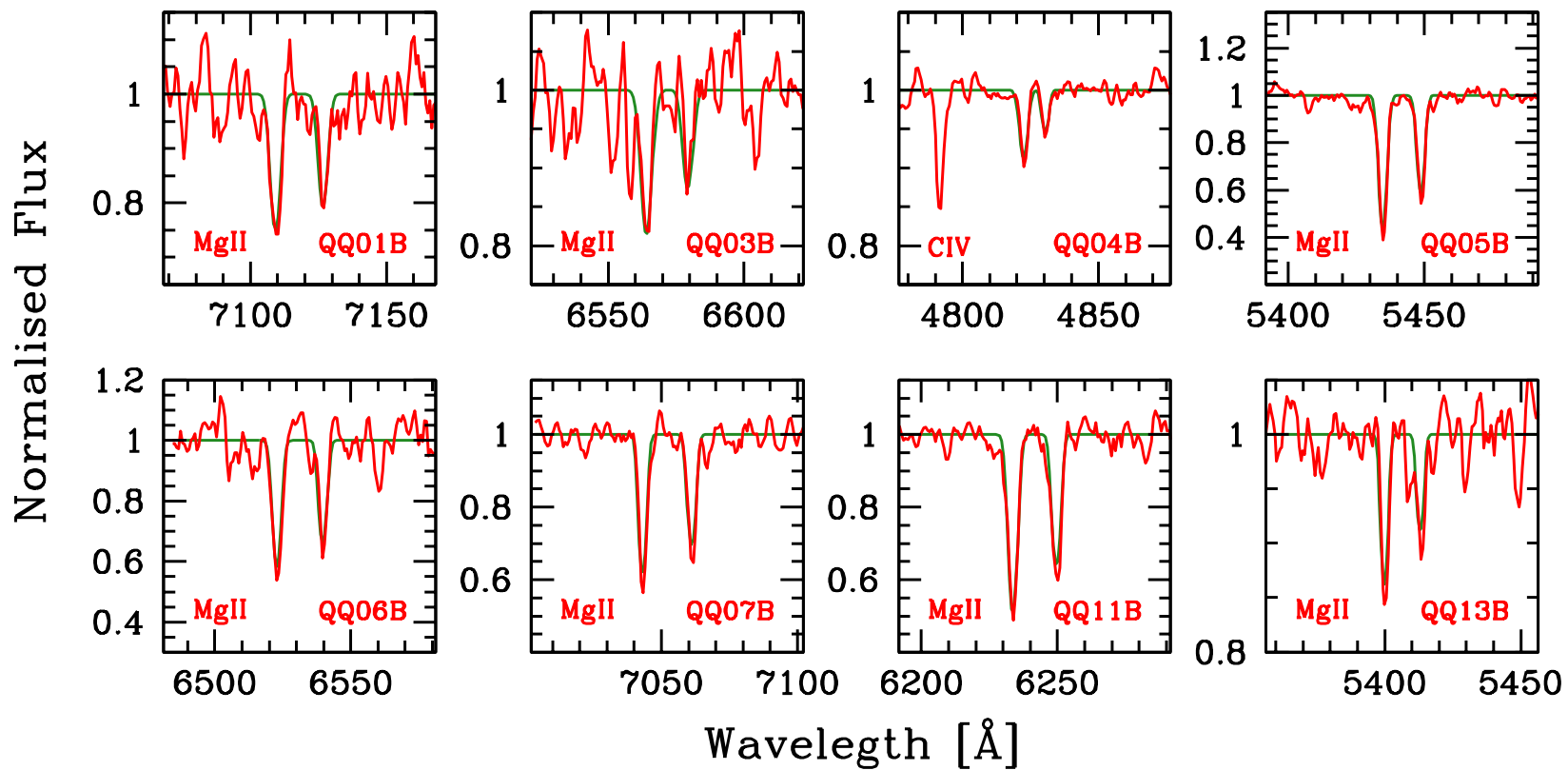


Figure 2.4: Close up of the normalised QSO_B spectra where the transverse absorption systems are detected (red line) and the fit performed as described in Section 2.2 (green line). The identification of the feature at $\sim 4791 \text{ \AA}$ present in the spectra of QQ04B is uncertain due to the presence of a nearby broad absorption line. It seems not associated to any of the detected CIV absorption systems.

Table 2.4: Same of Table 2.3, but for CIV absorption systems.

CIV						
ID	$\lambda 1548$		$\lambda 1551$		DR	z_{abs}
	λ_{abs} [Å]	EW_r [Å]	λ_{abs} [Å]	EW_r [Å]		
(01)	(02)	(03)	(04)	(05)	(06)	(07)
QQ04F	4830.3	1.42 ± 0.12	4838.1	1.36 ± 0.12	1.04 ± 0.02	2.1198 ± 0.0003
QQ04B	4822.4	0.12 ± 0.02	4830.1	0.06 ± 0.02	2.00 ± 0.21	2.1147 ± 0.0002
QQ09F	...	< 0.39	...	< 0.39
QQ09B	...	< 0.38	...	< 0.38
QQ10F	4751.3	0.14 ± 0.03	4759.1	0.13 ± 0.07	1.08 ± 0.35	2.0689 ± 0.0005
QQ10B	...	< 0.23	...	< 0.23

Only QQ04B shows a strong CIV absorption feature close to z_F (see Figure 2.4), formally yielding a covering factor of $k(\text{CIV}) \sim 33\%$. However, this feature is superimposed to the CIV broad emission lines of the QSO_B, and we can not exclude that it is instead a LOS absorption system associated to the QSO_B (see Appendix B). In the literature only few cases of CIV transverse absorption systems have been discovered, thus a sound value for the CIV covering factor around quasar is still missing. Bowen et al. (2006) have detected a CIV absorption system in correspondence of a Mg II one in a quasar pair separated by a projected distance of 26 kpc. In their sample Tytler et al. (2009) found 16 CIV absorption features close in redshift to a quasar, but both the small redshift difference between QSO_F and QSO_B and the large projected distance ($\text{pd} \gg 400$ kpc) of pairs they investigate do not allow to put firm constraints on the covering factor of the CIV strictly related to the quasars. Concerning galaxies, Chen et al. (2001) have shown that at impact parameter $\lesssim 150$ kpc the CIV covering factor is nearly unity.

2.3.2 Line-of-sight absorption systems

While no LOS absorption systems are observed for Mg II, these are present in 2 out of 3 spectra for CIV (see Figure 2.5). This is in good agreement with Vanden Berk et al. (2008) and Shen & Ménard (2012) who show that the occurrence of Mg II associated LOS absorption features in SDSS spectra is only of a few percent, and with Vestergaard (2003) that investigate a sample of moderate redshift quasar and found LOS narrow CIV absorption lines in $\gtrsim 50\%$ of them (see also, Wild et al. 2008). We stress that in general we can not discriminate between an origin of these absorbers close to the black hole, in the host galaxy, or in the surrounding halo (see for instance Crenshaw et al. 2003).

2.4 The EW–host galaxy mass relation

In Figure 2.6 we plot the rest frame equivalent width of Mg II transverse absorption systems against the QSO_F impact parameter. In spite of the small sample considered we

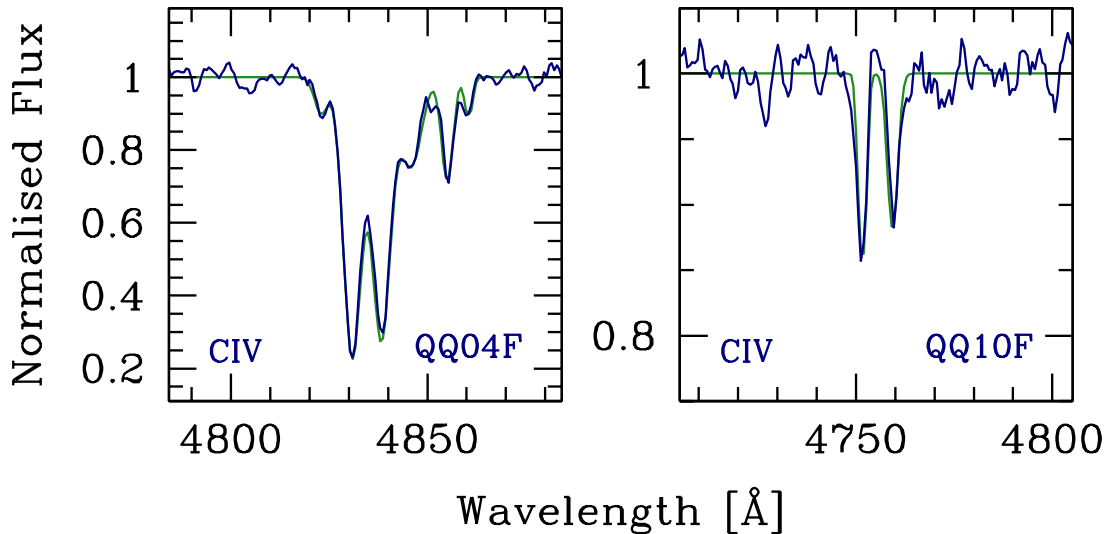


Figure 2.5: Close up of the normalised spectra of the quasars QQ04F and QQ10F for which the associated LOS absorption features are detected (blue line). The fits performed as described in Section 2.2 are shown with green lines. For notes on the different C IV doublets superimposed to the broad emission line of QQ04F see Appendix B)

note that many strong (i.e., $EW_r > 1 \text{ \AA}$) absorption systems are located up to separations larger than 70 kpc, in contrast to what observed in normal galaxies (see e.g., Chen et al. 2010a). We here assume that the Mg II absorption features are due to the gaseous halo of the quasars. However, we can not exclude the possibility that some of these systems are due to intervening galaxies. In Section 2.6 we will deal with alternative hypothesis.

Concerning galaxies, high resolution observations show that Mg II absorbers are often splitted in several discrete components (e.g., Churchill & Vogt 2001), suggesting a clumpy nature of the gaseous halo. Thus the EW_r of an absorption line is roughly proportional to the number of absorbing component along the line of sight (e.g., Petitjean & Bergeron 1990; Churchill et al. 2003). For the sake of simplicity, we can consider that the distribution of the cool gas around galaxies follow a spherical profile (e.g., Srianand & Khare 1993, 1994; Tinker & Chen 2008; Chelouche et al. 2008) and that the EW_r reflects the potential well of the dark matter halo. In other word, at a given radius, more massive systems sustain larger gaseous haloes that are responsible for stronger absorption lines due to the larger number of clouds intercepted. Assuming that the mass of the quasar host galaxy (M_{host}) traces the mass of the extended dark matter halo (see e.g., More et al. 2011), despite the uncertainties on the mass–to–light ratio, the EW_r of the absorption features is expected to follow a relation:

$$EW_r \propto \frac{M_{\text{host}}^\alpha}{pd^\beta}. \quad (2.5)$$

The two coefficients α and β have been estimated by Chen et al. (2010b) in a sample of 94 low redshift galaxies ($z < 0.5$): $\alpha = 1.8 \pm 0.1$ and $\beta = 0.34 \pm 0.06$ (see Figure 2.7).

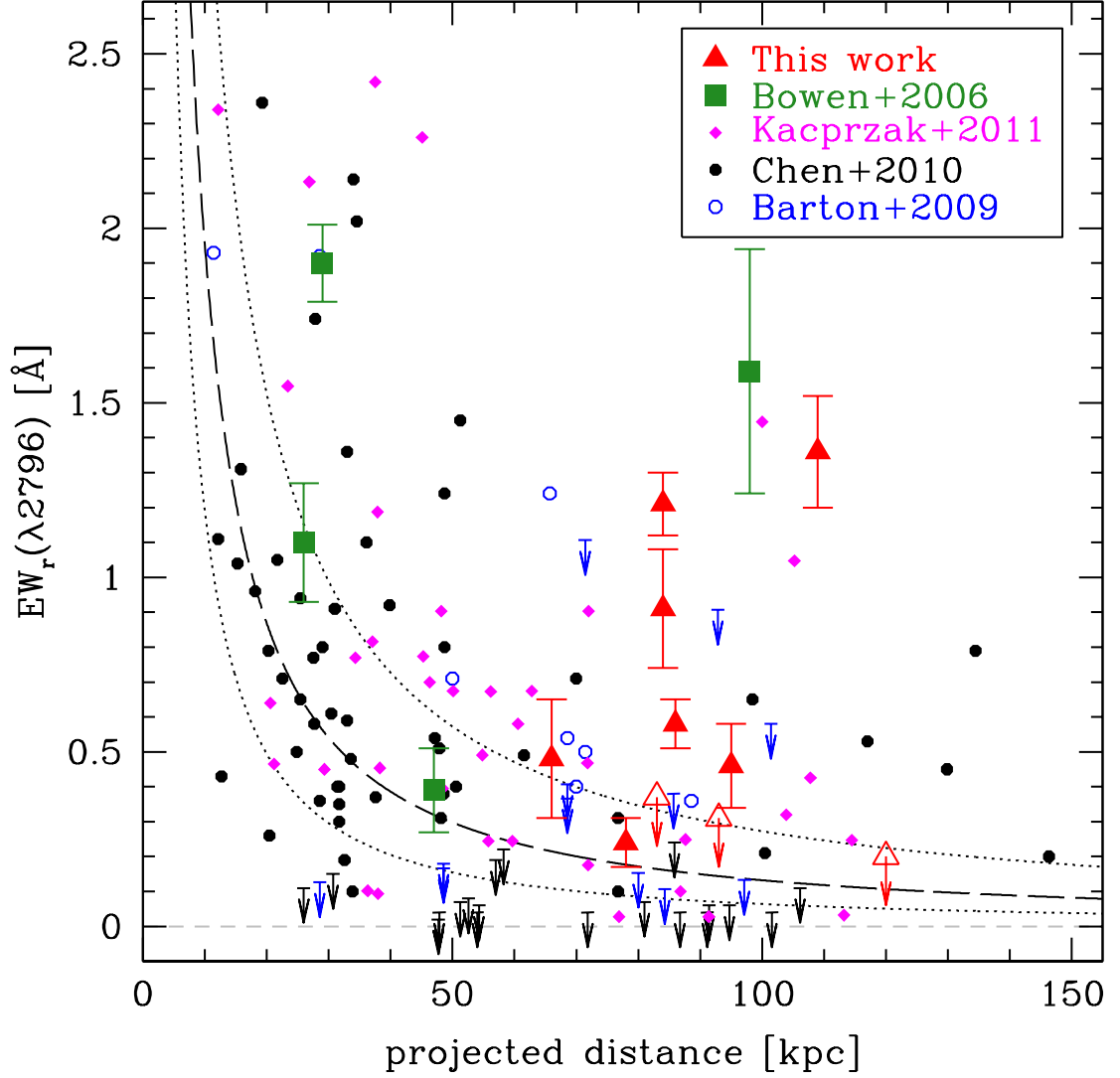


Figure 2.6: Rest frame EW of Mg II($\lambda 2796$) absorption line as a function of the projected distance. Red filled triangle are the QSO_F in which this feature is detected and the empty ones are the 2σ upper limits. Green squares are data for quasars from Bowen et al. (2006). Magenta diamonds, black filled points, and blue empty circles are absorption features associated to galaxies from Kacprzak et al. (2011), Chen et al. (2010a), and Barton & Cooke (2009). Black dashed line shows the best fit of the anti-correlation proposed by Chen et al. (2010b) and the associated 1σ uncertainties (dotted lines).

2.4 The EW–host galaxy mass relation

It is worth noting that the correlation between the EW_r and the mass of the halo is still not well established. For instance, Bouché et al. (2006), from an analysis of the relation between Mg II absorbers and luminous red galaxies in the SDSS found an anti-correlation between the absorber halo mass and EW_r , i.e., on average very strong absorbers ($EW_r \gtrsim 2 \text{ \AA}$) arise in less massive dark matter haloes ($\sim 10^{11} M_\odot$) while absorbers with $EW_r \sim 0.3 - 1.2 \text{ \AA}$ in the more massive one ($\sim 10^{12.5} M_\odot$). In addition Charlton & Churchill (1996) show that the Mg II distribution could be satisfactorily explained with both an extended disk geometry as well as a spherical one. From a sample of 40 galaxies at redshift ~ 0.5 , Kacprzak et al. (2011) suggest that the Mg II gas is distributed following a flattened halo that is co-planar and coupled to the inclination of the galaxy disc (see also, Kacprzak et al. 2012).

In order to determine the mass of the host galaxy (M_{host}) of QSO_F we consider the $M_{\text{BH}}-M_{\text{host}}$ relation presented by Decarli et al. (2010c) that is based on the investigation of 96 quasars with known host galaxy luminosities in the redshift range $0.07 < z < 2.74$:

$$\log \frac{M_{\text{BH}}}{M_{\text{host}}} = (0.28 \pm 0.06)z - (2.91 \pm 0.06). \quad (2.6)$$

where z is the quasar redshift. The black hole masses are estimated using the virial method applied to the gas of the BLR. These could be inferred from the width of broad emission lines and from the continuum luminosity (λL_λ), as expected from a photoionisation model (e.g., Kaspi et al. 2000). Following the recipes in Vestergaard & Peterson (2006) and of Vestergaard & Osmer (2009), one has:

$$\lg \frac{M_{\text{BH}}}{10^6 M_\odot} = \lg \left[\frac{\text{FWHM}(\text{Mg II})}{10^3 \text{ km/s}} \right]^2 + \lg \left[\frac{\lambda L_\lambda(5100 \text{ \AA})}{10^{44} \text{ erg/s}} \right]^{0.50} + 0.96 \quad (2.7)$$

$$\lg \frac{M_{\text{BH}}}{10^6 M_\odot} = \lg \left[\frac{\text{FWHM}(\text{C IV})}{10^3 \text{ km/s}} \right]^2 + \lg \left[\frac{\lambda L_\lambda(1350 \text{ \AA})}{10^{44} \text{ erg/s}} \right]^{0.53} + 0.66 \quad (2.8)$$

The uncertainties associated to these estimates are dominated by the dispersion of the relation between the radius of the BLR and the luminosity of the continuum and are typically around $\sim 0.4 \text{ dex}$ (e.g., Vestergaard & Peterson 2006; Shen et al. 2011). The mass of the black holes calculated for the QSO_F are listed in Table 2.1.

In Figure 2.7 we show the distribution of the EW_r as a function of the impact parameter rescaled for the stellar mass for quiescent galaxies from Barton & Cooke (2009) and Chen et al. (2010b) (on average $M_{\text{gal}} \sim 10^{10} M_\odot$) and for the host of quasars (on average $M_{\text{host}} \sim 2 \times 10^{11} M_\odot$). Taking into account the mass, the Mg II absorption systems associated to quasars have a distribution close to that of galaxies. The value of the χ^2 for our data estimated on the relations presented by Chen et al. (2010a,b) prior and after accounting for the galaxy mass improves of a factor ~ 3 . This is in agreement with studies that suggest that the haloes of quasars are similar to that of normal galaxies (e.g., Chelouche et al. 2008).

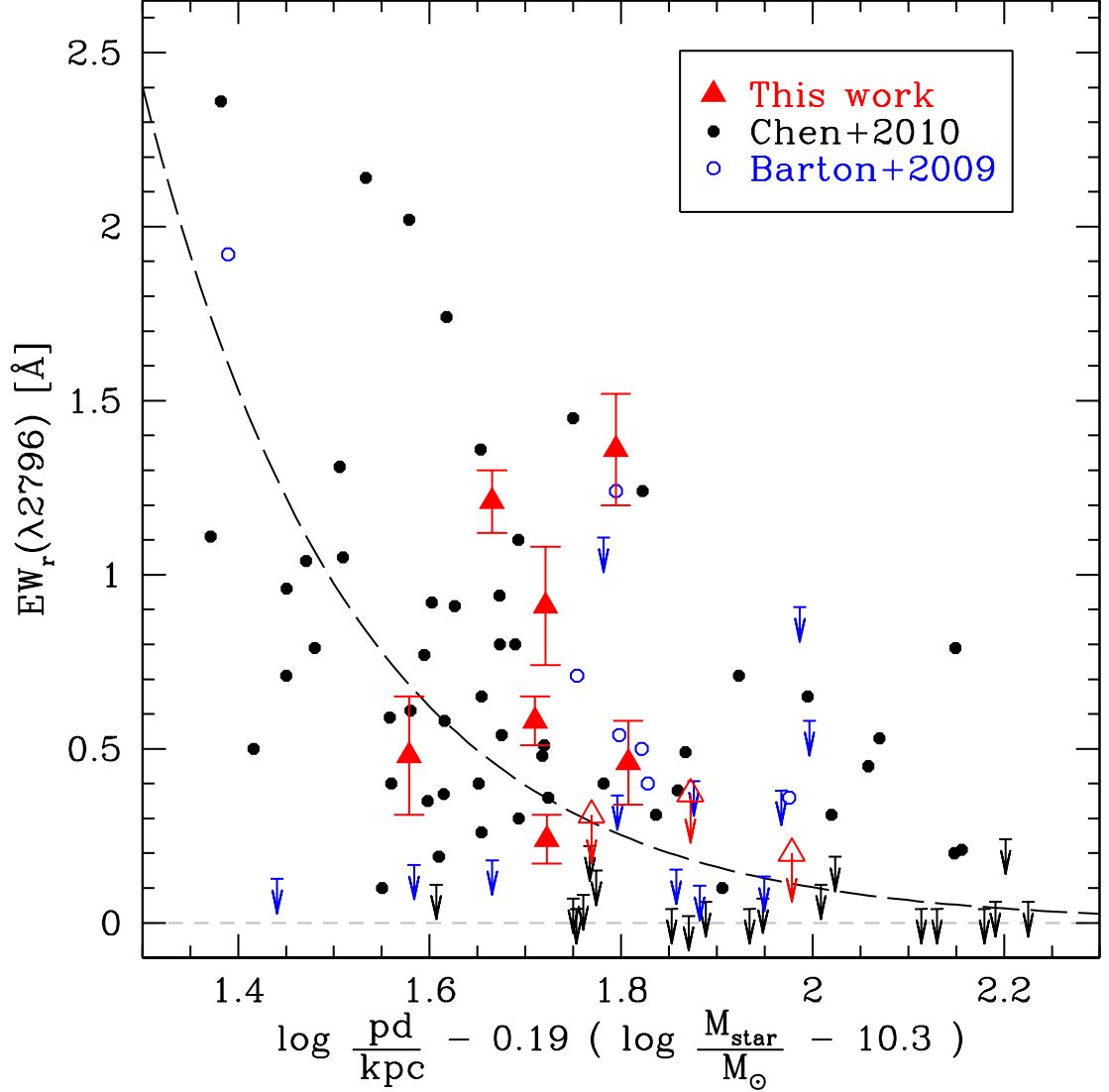


Figure 2.7: Rest frame EW of Mg II($\lambda 2796$) absorption line as a function of projected distance and stellar mass for quasars and galaxies. Red filled triangles are systems for which the absorption system was detected, while the empty ones are 2σ upper limits. Empty blue and filled black circle are data for galaxies from Barton & Cooke (2009) and Chen et al. (2010b), respectively. Black dashed line is the EW_r vs. projected distance anti-correlation for galaxies including the scaling relation with stellar mass proposed by Chen et al. (2010b). For the x-axis we have adopted the same projection of Figure 3 in Chen et al. (2010b).

2.5 Effects of the quasar radiation

The presence of the intense radiation field coming from the central SMBH should have a substantial effect in the thermal state of the gaseous halo. Chelouche et al. (2008) model the distribution of cool gas around quasars suggesting that it is filled with clouds having size of ~ 1 pc and density of $\sim 10^{-2} \text{ cm}^{-3}$. Under these conditions a quasars with luminosity of 10^{46} erg/s (the average of our sample calculated from the bolometric corrections given in Richards et al. 2006, see Table 2.1) can heat the cool gas within ~ 100 kpc up to a temperature of $T \sim 10^5 \text{ K}$, allowing the existence of only few Mg II absorbers. Wild et al. (2008) from a sample Mg II absorber with equivalent width larger than 0.3 \AA directly associated to the quasars, found that the SMBH emission destroys Mg II clouds out to at least 800 kpc. Since the quasar radiation is thought to be emitted into cones (Antonucci 1993), an anisotropy of the distribution of absorbers is thus expected (e.g., Hennawi et al. 2006b). If the UV emission of the central black occurs along the line of sight, the transverse absorption features will be not affected by it, and the quasar luminosity will have little impact on the extend Mg II absorbing gas at large galactic radii. On the contrary, Mg II absorbers along the line of sight will be photoionised by the quasar emission (see Figure 2.8 and Elvis 2000).

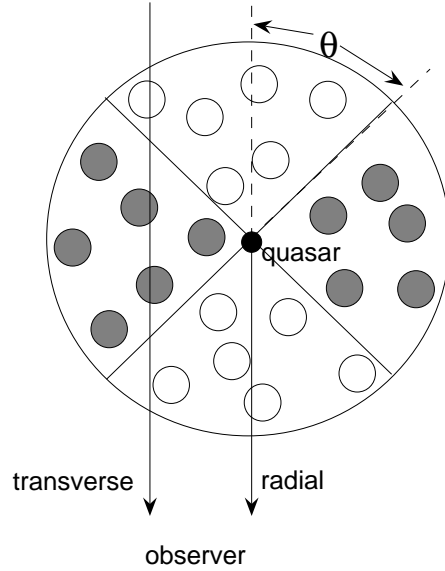


Figure 2.8: Distribution of the gas around a quasars. If the SMBH emits its ionising radiation into a cone with opening angle θ , the cool gas clouds which are exposed to it (open circle) are heated, while the remaining (filled circles) remain cool and their properties resemble those of haloes associated with non active galaxies. Figure from Chelouche et al. (2008).

C IV and Mg II are believed to reside in the same halo clouds, however the ionising region of the former is expected to be smaller than that of the latter, consistent with its higher ionisation energy. C IV absorbers could survive within ~ 100 kpc, even though the radiation field of the quasar (Chelouche et al. 2008). The origin of the C IV LOS absorbers could also be associated to the region closer to the quasar. For instance, Wild et al. (2008), investigating the C IV LOS absorption system in a sample of ~ 7400 C IV absorbers from the SDSS, have found that $\sim 40\%$ of the systems within 3000 km/s of the quasar are due to a gas outflow from the central black hole (see also, Nestor et al. 2005).

2.6 Origin of the absorption systems

Although our sample of 13 quasar pairs does not allow us to put firm constraints, we can comment on the possible origin of the absorbing gas.

A simple explanation for the most intense and distant absorption lines detected around quasars is that these are due to a chance superposition of satellite galaxies or to the presence of tidal tails due to recent merger episodes (see e.g., Fumagalli et al. 2011; Keeney et al. 2011). This scenario is supported by studies suggesting that, despite the wide variety of environments in which they are detected, quasars seem to prefer galactic environment richer than average (e.g., Wold et al. 2001; Serber et al. 2006; Hutchings et al. 2009). However, the high covering factor and the observational evidence of galaxies surrounded by cool gas up to a radius of ~ 100 kpc, allow us to fairly assume the link between absorbers and the quasar haloes. In support of this we also roughly estimate the the H I column density from the rest frame equivalent width of Mg II by applying to our study the empirical relations found by Ménard & Chelouche (2009) in the sample of low-redshift Lyman absorbers of Rao et al. (2006). All the detected systems have $\lg(N_{\text{HI}}/\text{cm}^2) < 19.6$, that is unlikely associated to galactic disc (e.g., Zwaan et al. 2005). However, we can not exclude the possibility that the absorptions origin from extra-planar neutral gas associated to spiral galaxies (e.g., Sancisi et al. 2008).

If the absorbers are associated to the quasar gaseous halos, the improvement of the anti-correlation between EW_r and projected distance due to the addition of the galaxy mass as parameter is naturally explained in the inflow scenario. As suggested by Chen et al. (2010b) more massive galaxies have more extended halos of cool gas and thus the observed Mg II absorbers arise in infalling clouds. However, we note that only the weaker absorption systems are thought to be associated to inflows of gas (the few absorption systems observed by Chen et al. at separations larger than 70 kpc have typically $\text{EW}_r \lesssim 0.7 \text{ \AA}$), while the stronger ones to outflows (e.g., Zibetti et al. 2007). The inflows of gas responsible of the quasar activity may produce intense star formation episodes and strong winds (e.g., Di Matteo et al. 2005; Hopkins et al. 2005; Maiolino et al. 2012) that might give rise to the stronger detected absorption lines. This is also supported by the recent discovery of signature of high star formation rate and gas outflows in the quasar host galaxies (Floyd et al. 2012; Sanmartim et al. 2012).

2.7 Conclusions

In this Chapter we have studied 13 close projected quasar pairs ($60 \text{ kpc} < \text{pd} < 120 \text{ kpc}$) observed with FORS2 at ESO-VLT. In 7 out of 10 systems we have detected the Mg II doublet on the QSO_B spectrum in correspondence to the QSO_F, while only one association out of 3 is found for CIV. Considering also the 4 absorption systems discovered by Bowen et al. (2006), we estimate an high covering factor for the cool gas surrounding quasars ($k(\text{Mg II}) \sim 75\%$ for absorption systems with $\text{EW}_r \gtrsim 0.3 \text{ \AA}$).

We compare our study with those performed for inactive galaxies by Kacprzak et al. (2011), Chen et al. (2010a,b), and Barton & Cooke (2009). If we consider EW_r as a function of both the projected distance and the mass of the systems, we find that the haloes of quasars are similar to that of galaxies. This suggests that the Mg II absorbers

are associated with gas inflows, as could be expected if the quasar nuclear activity were driven by intense gas accretion onto the SMBH. However, alternative origins for the stronger absorption features ($EW_r \gtrsim 0.5 \text{ \AA}$) are possible. Those could be associated to intervening galaxies or to outflows of gas due to star formation episodes.

Finally, we note that along the line of sight we do not detect any Mg II absorbers of the same strength of the transverse one. These results are in agreement with models that consider a non isotropic emission of the quasar, which are hosted by gaseous haloes more massive than those of inactive galaxies.

2 *The VLT sample*

3 The SDSS sample

In this Chapter we introduce our ongoing spectroscopic programme aimed to detect Mg II absorption features in a sample of 33 quasar pairs driven from the Schneider et al. (2010) SDSS catalogue (Section 3.1). We have already collected optical and near–infrared spectra for 20 of these sources with the Optical System for Imaging and low–intermediate Resolution Integrated Spectroscopy (OSIRIS Cepa et al. 2003) at the GTC, and the analysis of these data is in progress.

As premise for this study, we have analysed the SDSS spectra of the 78 quasar pairs with projected separation $pd \leq 200$ kpc, for which it is possible to investigate the presence of Mg II or C IV absorption systems associated to the foreground quasars in the wavelength range explored by the SDSS (i.e., 3800 Å–9200 Å; Section 3.2). The properties of the detected systems are compared with the results presented in Farina et al. (2012b) and in Chapter 2 (Sections 3.2.1 and 3.2.2).

3.1 The OSIRIS–GTC sample

In order to strengthen the results presented in Chapter 2 and in Farina et al. (2012b), we consider to enlarge our sample searching in the Schneider et al. (2010, see Appendix A) catalogue for projected quasar pairs with separations $pd \leq 200$ kpc (at the redshift of the foreground quasars), and to take advantage of the exquisite capabilities of OSIRIS, the imager and spectrograph located in the Nasmyth–B focus of GTC. OSIRIS covers the optical and near–IR wavelength range (from 3650 Å to 10500 Å) with a field–of–view of $8'.0 \times 5'.2$ (with a plate scale of $0''.127$) that allows, by using the $8'.67$ slit, to observe at the same time two sources separated in the sky by up to $\sim 7'.0$ ¹.

We selected quasar pairs that match the following constraints:

- i) the projected separation is $pd \leq 200$ kpc;
- ii) the redshifts of the fore– and back–ground quasars combine so that the Mg II absorption lines at $z = z_F$ fall within the wavelength range observed with OSIRIS high resolution grisms: R2500V, R2500R, and R2500I (see Table 3.1), and that do

Table 3.1: Properties of the considered OSIRIS grisms. (01) grism name, (02) central wavelength, (03) spectral range and, (04) spectra resolution at the central wavelength ($0''.6$ slit).

GRISM	λ_c [Å]	range [Å]	R
(01)	(02)	(03)	(04)
R2500V	5210	4500 – 6000	2515
R2500R	6590	5575 – 7685	2475
R2500I	8740	7330 – 10000	2503

¹The reduced distance allowed is due to the obscuration present on the edges of OSIRIS field–of–view, and to manufacturing defects of the slit.

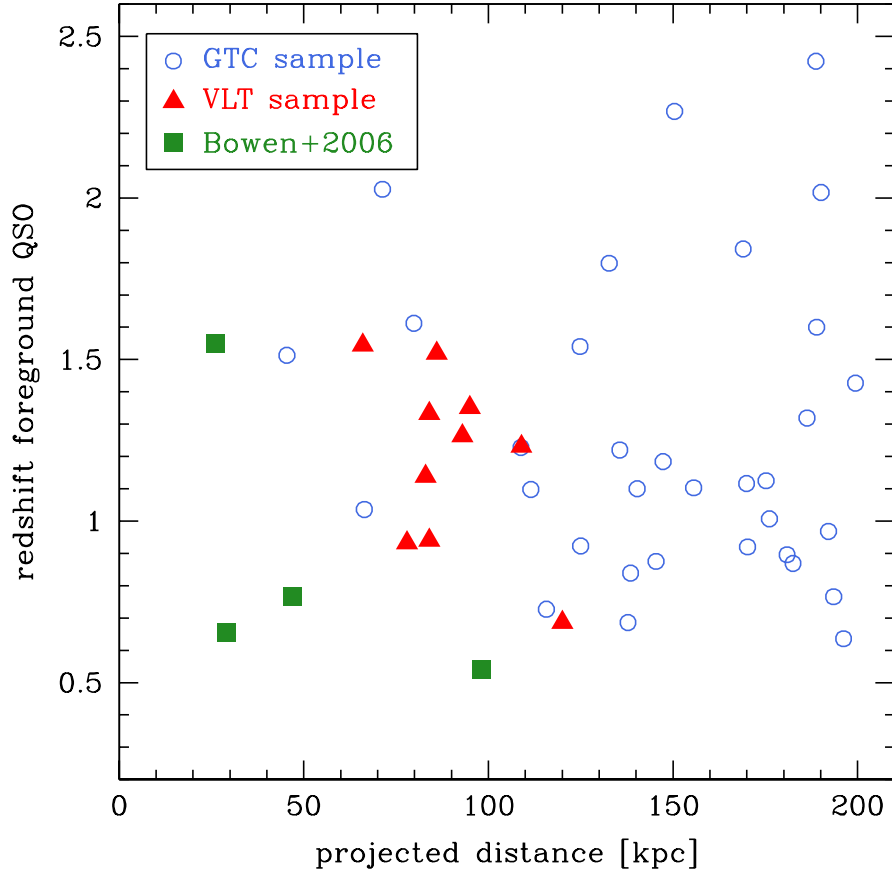


Figure 3.1: Distribution of close projected pairs investigated for the presence of Mg II absorption systems in the $pd-z_F$ plane. Empty blue circles are the sample of systems proposed for OSIRIS-GTC observations. Red triangles and green squares are from the sample of Farina et al. (2012b, see Chapter 2) and Bowen et al. (2006), respectively.

not overlap with important sky features or narrow emission lines in the spectrum of the background target;

iii) the QSO_B is brighter than $r < 20.1$.

The last restriction was adopted to make our GTC programme ideal as filler. Indeed, the observations can be done with seeing up to $1''.5$, while ensuring a good spectra ($S/N \sim 30$) in a reasonable amount of observing time.

The final sample consists of 33 pairs (see Figure 3.1) in the redshift range $0.6 \lesssim z_F \lesssim 2.4$. The average projected separation is $\langle pd \rangle \sim 150$ kpc, thus these systems will allow us to obtain information on the outer regions of the quasar gaseous haloes. Spectra for 20 pairs was already gathered at GTC, while the remaining 13 will be observed in the next semester.

3.2 Analysis of SDSS spectra

The Schneider et al. (2010, see Appendix A) catalogue contains 99 quasar pairs with projected separation $pd \leq 200$ kpc at the redshift of the foreground quasar. From this list we focussed only on those systems in which Mg II and C IV absorptions systems associated to QSO_F (see Section 2.3) fall within the SDSS spectra observational window (i.e., from 3800 Å to 9200 Å). This limit the redshift of the foreground targets to be in the range: $0.35 \lesssim z_F \lesssim 2.29$ for Mg II and $1.45 \lesssim z_F \lesssim 4.94$ for C IV. As additional constraint, we also removed all the pairs in which the absorptions lines could overlap with strong sky features and/or narrow emission lines in the spectra of QSO_B. The final sample consists of 74 systems suitable for the study of Mg II and 20 for the C IV (see Table 3.2 and Figure 3.2).

It is worth noting that the typical signal-to-noise of the considered spectra is low ($S/N \sim 5$, see Figure 3.2) and that the SDSS reduction pipeline often fail to remove some night sky emission lines (in particular the OH forest), that leave significant residuals in the red part of the spectra (i.e., at wavelength $\lambda \gtrsim 7500$ Å, see Figure 3.3). Thus, the SDSS spectra allow us to detect only the stronger ($EW \gtrsim 1$ Å) metal absorption lines associated to quasars, and higher signal-to-noise spectra are mandatory to study the distribution of the cool gas as a function of the projected distance and of the host galaxy stellar mass down to a sensitive limit ($EW_r \sim 0.3$ Å).

For the analysis of the spectra we follow the same procedures presented in Section 2.2. We consider an absorption feature as associated to the foreground quasar if it lie within ± 1000 km/s from z_F (see Section 2.3). The results of this analysis are listed in Tables 3.3 and 3.4.

3.2.1 MgII absorption systems associated to quasars

In the spectra of QSO_B we detect 6 transverse Mg II absorption systems associated to QSO_F (see Table 3.3 and Figure 3.4). Excluding from our sample the systems that do not allow to derive stringent constraint on the minimum detectable equivalent width, we are able to roughly estimate a covering fraction of $k(\text{Mg II}) \sim 50\%$ for $EW_r(\text{Mg II}) \gtrsim 0.6$ Å. If we include also the results presented in the previous Chapter and in Bowen et al. (2006), we infer $k(\text{Mg II}) \sim 46\%$ for $EW_r(\text{Mg II}) \gtrsim 0.6$ Å at separation $pd < 200$ kpc. This high covering fraction suggests that the Mg II haloes of quasar may extend up to radius as large as 200 kpc. However, one should consider that the probability to intercept an intervening galaxy increase with the separations and that the galactic environment of quasars is typically richer than average (Wold et al. 2001; Söchting et al. 2002; Serber et al. 2006; Hutchings et al. 2009), thus the strong absorption systems detected at large projected separations could be due to intercepted galactic discs, rather than to the quasar haloes.

In Figure 3.4 we show the distribution of the Mg II rest frame equivalent widths as a function of impact parameters and host galaxy masses estimated with the $M_{\text{BH}}-M_{\text{host}}$ relation presented by Decarli et al. (2010c, see Section 2.4). The stronger absorption systems ($EW_r \gtrsim 1$ Å) do not seem to follow the relations proposed by Chen et al. (2010a,b), even if we consider to stellar mass of the galaxies. This suggests that the absorbing clouds of these systems are not associated to gas inflows, but more probably to

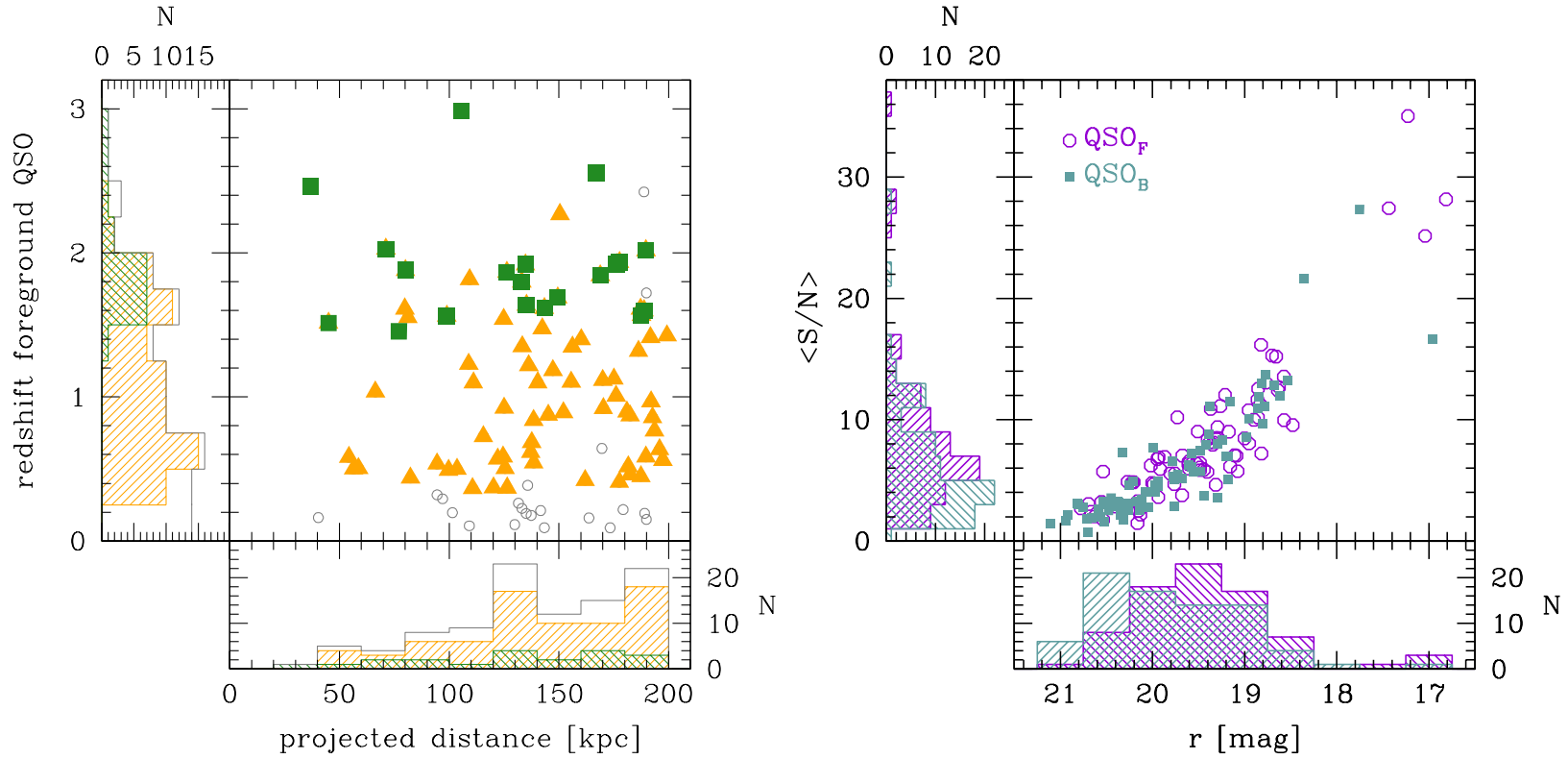


Figure 3.2: Properties of the SDSS quasar pairs with projected separation $pd \leq 200$ kpc in the Schneider et al. (2010) catalogue. *Left panel* — Distribution of the systems in the pd - z_F plane. The pairs suitable for the study of Mg II and C IV absorption features are highlighted with orange triangles and green squares, respectively. The open grey dots mark the systems not considered in our study.

Right panel — Average signal-to-noise per pixel of SDSS spectra as a function of the r -band magnitude of the quasars. Violet circles point to the foreground quasars and the light blue squares to the background ones. Only $\sim 20\%$ of the spectra have a signal-to-noise higher than $S/N \sim 10$, that allow to detect weaker absorption features associated to quasars ($EW \lesssim 1 \text{ \AA}$).

Table 3.2: Properties of the quasar pairs selected from the Schneider et al. (2010) catalogue. (01) our identification label of the pair, (02,03) redshifts from broad emission line, (04,05) catalogue r-band magnitude of the quasars, (06) angular and (07) projected separation, (09) bolometric luminosity of the foreground quasar (see Section 2.4 for details), (10) black hole mass of the foreground quasar (see Section 2.4 for details). The label F and B refer to the foreground and to the background quasar, respectively.

ID	$z_{\text{bl,F}}$	$z_{\text{bl,B}}$	r_{F}	r_{B}	$\Delta\theta$	pd	$L_{\text{bol,F}}$	$M_{\text{BH,F}}$
(01)	(02)	(03)	(05)	(06)	[arcsec]	[kpc]	[10^{46} erg/s]	[$10^8 M_{\odot}$]
(01)	(02)	(03)	(05)	(06)	(07)	(08)	(09)	(10)
QQS01	1.615	2.093	20.16	20.17	16.9	143	0.96±0.03	7.8
QQS02	1.921	2.093	20.16	20.17	21.0	176	0.97±0.17	14.0
QQS03	1.637	1.652	20.63	20.80	16.0	135	0.94±0.02	3.8
QQS04	0.505	1.181	18.82	19.76	9.6	58	0.34±0.02	4.2
QQS05	0.562	1.404	19.76	20.33	30.5	197	0.30±0.01	3.3
QQS06	2.027	2.087	19.26	19.57	8.5	71	5.68±0.19	21.9
QQS07	1.612	2.716	19.41	19.42	9.4	79	3.55±0.06	7.1
QQS08	1.125	1.330	19.93	19.77	21.4	175	1.03±0.02	4.7
QQS09	1.319	1.744	19.17	17.75	22.2	186	2.70±0.06	12.4
QQS10	0.366	0.712	18.85	20.32	21.8	110	0.21±0.01	0.5
QQS11	1.007	1.259	19.08	19.38	22.0	176	0.77±0.02	3.0
QQS12	1.351	1.698	20.13	20.27	15.9	133	0.58±0.02	4.8
QQS13	0.923	1.019	20.27	18.78	16.0	125	0.49±0.01	2.9
QQS14	0.408	1.019	19.60	18.78	32.7	177	0.16±0.01	1.6
QQS15	1.688	2.163	18.85	19.67	17.7	149	5.30±0.04	12.8
QQS16	0.492	0.985	19.40	18.84	16.5	99	0.30±0.01	1.9
QQS17	0.858	1.646	19.92	20.53	25.1	192	0.42±0.01	3.5
QQS18	0.875	2.229	19.76	20.21	18.8	145	0.45±0.01	1.6
QQS19	0.686	1.035	19.11	19.29	19.4	137	0.39±0.01	1.7
QQS20	1.036	3.213	19.94	20.04	8.2	66	0.43±0.01	0.9
QQS21	0.727	2.310	20.13	20.25	16.0	115	0.14±0.01	1.2
QQS22	2.460	2.462	19.68	20.14	4.5	36	3.10±0.23	2.3
QQS23	1.600	2.161	18.66	20.36	22.3	188	7.01±0.05	9.3
QQS24	1.842	2.443	18.57	20.12	20.0	168	7.01±0.29	18.5
QQS25	0.893	0.900	19.53	16.96	19.6	152	0.76±0.01	16.6
QQS26	0.423	1.953	19.95	20.58	29.3	162	0.18±0.01	0.5
QQS27	1.611	3.054	20.55	20.51	22.1	187	1.24±0.05	8.1
QQS28	0.438	1.763	18.95	21.10	14.6	82	0.36±0.01	4.0
QQS29	1.184	2.664	20.40	20.11	17.8	147	0.48±0.03	2.9
QQS30	0.501	0.501	19.38	19.55	9.3	56	0.28±0.01	1.4
QQS31	0.766	1.480	18.70	19.57	26.2	193	1.05±0.01	3.2
QQS32	0.536	0.536	19.37	19.38	15.0	94	0.37±0.01	1.9
QQS33	0.839	1.738	19.29	20.25	18.2	138	0.61±0.01	3.3
QQS34	1.348	3.285	17.23	20.38	18.6	156	16.20±0.33	17.5
QQS35	0.543	0.543	19.61	18.81	21.8	138	0.32±0.01	6.3
QQS36	0.896	1.917	19.31	19.24	23.3	181	0.84±0.02	1.6
QQS37	0.571	1.171	19.08	19.60	18.7	122	0.32±0.03	2.0

3 The SDSS sample

Table 3.2: continued. The analysis of the spectra of the alleged foreground quasar of the pair QQS54 suggests that this source is indeed a star.

ID	$z_{\text{bl,F}}$	$z_{\text{bl,B}}$	r_{F}	r_{B}	$\Delta\theta$	pd	$L_{\text{bol,F}}$	$M_{\text{BH,F}}$
(01)	(02)	(03)	(05)	(06)	[arcsec] (07)	[kpc] (08)	$[10^{46} \text{ erg/s}]$ (09)	$[10^8 M_{\odot}]$ (10)
QQS38	1.866	1.882	16.81	20.34	15.0	126	29.44±0.57	66.8
QQS39	1.400	1.739	19.21	20.81	19.0	160	2.64±0.03	9.2
QQS40	0.585	1.569	18.57	20.94	28.8	189	0.96±0.01	0.7
QQS41	1.513	1.891	20.53	19.48	5.3	45	0.51±0.01	10.1
QQS42	1.540	3.053	19.48	19.72	14.7	124	2.58±0.05	12.6
QQS43	1.100	2.964	20.53	19.76	17.2	140	0.20±0.01	3.9
QQS44	0.968	1.212	17.43	19.29	24.2	192	4.97±0.04	17.9
QQS45	1.098	2.521	20.01	20.45	13.6	111	0.89±0.01	2.6
QQS46	2.985	3.002	18.47	19.47	13.7	105	27.40±0.44	173.9
QQS47	0.449	0.687	20.15	20.92	32.7	187	0.10±0.01	0.3
QQS48	1.936	1.959	20.77	19.15	21.2	177	1.52±0.19	2.5
QQS49	1.455	1.457	17.04	18.61	9.1	77	13.39±0.16	16.7
QQS50	1.220	1.774	19.34	18.67	16.4	136	1.92±0.01	11.3
QQS51	0.499	0.998	19.73	19.19	17.0	103	0.32±0.01	6.1
QQS52	0.371	1.628	18.62	18.77	23.5	120	0.28±0.01	1.6
QQS53	2.017	2.173	20.66	20.44	22.7	189	1.85±0.20	6.6
QQS54	...	4.230	19.98	20.71	13.0
QQS55	1.918	2.271	20.69	20.75	16.0	134	1.80±0.15	5.9
QQS56	0.584	1.598	18.82	18.85	18.9	124	0.70±0.01	2.5
QQS57	1.116	2.968	19.44	19.97	20.8	170	0.98±0.03	9.1
QQS58	1.798	2.277	19.80	18.80	15.8	133	1.98±0.04	8.0
QQS59	2.268	3.315	19.33	20.31	18.3	150	7.09±0.17	47.3
QQS60	1.566	1.578	20.00	19.44	22.2	187	0.79±0.02	20.6
QQS61	0.369	1.193	19.15	19.17	24.8	126	0.14±0.01	1.6
QQS62	1.563	1.564	19.29	18.98	11.7	98	2.51±0.04	15.2
QQS63	0.616	1.745	20.22	18.53	20.3	137	0.25±0.01	1.1
QQS64	1.552	2.658	18.89	20.69	9.6	81	3.99±0.04	6.9
QQS65	0.517	1.489	18.76	20.37	29.3	181	0.65±0.03	0.7
QQS66	1.475	3.444	18.83	20.65	16.9	142	3.61±0.04	21.5
QQS67	0.636	2.275	19.48	19.93	28.6	195	0.45±0.02	6.5
QQS68	1.103	2.341	19.86	19.96	19.0	155	1.12±0.01	2.7
QQS69	0.504	1.600	18.86	19.99	20.5	125	0.54±0.01	1.6
QQS70	0.920	1.649	19.50	18.95	21.7	170	0.78±0.01	1.5
QQS71	1.880	1.890	18.63	18.36	9.5	80	11.30±0.18	22.7
QQS72	2.553	2.570	19.48	20.56	20.8	167	4.00±0.13	9.5
QQS73	1.228	1.514	19.61	20.08	13.1	108	1.38±0.02	10.3
QQS74	0.869	1.465	20.20	19.18	23.7	182	0.42±0.01	3.0
QQS75	0.460	0.487	19.00	19.94	31.4	182	0.31±0.01	1.4
QQS76	0.582	1.942	18.95	20.50	8.3	54	0.44±0.01	1.7
QQS77	1.414	1.819	19.31	20.47	22.7	191	1.28±0.02	5.2
QQS78	1.427	1.946	19.67	19.78	23.6	199	1.64±0.02	6.9

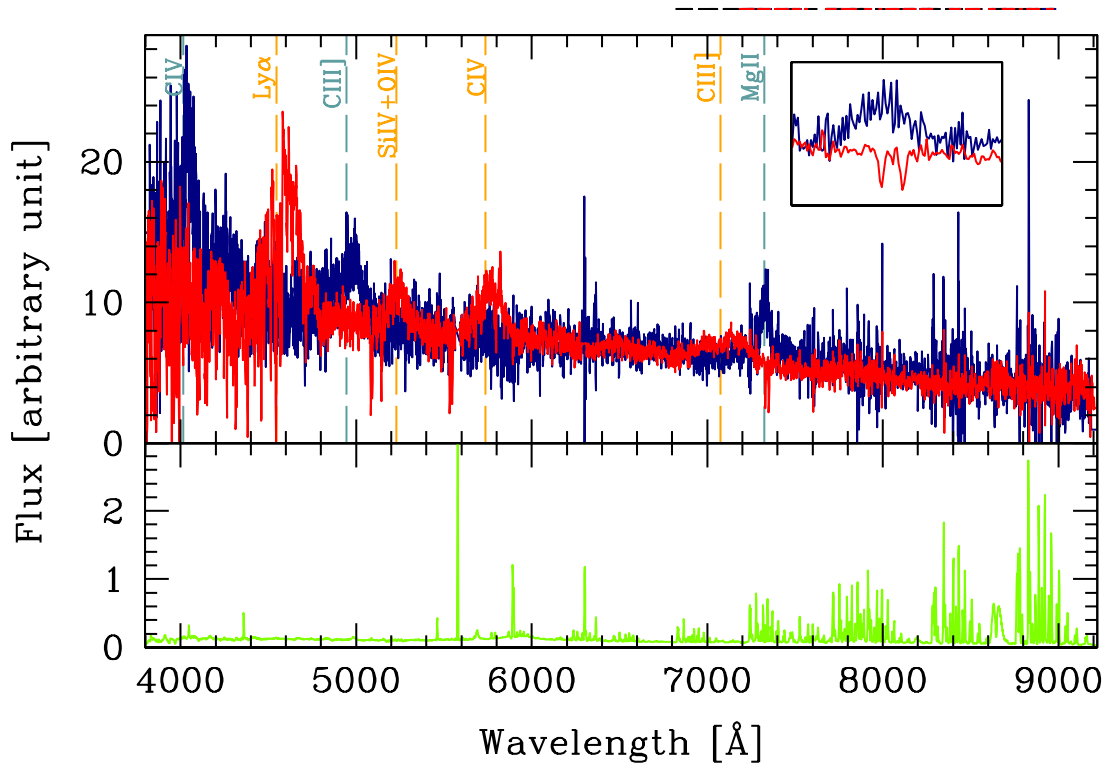


Figure 3.3: Spectra of the quasar pair QQS07 with projected separation $pd = 79$ kpc. The foreground and the background quasars are shown in blue and red, respectively. Most prominent quasar broad emission lines are marked with vertical dashed lines and the sky emission spectra is in the bottom panel. In the inset we show the detection of the Mg II absorption lines at the redshift of the foreground quasar. The decay of the SDSS spectral quality at $\lambda \gtrsim 7500$ Å is apparent.

intervening galaxies or to star formation driven outflows (see Section 2.6).

We observe also 4 LOS Mg II absorption lines associated to QSO_F . This small number of detections is consistent with the studies of Vanden Berk et al. (2008) and Shen & Ménard (2012) that are based on the analysis of hundreds of quasar spectra. The presence of these LOS absorption features could be due to external galaxies clustering around the quasar (e.g., Weymann et al. 1979); to the gaseous halos of the quasar host galaxy (e.g., Heckman et al. 1990, 1991); or originating from the vicinity of the SMBH (e.g., Hamann et al. 1995; Barlow & Sargent 1997). However, our sample is too small to allow us to distinguish between the possible origins.

3.2.2 CIV absorption systems associated to quasars

The SDSS spectra reveal the presence of 2 CIV transverse absorption features associated to QSO_F (see Table 3.4 and Figure 3.5). It is worth noting that both the spectra of the quasar pair QQS03 show the CIV absorption feature at the same redshift, we are thus probably detecting an intervening system blueshifted of ~ 1000 km/s from the

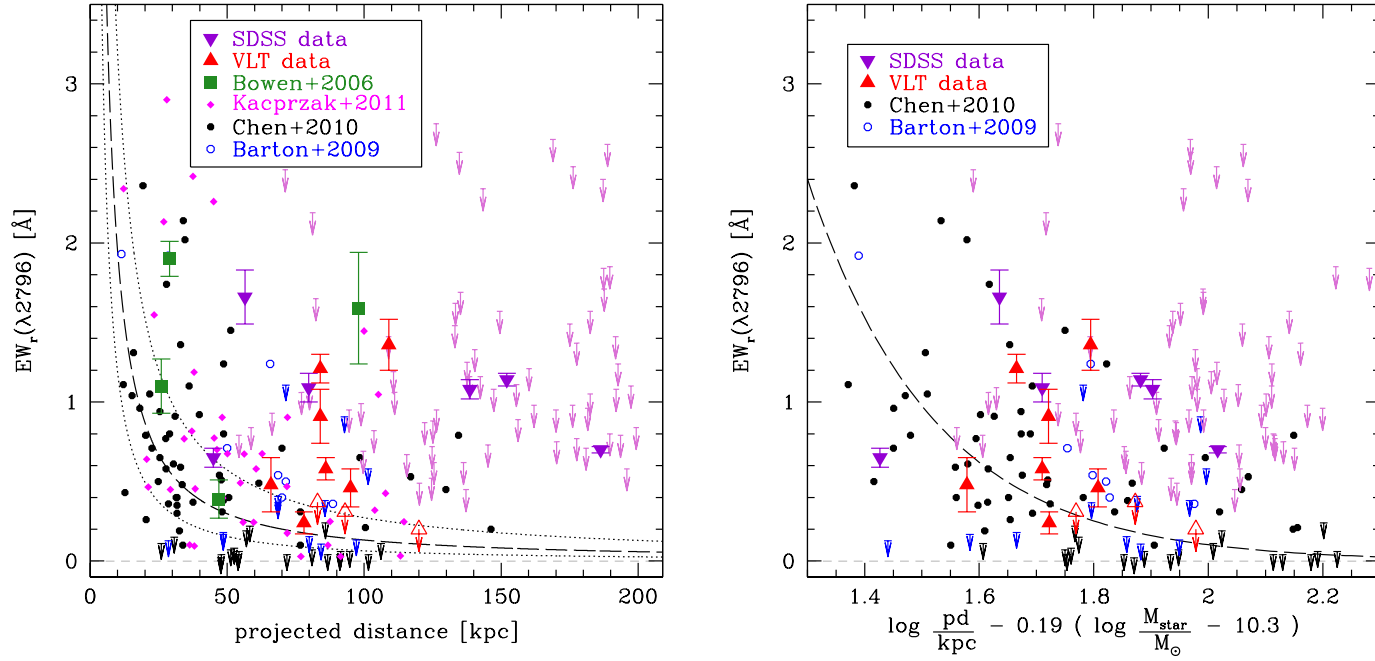


Figure 3.4: Rest frame EW of Mg II($\lambda 2796$) absorption line as a function of the projected distance and stellar mass for quasars and galaxies. Violet filled triangles are QSO_F in which this feature is detected and pale pink arrows are the 2σ upper limits. Red filled and empty triangles are data from the VLT sample (see Chapter 2). Green squares are data for quasars from Bowen et al. (2006). Magenta diamonds, black filled points, and blue empty circles are absorption features associated to galaxies from Kacprzak et al. (2011), Chen et al. (2010a), and Barton & Cooke (2009).

Left Panel — Black dashed line shows the best fit of the anti-correlation proposed by Chen et al. (2010b) and the associated 1σ uncertainties (dotted lines).

Right panel — Black dashed line is the EW_r vs. projected distance anti-correlation for galaxies including the scaling relation with stellar mass proposed by Chen et al. (2010b). For the x-axis we have adopted the same projection of Figure 3 in Chen et al. (2010b).

quasars.

Chen et al. (2001) detect the presence of a CIV envelope with an abrupt boundary at ~ 150 kpc (see Figure 3.5). The upper limits derived from the analysis of SDSS data does not allow to determine whether this CIV halo is present or not around quasars. However, the presence of two absorption systems at 117 kpc and at 177 kpc suggests that the CIV cool gas surrounding the quasar host galaxies, if exist, could extent up to these large radius.

We also detect 9 CIV LOS absorption system (see Table 3.4). These systems are commonly observed in quasar spectra and, even if the origin of these absorption is not clear, most of these are thought to be associated to outflows of gas from the SMBH (e.g., Vestergaard 2003; Wild et al. 2008, and Section 2.3).

3.3 Conclusions

In this Chapter we have introduced the sample of 33 quasar pairs that are part of our ongoing OSIRIS–GTC programme aimed to confirm the results presented in Chapter 2 and to estimate the size of the Mg II quasar gaseous haloes.

As a preliminary study for this work, we have analysed the SDSS spectra of 78 pairs with separations between ~ 50 kpc and ~ 200 kpc in order to detect Mg II and CIV metal absorption lines within 1000 km/s from the quasars. Due to the low signal–to–noise of these data, we are able to reveal the presence of only few (strong) absorption lines. Reliable estimate for the covering fraction of cool gas around the quasar host galaxies require spectra with an higher signal–to–noise that will allow to observe absorbing systems as faint as $EW_r \sim 0.3 \text{ \AA}$. The analysis of the high quality data collected at GTC, will be a breakthrough in our comprehension of the origins of the cool gas surrounding quasars and of the mechanisms that regulate the ignition of the quasar activity.

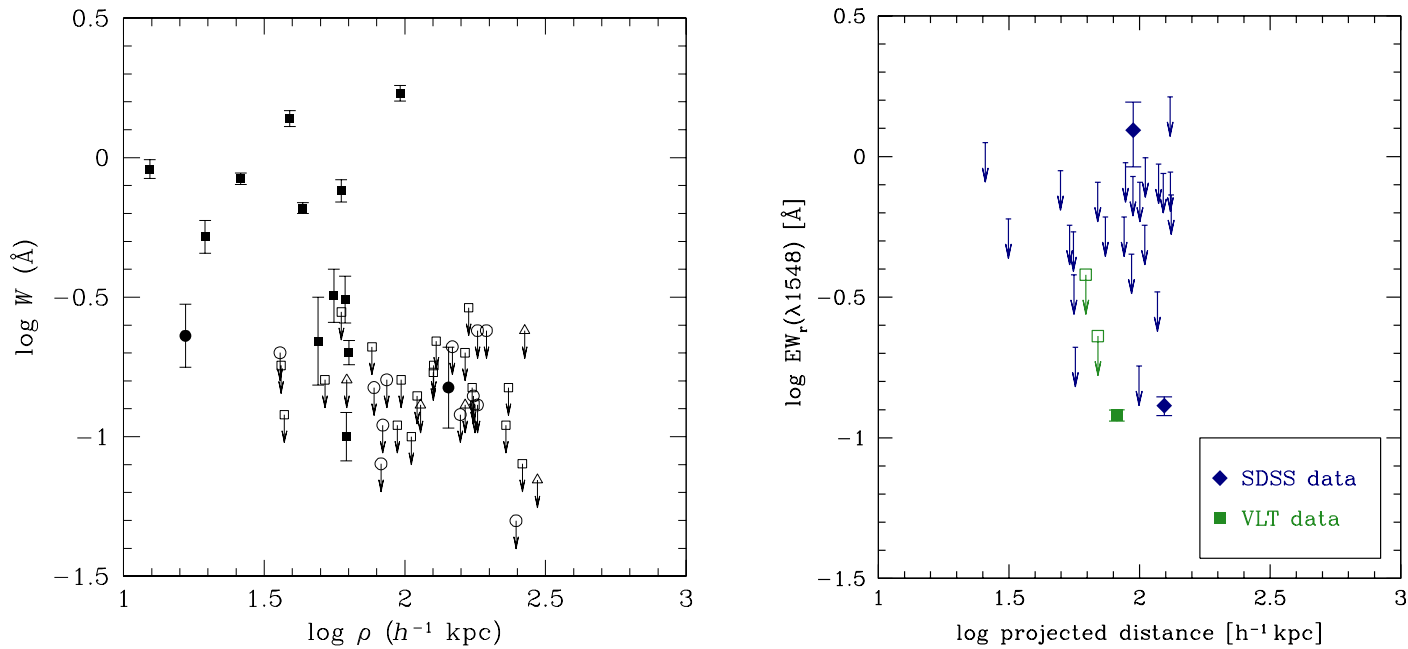


Figure 3.5: Logarithm of the rest frame EW of CIV($\lambda 1548$) absorption line vs. logarithm of projected distance for quasars and galaxies.

Left panel — Distribution of the data for galaxies from Chen et al. (2001). Circles are early-type elliptical or S0 galaxies, triangles represent early-type spiral galaxies, and squares late-type spiral galaxies. Closed points indicate detections while the open ones are 3σ upper limits of non-detections (Figure from Chen et al. 2001)

Right panel — Distribution of the data for quasars. Black diamonds and red squares are data from the SDSS and VLT spectra, respectively. Arrow represent 2σ upper limits.

Table 3.3: Properties of the Mg II absorption features associated to QSO_F. (01,05) our identification label of the quasar, (02,03,06,07) rest frame equivalent width, and (04,08) redshift of the absorption. If no absorption system is present, the 2σ upper limit for the EW_r is quoted. The label F and B refer to absorption systems observed on the spectra of the foreground and of the background quasar, respectively.

Mg II							
ID	EW _r (λ2796)	EW _r (λ2803)	z _{abs}	ID	EW _r (λ2796)	EW _r (λ2803)	z _{abs}
(01)	[Å]	[Å]	(04)	(05)	[Å]	[Å]	(08)
QQS01F	< 0.95	< 0.95	...	QQS09F	< 0.53	< 0.53	...
QQS01B	< 2.34	< 2.34	...	QQS09B	0.70 ± 0.02	0.50 ± 0.02	1.377 ± 0.001
QQS02F	< 1.38	< 1.38	...	QQS10F	< 0.61	< 0.61	...
QQS02B	< 2.48	< 2.48	...	QQS10B	< 1.19	< 1.19	...
QQS03F	< 1.60	< 1.60	...	QQS11F	< 0.53	< 0.53	...
QQS03B	< 1.69	< 1.69	...	QQS11B	< 0.98	< 0.98	...
QQS04F	0.65 ± 0.05	0.80 ± 0.07	0.562 ± 0.001	QQS12F	< 0.82	< 0.82	...
QQS04B	< 0.84	< 0.84	...	QQS12B	< 1.62	< 1.62	...
QQS05F	2.77 ± 0.33	2.14 ± 0.25	0.618 ± 0.001	QQS13F	< 0.52	< 0.52	...
QQS05B	< 1.10	< 1.10	...	QQS13B	< 0.88	< 0.88	...
QQS06F	< 0.90	< 0.90	...	QQS14F	< 0.60	< 0.60	...
QQS06B	< 2.46	< 2.46	...	QQS14B	< 0.77	< 0.77	...
QQS07F	< 0.89	< 0.89	...	QQS15F	< 0.51	< 0.51	...
QQS07B	1.09 ± 0.09	1.22 ± 0.10	1.672 ± 0.001	QQS15B	< 1.57	< 1.57	...
QQS08F	< 0.61	< 0.61	...	QQS16F	< 0.52	< 0.52	...
QQS08B	< 1.49	< 1.49	...	QQS16B	< 0.69	< 0.69	...

Table 3.3: continued.

ID	EW _r (λ2796) [Å]	EW _r (λ2803) [Å]	z _{abs}	ID	EW _r (λ2796) [Å]	EW _r (λ2803) [Å]	z _{abs}
(01)	(02)	(03)	(04)	(05)	(06)	(07)	(08)
QQS17F	< 0.50	< 0.50	...	QQS28F	< 0.63	< 0.63	...
QQS17B	< 1.24	< 1.24	...	QQS28B	< 1.65	< 1.65	...
QQS18F	< 0.57	< 0.57	...	QQS29F	< 0.88	< 0.88	...
QQS18B	< 0.73	< 0.73	...	QQS29B	< 1.08	< 1.08	...
QQS19F	< 0.60	< 0.60	...	QQS30F	< 0.60	< 0.60	...
QQS19B	< 1.25	< 1.25	...	QQS30B	1.66 ± 0.17	1.30 ± 0.14	0.558 ± 0.001
QQS20F	< 0.70	< 0.70	...	QQS31F	< 0.66	< 0.66	...
QQS20B	< 0.93	< 0.93	...	QQS31B	< 0.79	< 0.79	...
QQS21F	< 0.72	< 0.72	...	QQS32F	< 0.58	< 0.58	...
QQS21B	< 0.67	< 0.67	...	QQS32B	< 0.95	< 0.95	...
QQS23F	< 0.51	< 0.51	...	QQS33F	< 0.53	< 0.53	...
QQS23B	< 2.62	< 2.62	...	QQS33B	< 1.16	< 1.16	...
QQS24F	< 0.92	< 0.92	...	QQS34F	< 0.31	< 0.31	...
QQS24B	< 2.65	< 2.65	...	QQS34B	< 0.89	< 0.89	...
QQS25F	< 0.52	< 0.52	...	QQS35F	< 0.52	< 0.52	...
QQS25B	1.14 ± 0.04	0.91 ± 0.04	0.950 ± 0.001	QQS35B	1.08 ± 0.06	0.91 ± 0.04	0.600 ± 0.001
QQS26F	< 0.64	< 0.64	...	QQS36F	< 0.47	< 0.47	...
QQS26B	< 0.98	< 0.98	...	QQS36B	< 0.71	< 0.71	...
QQS27F	< 1.34	< 1.34	...	QQS37F	< 0.60	< 0.60	...
QQS27B	< 2.40	< 2.40	...	QQS37B	< 0.87	< 0.87	...

Table 3.3: continued.

ID	$EW_r(\lambda 2796)$ [Å]	$EW_r(\lambda 2803)$ [Å]	z_{abs}	ID	$EW_r(\lambda 2796)$ [Å]	$EW_r(\lambda 2803)$ [Å]	z_{abs}
(01)	(02)	(03)	(04)	(05)	(06)	(07)	(08)
QQS38F	< 0.44	< 0.44	...	QQS49F	< 0.44	< 0.44	...
QQS38B	< 2.75	< 2.75	...	QQS49B	< 1.06	< 1.06	...
QQS39F	< 0.55	< 0.55	...	QQS50F	< 0.52	< 0.52	...
QQS39B	< 1.21	< 1.21	...	QQS50B	< 0.62	< 0.62	...
QQS40F	< 0.53	< 0.53	...	QQS51F	< 0.42	< 0.42	...
QQS40B	< 1.85	< 1.85	...	QQS51B	< 0.82	< 0.82	...
QQS41F	< 0.58	< 0.58	...	QQS52F	< 0.37	< 0.37	...
QQS41B	0.65 ± 0.06	0.61 ± 0.06	1.572 ± 0.001	QQS52B	< 0.49	< 0.49	...
QQS42F	< 0.56	< 0.56	...	QQS53F	< 0.42	< 0.42	...
QQS42B	< 0.72	< 0.72	...	QQS53B	< 0.80	< 0.80	...
QQS43F	< 1.00	< 1.00	...	QQS54F
QQS43B	< 1.33	< 1.33	...	QQS54B
QQS44F	< 0.32	< 0.32	...	QQS55F	< 1.08	< 1.08	...
QQS44B	< 1.08	< 1.08	...	QQS55B	< 2.57	< 2.57	...
QQS45F	< 0.73	< 0.73	...	QQS56F	< 0.53	< 0.53	...
QQS45B	< 1.06	< 1.06	...	QQS56B	< 0.52	< 0.52	...
QQS47F	< 0.86	< 0.86	...	QQS57F	< 0.57	< 0.57	...
QQS47B	< 1.84	< 1.84	...	QQS57B	< 0.95	< 0.95	...
QQS48F	< 0.99	< 0.99	...	QQS58F	< 0.99	< 0.99	...
QQS48B	< 1.37	< 1.37	...	QQS58B	< 1.48	< 1.48	...

Table 3.3: continued.

ID	EW _r (λ 2796)	EW _r (λ 2803)	z _{abs}	ID	EW _r (λ 2796)	EW _r (λ 2803)	z _{abs}
(01)	[\AA] (02)	[\AA] (03)	(04)	(05)	[\AA] (06)	[\AA] (07)	(08)
QQS59F	< 2.09	< 2.09	...	QQS69F	< 0.61	< 0.61	...
QQS59B	< 5.67	< 5.67	...	QQS69B	< 0.62	< 0.62	...
QQS60F	< 0.69	< 0.69	...	QQS70F	< 0.63	< 0.63	...
QQS60B	< 1.71	< 1.71	...	QQS70B	< 0.75	< 0.75	...
QQS61F	< 0.64	< 0.64	...	QQS71F	0.77 ± 0.04	0.56 ± 0.03	1.940 ± 0.001
QQS61B	< 0.95	< 0.95	...	QQS71B	< 1.09	< 1.09	...
QQS62F	< 0.44	< 0.44	...	QQS73F	< 0.60	< 0.60	...
QQS62B	< 0.99	< 0.99	...	QQS73B	< 1.41	< 1.41	...
QQS63F	< 0.68	< 0.68	...	QQS74F	< 0.59	< 0.59	...
QQS63B	< 0.45	< 0.45	...	QQS74B	< 1.05	< 1.05	...
QQS64F	< 0.65	< 0.65	...	QQS75F	< 0.56	< 0.56	...
QQS64B	< 2.19	< 2.19	...	QQS75B	< 1.57	< 1.57	...
QQS65F	0.50 ± 0.03	0.60 ± 0.04	0.574 ± 0.001	QQS76F	< 0.58	< 0.58	...
QQS65B	< 0.96	< 0.96	...	QQS76B	< 0.79	< 0.79	...
QQS66F	< 0.57	< 0.57	...	QQS77F	< 0.66	< 0.66	...
QQS66B	< 1.16	< 1.16	...	QQS77B	< 1.41	< 1.41	...
QQS67F	< 0.55	< 0.55	...	QQS78F	< 0.59	< 0.59	...
QQS67B	< 0.58	< 0.58	...	QQS78B	< 0.84	< 0.84	...
QQS68F	< 0.71	< 0.71	...				
QQS68B	< 1.11	< 1.11	...				

Table 3.4: Properties of the CIV absorption features associated to QSO_F. (01,05) our identification label of the quasar, (02,03,06,07) rest frame equivalent width, and (04,08) redshift of the absorption. If no absorption system is present, the 2σ upper limit for the EW_r is quoted. The label F and B refer to absorption systems observed on the spectra of the foreground and of the background quasar, respectively.

CIV							
ID	EW _r (λ1548)	EW _r (λ1551)	z _{abs}	ID	EW _r (λ1548)	EW _r (λ1551)	z _{abs}
(01)	[Å]	[Å]	(04)	(05)	[Å]	[Å]	(08)
QQS01F	< 0.45	< 0.45	...	QQS22F	0.76 ± 0.12	0.69 ± 0.11	2.560 ± 0.001
QQS01B	< 0.81	< 0.81	...	QQS22B	< 1.12	< 1.12	...
QQS02F	< 0.47	< 0.47	...	QQS23F	1.11 ± 0.06	0.73 ± 0.04	1.700 ± 0.001
QQS02B	< 0.87	< 0.87	...	QQS23B	< 0.73	< 0.73	...
QQS03F	1.06 ± 0.16	1.14 ± 0.16	1.737 ± 0.001	QQS24F	0.55 ± 0.04	0.45 ± 0.03	1.942 ± 0.001
QQS03B	1.24 ± 0.32	1.24 ± 0.37	1.737 ± 0.001	QQS24B	< 0.94	< 0.94	...
QQS06F	< 0.56	< 0.56	...	QQS27F	< 0.38	< 0.38	...
QQS06B	< 0.89	< 0.89	...	QQS27B	< 1.63	< 1.63	...
QQS07F	< 0.35	< 0.35	...	QQS38F	< 0.24	< 0.24	...
QQS07B	< 0.54	< 0.54	...	QQS38B	< 0.95	< 0.95	...
QQS15F	0.11 ± 0.01	0.13 ± 0.01	1.788 ± 0.001	QQS41F	< 0.27	< 0.27	...
QQS15B	< 0.57	< 0.57	...	QQS41B	< 0.60	< 0.60	...

Table 3.4: continued.

ID	EW _r (λ1548) [Å]	EW _r (λ1551) [Å]	z _{abs}	ID	EW _r (λ1548) [Å]	EW _r (λ1551) [Å]	z _{abs}
(01)	(02)	(03)	(04)	(05)	(06)	(07)	(08)
QQS42F	< 0.44	< 0.44	...	QQS60F	< 0.34	< 0.34	...
QQS42B	< 0.61	< 0.61	...	QQS60B	< 0.88	< 0.88	...
QQS46F	< 0.21	< 0.21	...	QQS62F	0.32 ± 0.02	0.23 ± 0.02	1.662 ± 0.001
QQS46B	< 0.61	< 0.61	...	QQS62B	< 0.81	< 0.81	...
QQS48F	< 0.39	< 0.39	...	QQS64F	0.16 ± 0.01	0.07 ± 0.01	1.652 ± 0.001
QQS48B	0.13 ± 0.01	0.10 ± 0.01	2.036 ± 0.001	QQS64B	< 0.40	< 0.40	...
QQS49F	< 0.19	< 0.19	...	QQS66F	< 0.32	< 0.32	...
QQS49B	< 0.57	< 0.57	...	QQS66B	< 0.18	< 0.18	...
QQS55F	< 0.41	< 0.41	...	QQS71F	1.20 ± 0.11	0.99 ± 0.09	1.980 ± 0.001
QQS55B	< 0.85	< 0.85	...	QQS71B	< 0.70	< 0.70	...
QQS58F	1.38 ± 0.17	1.30 ± 0.15	1.898 ± 0.001	QQS72F	< 0.33	< 0.33	...
QQS58B	< 0.45	< 0.45	...	QQS72B	< 0.33	< 0.33	...
QQS59F	< 0.28	< 0.28	...				
QQS59B	< 0.99	< 0.99	...				

Part II

Physical systems of multiple quasars

4 The study of physical systems of multiple quasars

In the current hierarchical scenario of galaxy formation and evolution, interactions and mergers are thought to have a dominant role in the building up and in the growth of massive galaxies (e.g., White & Rees 1978), and in the ignition of the quasar activity. In fact, in this framework, we know that:

- a) galaxies regularly interact and merge (e.g., Toomre & Toomre 1972);
- b) SMBHs reside at the centre of almost every massive galaxies (e.g., Richstone et al. 1998);
- c) major merger event could trigger inflows of gas down to the circumnuclear regions that could result in a burst of quasar emission (e.g., Di Matteo et al. 2005).

These facts suggest that binary SMBHs should be commonplace, and thus also quasar pairs (if the two SMBHs are actively accreting at the same time). In the past, the search for physical systems of quasars (i.e., two quasars with small projected separation and almost at the same redshift) was limited by the little number of quasars known. The inspection of ~ 10000 quasars in the Large Bright Quasar Survey (Hewett et al. 1995) has driven to the discovery of 16 pairs with projected separation $pd \lesssim 100$ kpc, only 10 of which are confirmed physical association (Kochanek et al. 1999; Mortlock et al. 1999). A great improvement to this kind of analysis was given by the SDSS (York et al. 2000), in particular thanks to its large spectroscopic (~ 100000 objects, Schneider et al. 2010) and photometric (~ 1000000 sources, Richards et al. 2009) quasar catalogues. The benefits given by this larger statistic are apparent. For instance, Hennawi et al. (2006b) conducted an extensive search of quasar pair on the SDSS database and found, in the redshift range $0.5 \leq z \leq 3.0$, 221 pairs with $pd < 1.5$ Mpc and velocity difference along the line-of-sight $\Delta V_{\text{LOS}} < 2000$ km/s.

The increasing number of known quasar pairs has allowed to study their small scale clustering properties. Djorgovski (1991) first pointed out that the handful of binary quasars known at the time highlighted the evidence of an increment of the number of pairs respect to the simple extrapolations of the larger scale two-point correlation function of quasar down to scales of $\lesssim 150$ kpc, and he proposed that this was due to the increase of quasar activity during merger events. This enhancement of quasar clustering, even if at scale smaller than those proposed by Djorgovski et al. (i.e., $\lesssim 50$ kpc), was confirmed by several authors from larger sample of pairs (e.g., Hennawi et al. 2006b, 2010; Myers et al. 2007a,b; Foreman et al. 2009; Shen et al. 2010; Kayo & Oguri 2012).

Additional evidences for enhanced small-scale clustering come from the mere existence of few systems with more than two physically associated quasars, which are expected to

4 The study of physical systems of multiple quasars

be even more elusive objects. So far only two quasar triplet are known QQQ J1432-0106 at $z = 2.08$ (Djorgovski et al. 2007) and QQQ J1519+0627 at $z = 1.51$ (Farina et al. 2012c, see also Chapter 6). At smaller projected separations and lower luminosities, Liu et al. (2011) recently discovered a triple AGN in the galaxy SDSS J1027+1749 at $z = 0.07$, and Schawinski et al. (2011) serendipitously observed three low mass ($< 10^7 M_{\odot}$) accreting black holes in a galaxy at $z = 1.35$.

The galactic environment of the quasars pairs is expected to be particularly rich. In fact quasars are expected to be associated with high peaks of the Gaussian fluctuations that inhabit preferentially in regions where rich clusters evolve (e.g., Efstathiou & Rees 1988), and the probability for merger to occur in dense region increase (e.g., Hopkins et al. 2008). Quasar pairs are thus expected to be signposts for high redshift clusters, for instance Boris et al. (2007) investigate the field of four wide separation quasar pairs at redshift $z \sim 1$ ($300 \text{ kpc} \lesssim \text{pd} \lesssim 1100 \text{ kpc}$, $300 \text{ km/s} \lesssim \Delta V_{\text{LOS}} \lesssim 1300 \text{ km/s}$) and detect evidences of large scale structure for three of them, while one seems to be an isolated system. Intriguingly, pairs are often found also in poor environment. Green et al. (2011) did not found any extended X-ray emission nor optical galaxy excess associated seven binary quasars with $\text{pd} < 30 \text{ kpc}$, $\Delta V_{\text{LOS}} < 800 \text{ km/s}$, and $z < 1$. At higher redshift ($z = 4.25$), Fukugita et al. (2004) investigate the environment of a pair of quasars separated by $\sim 225 \text{ kpc}$ and with a velocity difference of 860 km/s . They did not detect any significant enhancement in the galaxy density around the pair. It is noticeable that the first discovered spatially resolved binary quasar ($\text{pd} = 21 \text{ kpc}$, $\Delta V_{\text{LOS}} = 215 \text{ km/s}$) that clearly inhabits in an ongoing galaxy merger Green et al. (2010) does not show any evidence for the presence of a surrounding galaxy cluster.

In this scenario is therefore fundamental to study the dynamical properties and the richness of the environment of physical quasar systems. In Chapter 5 we present the study of the dynamical mass of six physical quasar pairs, for which the SDSS spectra allow to accurately determine the relative velocity difference from the study of [O III] forbidden emission lines. In Chapter 6 we present the discovery of QQQ J1519+0627 the second case know of quasar triplet. The study of these physical systems allow to place constraints on the dark mass present in this systems and on the role of the galactic environment in the simultaneous ignition of the quasar activity in two or more quasars.

5 Six physical pairs of quasars

In this Chapter we investigate six low redshift quasar pairs with projected distance $pd \leq 500$ kpc and systemic velocity difference along the line-of-sight $\Delta V_{\text{LOS}} \leq 500$ km/s. We accurately estimate their dynamical masses from narrow emission lines and, in order to derive limits on the dark mass present in these systems, we compare them with the stellar mass of the host-galaxies (Section 5.3) and with the richness of their galactic environment (Section 5.4). The results and the analysis reported here come principally from Farina et al. (2011).

5.1 Sample selection

We mine the Schneider et al. (2010, see Appendix A.1.1) catalogue of spectroscopically confirmed quasars to find pairs suitable for the study of the dynamic of the system. We select as *pairs* two quasars that have:

- i) projected separation $pd \leq 500$ kpc;
- ii) line-of-sight velocity difference based on the catalogue redshift $\Delta V_{\text{LOS}} \leq 500$ km/s;
- iii) redshift $z \leq 0.8$.

The latter constraint is imposed to have the [O III] narrow lines well inside the observational window explored by SDSS spectra (i.e., 3900 Å–9100 Å). These are indeed the strongest emission lines that allow to trace the systemic velocity of the quasars (see Section 5.2). The properties of the 6 pairs we found which satisfy the above criteria are listed in Table 5.1 and the SDSS spectra are shown in Figure 5.1.

Due to the large separation between the quasars one could argue that the redshift differences are related to the Hubble Flow and therefore measure the physical radial distances rather than the velocity differences. However, from a simple statistical estimate, we are able to exclude this possibility. In the Schneider et al. (2010) catalogue there are 35 pairs with $z \leq 0.8$, $pd \leq 4$ Mpc and a physical radial separation, calculated from the redshift, $rd \leq 4$ Mpc. Assuming that the 29 systems with $pd > 0.5$ Mpc are homogeneously distributed, we expect to find ~ 1 pair with separation $pd \leq 0.5$ Mpc, while 6 are found. This argument is further strengthened once we consider that 3 more pairs with $pd \leq 0.5$ Mpc were expected in absence of the fiber collision limit (see Blanton et al. 2003, and Appendix A.1.1). Henceforth, we will assume that redshift differences between the quasars in our pairs are dominated by their mutual velocities.

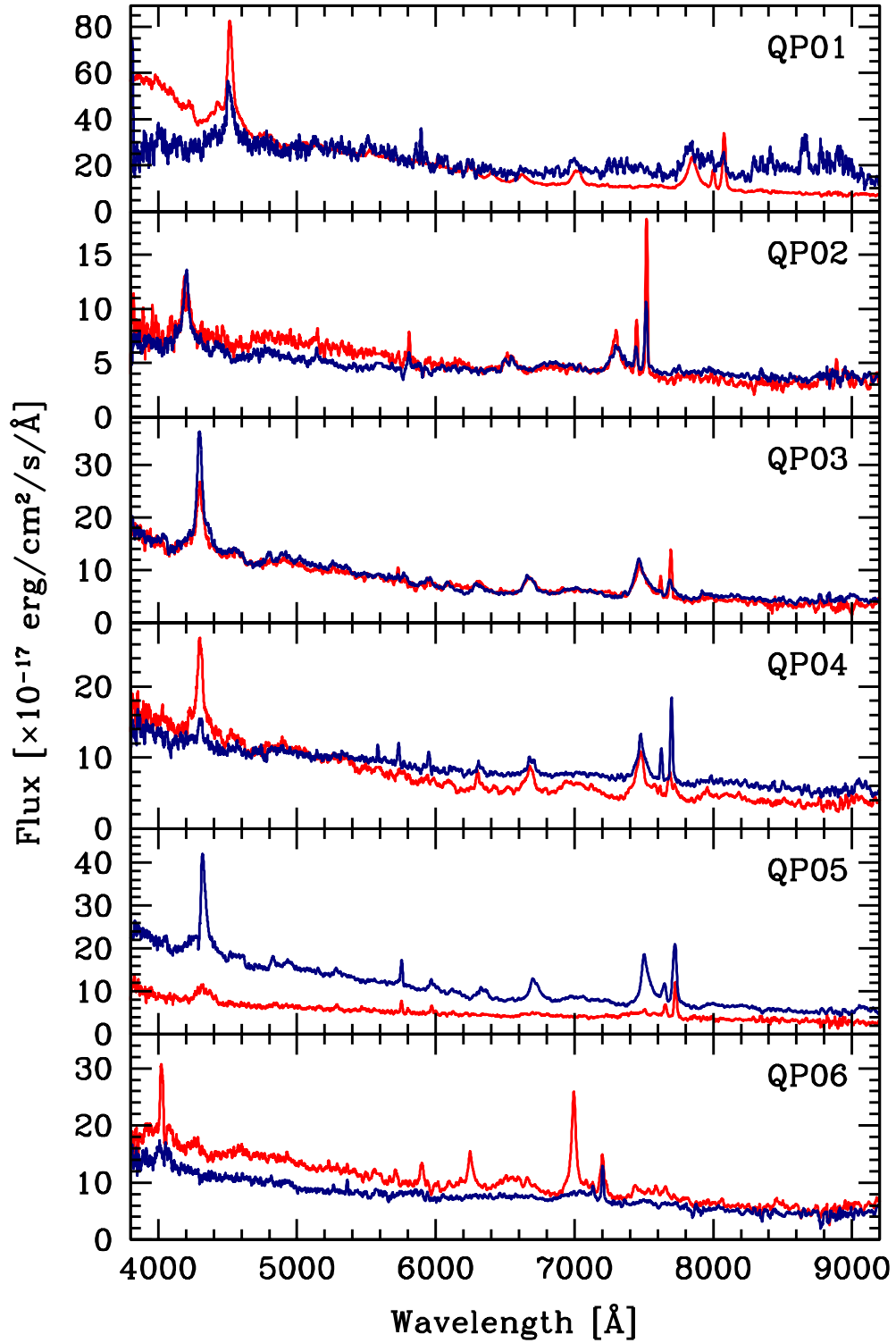


Figure 5.1: The SDSS spectra of the two quasars of each pair (background red line, foreground blue line). Data are smoothed with a 10 \AA boxcar filter. For the sake of comparison, the flux of the foreground quasars of QP01 is increased by a factor of 10.

5.2 Systemic velocity differences from [OIII] lines

Table 5.1: Properties of the selected quasar pairs. (01) our identification label of the quasars, right ascension (02) and declination (03) of the quasars, (04) catalogue redshift from Schneider et al. (2010), (05) absolute magnitude in V-band, angular (06) and proper (07) transverse separation, and (08) radial velocity difference derived from the catalogue redshifts.

ID	RA	DEC	z	M_V	$\Delta\theta$	pd	ΔV_{LOS}
(01)	[J2000] (02)	[J2000] (03)	(04)	[mag] (05)	[arcsec] (06)	[kpc] (07)	[km/s] (08)
QP01A	01:17:58.8	+00:20:21	0.6122	-22.38	44	300	149
QP01B	01:17:58.0	+00:21:04	0.6130	-24.65			
QP02A	07:47:59.7	+43:18:11	0.5010	-22.76	9	56	40
QP02B	07:47:59.0	+43:18:05	0.5012	-22.61			
QP03A	08:24:40.6	+23:57:10	0.5356	-23.19	15	94	176
QP03B	08:24:39.8	+23:57:20	0.5365	-23.19			
QP04A	08:45:41.5	+07:11:52	0.5363	-23.48	62	393	195
QP04B	08:45:41.1	+07:10:50	0.5373	-23.20			
QP05A	08:56:26.7	+51:11:18	0.5425	-22.81	22	139	175
QP05B	08:56:25.6	+51:11:37	0.5434	-23.59			
QP06A	12:49:03.3	+47:19:06	0.4375	-23.09	79	446	146
QP06B	12:48:56.6	+47:18:28	0.4382	-22.63			

5.2 Systemic velocity differences from [OIII] lines

The SDSS spectroscopic pipeline assigns a redshift to the spectra of each quasar by comparing the wavelengths of all the detected emission lines with the references rest-frame wavelengths taken from the composite template of Vanden Berk et al. (2001, see also Appendix A.1.1). This approach however prevents us to know the systemic redshift of the systems. It is well known that the redshifts of quasars derived from emission lines of various elements can differ by as much as 1000 km/s (e.g., Gaskell 1982; Tytler & Fan 1992; Bonning et al. 2007). Moreover broad emission lines often show asymmetric line profile (e.g., Shen & Loeb 2010) or/and strong absorption features (e.g., Weymann et al. 1991) that could invalidate the measure of their peak wavelength. The most reliable estimate of the systemic velocity of the quasars is thus obtained from the measurements of narrow forbidden lines, the most prominent of which are [O III] $_{\lambda 4949}$ and [O III] $_{\lambda 5007}$ (e.g., Nelson & Whittle 1996; Nelson 2000). In fact the narrow emission lines arise from gas predominantly orbitating in the potential well of the host galaxy, which could be different from that of the black hole (e.g., Merritt et al. 2006). Hewett & Wild (2010) compared the redshifts derived from [O III] emission lines and from the photospheric absorptions of the stars (i.e., the Ca II doublet at $\lambda = 3934.9 \text{ \AA}$ and $\lambda = 3969.6 \text{ \AA}$) in a sample of 825 quasars at redshift $z < 0.4$. They found that the [O III] line centroids are shifted by $45 \pm 5 \text{ km/s}$ to the blue with respect to the Ca II ones (see also, Boroson

2005). This offset has a little impact in our measurements, since we are interested in the relative difference between the two quasar redshifts.

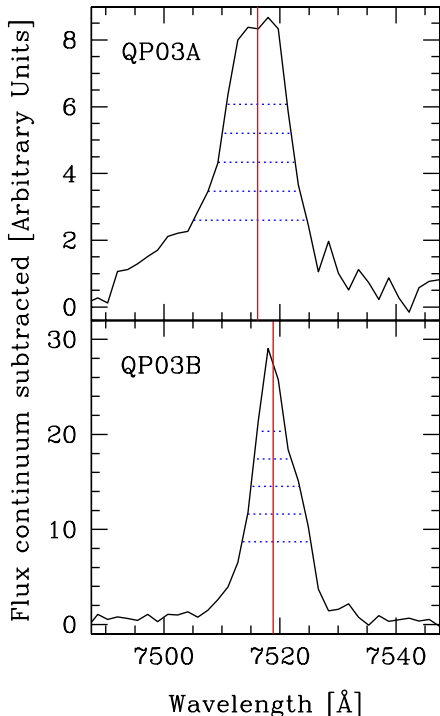


Figure 5.2: The normalised SDSS spectra of the two quasars of the pairs QP03 in the region around the emission line [O III] at $\lambda = 5007 \text{ \AA}$. The peak wavelength (red vertical lines) is the median value of the baricenter calculated considering only the flux above different thresholds (i.e., 30, 40, 50, 60, and 70%) of the line peak (blue dotted horizontal lines).

Under the hypothesis that all our pairs form bound systems, and thus that the measured velocity differences are due to the mutual interaction between the two quasars, we can infer the dynamical mass through the virial theorem:

$$M_{\text{vir}} = \frac{\Delta V^2 d}{G} \quad (5.1)$$

where ΔV is the relative velocity of the two components, d their separation, and G the gravitational constant. For circular orbits, it is possible to calculate the line-of-sight

The [O III] line centroids are evaluated from the variations of the baricenter position resulting from different flux thresholds (see Figure 5.2 for details). The peak position is given by the median of the individual measurement of the baricentre, and the corresponding uncertainty is given by their interquartile range. The redshifts and the radial velocity differences that result from these measurements are listed in Table 5.2.

5.3 The virial mass of quasar pairs

The probability that the six systems found are due to a simple chance superpositions is rather low. In fact, as first order test, we can estimate the number of quasar pairs expected in a random catalogue in which no correlations are present. A simple way to construct this catalogue is given by the redshift permutation method (e.g., Osmer 1981; Zhdanov & Surdej 2001). This consists in maintaining the positions of the quasars fixed, but to randomly permute the redshifts. The greatest advantage of this technique is that the geometry of the survey is automatically taken into account. However, even if most of the correlations between objects are destroyed, the angular correlation between quasars is preserved. Thus the result can be considered as an upper limit for the number of chance quasar pairs. In this random catalogue we expect to find ~ 0.4 pairs with $\Delta V_{\text{LOS}} \leq 500 \text{ km/s}$ and $\text{pd} \leq 500 \text{ kpc}$, while 6 are observed (see Figure 5.3), we thus assume that all the selected systems are physically associated.

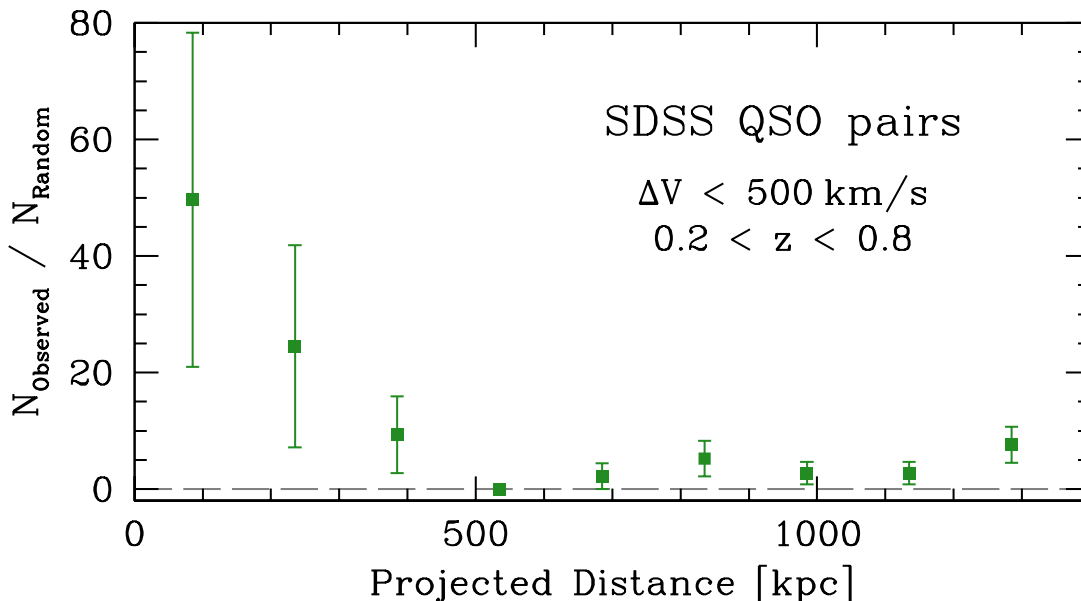


Figure 5.3: Ratio between the number of pairs at $0.2 < z < 0.8$ with $\Delta V_{\text{LOS}} < 500$ km/s present in the Schneider et al. (2010) quasar catalogue and those found in a random catalogue generated through the redshift permutation method. The poissonian uncertainties are shown. The increase of this ratio at separations $pd \lesssim 500$ kpc is apparent. Note that we do not correct for distortions in the redshift–space.

component of the relative velocity (ΔV_{LOS}) from the redshift difference (Δz). One has:

$$M_{\text{vir}} = C \left(\frac{c \Delta z}{1 + z} \right)^2 \frac{pd}{G} \quad (5.2)$$

where c is the speed of light, pd the proper transverse separation of the pair (see Table 5.1), and the factor C depends only on the inclination angle of the orbital plane (ι), and on the phase angle (ϕ). It is given by:

$$C^{-1} = (\sin \phi \sin \iota)^2 \times \sqrt{\sin^2 \phi + \cos^2 \phi \cos^2 \iota}. \quad (5.3)$$

The average value of C is $\langle C \rangle = 3.4$ and the minimum value is $C_{\text{min}} = 1$ (see Figure 5.4).

In Table 5.2 we list the minimum virial masses ($M_{\text{vir}}(\text{min})$), corresponding to $C = 1$) estimated for each pair of quasars, which represent the minimum masses of the systems to be bound. We note that the velocity difference measured for QP06 is consistent with 0 km/s. In this case we are probably observing the orbit of the pair nearly face on. It is of interest to compare these $M_{\text{vir}}(\text{min})$ with the stellar mass of the quasar host galaxies. Quasars are usually associated with massive, bulge dominated, galaxies (e.g., Disney et al. 1995; Dunlop et al. 2003; Floyd et al. 2004; Falomo et al. 2008; Kotilainen et al. 2009) with stellar masses that typically range from 0.3 to $1.3 \times 10^{12} M_{\odot}$ ¹

¹Estimated from quasars at $z < 1$.

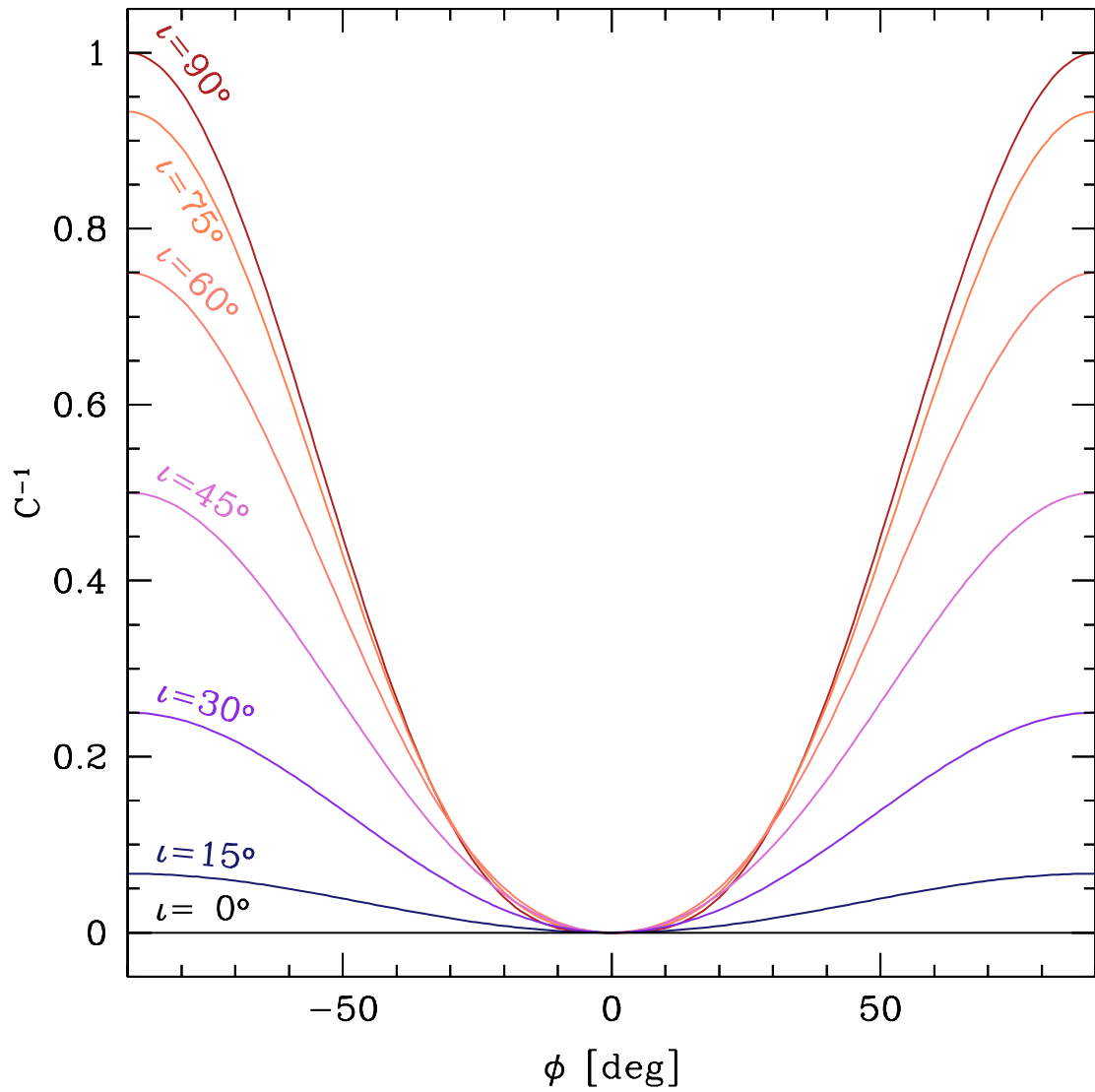


Figure 5.4: Factor C as a function of the phase angle (ϕ) for different values of the orbital plane inclination angle (i).

5.4 The galactic environment of quasar pairs

Table 5.2: Radial velocity difference and virial mass of the quasar pairs. (01) our identification label of the quasar pairs, (02, 03) redshifts measured from the [O III] narrow emission lines; (04) velocity difference from [O III]; (05) minimum virial mass compatible with the uncertainties of the measure of $\Delta V_{\text{LOS},n}$.

ID	$z_n(\text{A})$	$z_n(\text{B})$	$\Delta V_{\text{LOS},n}$ [km/s]	$M_{\text{vir}}(\text{min})$ [$10^{12} M_{\odot}$]
(01)	(02)	(03)	(04)	(05)
QP01	0.61142 ± 0.00078	0.61341 ± 0.00001	370 ± 171	2.8 – 20.4
QP02	0.50108 ± 0.00003	0.50174 ± 0.00001	132 ± 7	0.2 – 0.3
QP03	0.53527 ± 0.00009	0.53678 ± 0.00002	295 ± 21	1.6 – 2.2
QP04	0.53509 ± 0.00015	0.53754 ± 0.00002	478 ± 35	17.9 – 24.0
QP05	0.54322 ± 0.00003	0.54239 ± 0.00003	161 ± 9	0.7 – 0.9
QP06	0.43861 ± 0.00045	0.43859 ± 0.00001	4 ± 94	0.0 – 0.9

(see Decarli et al. 2010b,c, and references therein). For four quasar pairs (QP02, QP03, QP05, and QP06) the $M_{\text{vir}}(\text{min})$ is comparable with the typical masses of the host galaxies, while for the remaining two (QP01 and QP04) the minimum virial mass is substantially larger (see Table 5.2). If we consider the average value of C ($\langle C \rangle = 3.4$) instead of its minimum, then the above cases are further strengthened and also QP03 will exhibit a significant mass excess. It is noticeable that the median value of M_{vir} for our small sample ($6.5 \times 10^{12} M_{\odot}$) is consistent with the median mass of the dark matter host halos ($M_{\text{halo}} \sim 6 \times 10^{12} M_{\odot}$) estimated from the projected two-point correlation function by Myers et al. (2007a,b) (on the basis of ~ 300000 photometrically classified SDSS quasars) and by Richardson et al. (2012) (from ~ 48000 spectroscopically confirmed quasars).

It is possible that our pairs belong to a group or a cluster of galaxies and thus that the measured velocity differences depend on the overall mass distribution. In the next Section we investigate this possibility.

5.4 The galactic environment of quasar pairs

We here compare the number density of galaxies observed in SDSS i-band images with what expected if a cluster with projected velocity dispersion $\sigma_p \equiv \Delta V_{\text{LOS},n}$ (see below) were associated to our quasar pairs. This estimate is largely based on the relations between the galaxy distribution and virial mass presented by Girardi et al. (1995, 1998a,b), who studied the optical properties of 170 galaxy clusters at $z < 0.15$.

5.4.1 SDSS images analysis

In order to detect possible overdensities of galaxies we explore SDSS i-band images (sampling roughly to the rest frame V-band at redshift $z = 0.5$) in a area of $\sim 30 \text{ Mpc}^2$ around each quasar pairs. The magnitude limit in this band is 21.3 mag (York et al. 2000), thus it allows us to reach M^*+1 , where $M^* = -20.5$ is the characteristic luminosity

5 Six physical pairs of quasars

Table 5.3: Environment of quasar pairs. (01) our identification label of the quasar pairs, (02) density of galaxies in the region between 2 Mpc and 4 Mpc from the pairs, (03) number of galaxies detected in the inner 500 kpc, and (04) its corresponding density, and (05) minimum mass-to-light ratio that could have a galaxy cluster detected on SDSS i-band images (3σ over the background). The quoted uncertainties represent 1σ statistical fluctuations.

ID	n(bkg) [arcmin ⁻²]	N(<500 kpc)	n(<500 kpc) [arcmin ⁻²]	Υ
(01)	(02)	(03)	(04)	(05)
QP01	1.2±0.2	5	1.4±0.6	$\gtrsim 50$
QP02	1.4±0.1	8	1.4±0.5	$\gtrsim 10$
QP03	2.1±0.1	26	4.7±0.9	$\gtrsim 5$
QP04	1.9±0.1	15	2.7±0.7	$\gtrsim 150$
QP05	1.8±0.2	5	0.9±0.4	$\gtrsim 10$
QP06	1.9±0.2	12	2.3±0.7	...

of the galaxies at $z = 0.5$ (Wolf et al. 2003). The galaxy search is performed using **SExtractor** (Bertin & Arnouts 1996), assuming a detection threshold of 3 times the RMS of the sky background flux and masking region polluted by the presence of bright stars. The seeing of SDSS images range from $0.9''$ to $1.0''$ that at $z = 0.5$ correspond to a projected scale of ~ 6 kpc. A source is classified as *galaxy* if the STARCLASS parameter is lower than 0.2. The number counts of stars and galaxies we find are consistent with the study performed up to $I = 24$ mag by Postman et al. (1998) on a region of $4^\circ \times 4^\circ$, and with the prediction of the **TRILEGAL** package² (Girardi et al. 2005). In order to highlight a possible overdensity around the quasar pairs, we compute the number density of galaxies in annuli of 500 kpc radius, starting from the centre of each pair. We then compare the galaxy density in the first 500 kpc with that in the region between 2 Mpc and 4 Mpc, assumed as background. These values are reported in Table 5.3. Only for QP03 we measure a significant overdensity of galaxies in the central bin, in the other cases there are no evidences for density of galaxies that exceeds the background by more than 3σ .

5.4.2 Expected mass of the clusters

We now calculate the expected number density of galaxies associated to a cluster with projected velocity dispersion σ_p .

As a first step, the virial mass of a cluster ($M_{c,vir}$) is estimated as a function of σ_p . Assuming that the galaxy distribution traces the cluster potential well (e.g., Limber & Mathews 1960), $M_{c,vir}$ depends on the global velocity dispersion (σ) and on the positions of the galaxies:

$$M_{c,vir} = \frac{\sigma^2 R_{vir}}{G} \quad (5.4)$$

²<http://stev.oapd.inaf.it/cgi-bin/trilegal.1.4>

5.4 The galactic environment of quasar pairs

where the virial radius (R_{vir}) is given by the spatial average of the distances between any pair of galaxies (r_{ij}): $R_{\text{vir}}^{-1} = \langle r_{ij}^{-1} \rangle$. σ and R_{vir} could be translated into observable (projected) quantities (labelled with $_p$) assuming a spherical symmetry: $\sigma^2 = 3\sigma_p^2$ (e.g., The & White 1986; Merritt 1988), and $R_{\text{vir}} = \frac{\pi}{2}R_{p,\text{vir}}$ (e.g., Limber & Mathews 1960; Heisler et al. 1985). Thus Equation 5.4 becomes:

$$M_{c,\text{vir}} = \frac{3\pi}{2} \frac{\sigma_p^2 R_{p,\text{vir}}}{G}. \quad (5.5)$$

In a $\Omega_0 = 1$ Universe, considering a non-linear collapse, we can calculate the present density of a spherical virialised fluctuation (ρ_{vir}) in terms of the cosmological density (ρ_0 , see e.g., Peebles 1980):

$$\rho_{\text{vir}} = 18\pi^2 \rho_0 = 18\pi^2 \frac{3H_0^2}{8\pi G}. \quad (5.6)$$

If we consider that $M_{\text{vir}} = \frac{4}{3}\pi R_{\text{vir}}^3 \rho_{\text{vir}}$ from Equations 5.5 and 5.6 it is possible to obtain a linear relation between the projected virial radius and the projected velocity dispersion:

$$R_{p,\text{vir}} = a \sigma_p \quad (5.7)$$

where $a \sim 0.002 \text{ Mpc/km s}^{-1}$ (see also Girardi et al. 1998b). Therefore we are now able to calculate the virial mass of a galaxy cluster from the projected velocity dispersion:

$$M_{c,\text{vir}} = \frac{3\pi a}{2G} \sigma_p^3 \quad (5.8)$$

and, assuming a mass-to-light ratio Υ , its optical luminosity within the virial radius L_{tot} .

We assume that the galaxies of the cluster follow the Schechter luminosity function (Press & Schechter 1974; Schechter 1976):

$$\phi(L)dL = \left(\frac{\phi^*}{L^*}\right) \left(\frac{L}{L^*}\right)^\alpha e^{-\frac{L}{L^*}} dL \quad (5.9)$$

with parameters (i.e., the characteristic galaxy luminosity L^* and the faint-end slope of the function α) given by Wolf et al. (2003). The normalisation (ϕ^*) is estimated integrating ϕ over all the luminosities and comparing the result with L_{tot} :

$$l_{\text{tot}} = \int_0^\infty L' \phi(L') dL' \equiv \frac{L_{\text{tot}}}{\frac{4}{3}\pi R_{\text{vir}}^3}. \quad (5.10)$$

The number of galaxies brighter than the SDSS i-band magnitude limit at the redshift of the pair (L_{lim}) is:

$$N(L > L_{\text{lim}}) = \frac{4}{3}\pi R_{\text{vir}}^3 \int_{L_{\text{lim}}}^\infty \phi(L') dL' \quad (5.11)$$

where elliptical galaxy template by Mannucci et al. (2001) is used in order to compute k - and filter-corrections.

The distribution of the galaxies in a cluster is well represented by a King-like profile:

$$\rho_k(r) = \frac{\rho_{k0}}{\left[1 + \left(\frac{r}{R_c}\right)^2\right]^{\frac{3b}{2}}} \quad (5.12)$$

$$\Sigma_k(r) = \frac{\Sigma_{k0}}{\left[1 + \left(\frac{r}{R_c}\right)^2\right]^a} \quad (5.13)$$

where: $\rho_k(r)$ is the volume density of the galaxies with normalisation ρ_{k0} ; R_c is the core radius; $\Sigma_k(r)$ is the surface density of galaxies with normalisation $\Sigma_{k0} = 2\rho_{k0}R_c$; $b = \frac{2a+1}{3}$ and a are the parameters which describe the galaxy distribution in the external regions. In (Girardi et al. 1998b), the authors fit a King-like profile on 92 nearby galaxy clusters and found that typically $a \sim 0.70$ ($b \sim 0.8$) and that $R_c = 0.05 R_{\text{vir}}$. The value of ρ_{k0} (and thus of Σ_{k0}) could be fixed integrating $\rho_k(r)$ within the virial radius and forcing the results to be equal to $N(L > L_{\text{lim}})$.

In conclusion, we are now able to estimate the projected number density of galaxies associated to a cluster (Σ_k) given only the velocity dispersion (σ_p) and the mass-to-light ratio (Υ).

5.4.3 Limits on the mass-to-light ratio

In all cases but one, we do not find in SDSS images indications for overdensities of galaxies larger than 3 times the variation of the background. In Figure 5.5 we compare the expected density of galaxies with that observed in SDSS images. To explain their velocity differences, the pairs require mass-to-light ratio $\Upsilon > 10\text{--}150$ (see Table 5.3). These values are comparable with those reported in various studies on dynamical properties of galaxy clusters (e.g., Popesso et al. 2005, and references therein).

5.5 Conclusions

In this Chapter we have presented an accurate measure of the dynamical mass of 6 SDSS physical pairs of quasars for which the systemic velocity differences could be inferred from the [O III] narrow emission lines. In at least two cases this mass exceeds by a factor ~ 10 the stellar mass expected from the host galaxies. A possible explanation of this surplus is that the quasars are surrounded by dark matter haloes with masses similar to those inferred from larger sample of quasars by Myers et al. (2007a,b); Richardson et al. (2012). Alternatively, the quasar pairs could be harboured by cluster or group of galaxies that could give rise to the observed velocity differences. An analysis of SDSS i-band images shows that only one pair is associated to a significant overdensity of galaxies. For the remaining systems we are able to derive only lower limits on the mass-to-light ratio of the possible clusters ($\Upsilon \gtrsim 10\text{--}50$). It is worth noting that the strong lower limit imposed to QP04 ($\Upsilon \gtrsim 150$) suggests that the dynamical mass of the systems is most probably due to the mutual interaction between the two quasars rather than to the presence of a clusters.

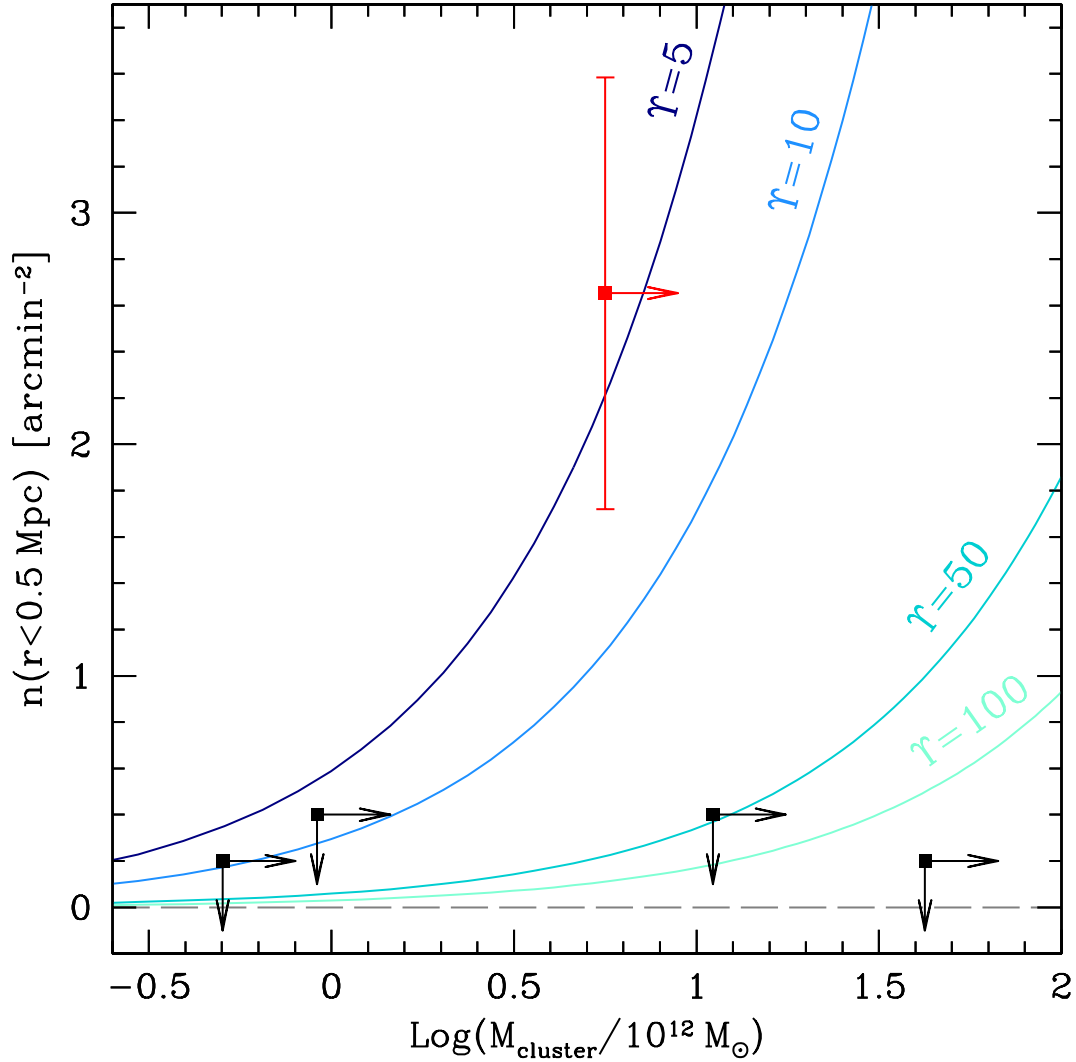


Figure 5.5: Expected central density of galaxies in SDSS *i*-band images as a function of the mass of the clusters for various value of the mass-to-light ratio (filled lines). Black square points are the quasar pairs for which no significant evidences of an overdensity of galaxies are present. For these systems we show 2σ upper limits. The red square points to QP03, for which SDSS images highlight a significant overdensity of galaxies in the first 500 kpc from the quasar pair.

5 *Six physical pairs of quasars*

In order to strengthen the evidence of the mass excess a larger sample of quasar pair is mandatory. One can explore the lists of already known quasar pairs (e.g., Hennawi et al. 2006b, 2010; Myers et al. 2008) or search for new pairs in the last SDSS spectroscopic catalogue (Pâris et al. 2012). Most of this systems are at redshift $z \gtrsim 0.8$ where the [O III] emission lines are shifted in the near infrared bands (for instance at $z = 1$ the [O III] doublet is at $\lambda \sim 10000 \text{ \AA}$). Excellent instrument capabilities are thus required to perform these studies.

6 One (new) physical triplet of quasars

In this Chapter we present our discovery of a new triplet of quasars (Farina et al. 2012c, see Appendix C). We give evidences that the three quasars form a physical system in Section 6.3 and we investigate their galactic environment with optical and near infrared broad band images in Section 6.4. Finally, we comment on the possible origin of this system in Section 6.5.

6.1 Sample selection

Quasar multiplets observed at close projected separations are rare (e.g., Hennawi et al. 2006b). Large spectroscopic surveys often fail to detect close quasar systems due to the fiber collision limits. For example in SDSS it is not possible to obtain the spectrum for both sources in a pair with separation $< 55''$ within a single plate (see Blanton et al. 2003, and Appendix A). To overcome this limitation, we have started a programme to search for close quasar triplets taking advantage of the large photometric sample of Richards et al. (2009, see Appendix A.1.2). Three quasars are selected as a candidate triplet if:

- i) at least one of them has spectroscopic redshift;
- ii) the other two reside within 500 kpc from it;
- iii) they have coincident (within the uncertainties) photometric redshift (estimated with the procedure suggested by Weinstein et al. 2004).

These criteria allow us to select a sample of 13 *bona fide* quasar triplet candidates, the observations of which is ongoing at the twin 6.5 m Magellan telescopes at Las Campanas Observatory (Chile) and at the 3.5 m telescope of the German–Spanish Astronomical Center at Calar Alto (Spain).

We here present our discovery of two quasars within $\sim 25''$ from the spectroscopic QSO SDSS J151947.3+062753 (hereafter QQQ1519A, Schneider et al. 2010) and located at a similar redshift ($\Delta V_{\text{LOS}} \lesssim 1000$ km/s). In Table 6.1 we list the properties of the quasars belonging to our newly discovered triplet, labelled QQQ J1519+0627, and, for comparison, of the components of the only other triple quasar system known so far: QQQ J1432-0106 (Djorgovski et al. 2007). In the following Section we describe the procedures and the results of the analysis of the spectroscopic and photometric data collected on QQQ J1519+0627.

Table 6.1: Properties of the triple quasar systems known to date. For each quasar, we list: (01) identification label, (02,03) position, (04) redshift, (05,06,07) magnitude observed in the z, J, and H bands, (08,09) angular and projected separation at the redshift of the system, and (10) line-of-sight velocity difference (ΔV_{LOS}). Data for QQQ J1432-0106 are from Djorgovski et al. (2007) and the SDSS database.

ID	RA	DEC	redshift	z	J	H	$\Delta\theta$	pd	ΔV_{LOS}
(01)	[J2000] (02)	[J2000] (03)	(04)	[mag] (05)	[mag] (06)	[mag] (07)	[arcsec] (08)	[kpc] (09)	[km/s] (10)
QQQ J1519+0627:									
– QQQ1519A	15:19:47.3	+06:27:53	1.504±0.001	18.86	18.81	18.55	$\Delta\theta(\text{A-B})=23.5$	pd(A-B)=198	$\Delta V(\text{A-B})=1100$
– QQQ1519B	15:19:45.7	+06:27:52	1.513±0.003	21.23	20.97	20.25	$\Delta\theta(\text{B-C})= 3.7$	pd(B-C)= 31	$\Delta V(\text{B-C})= 850$
– QQQ1519C	15:19:45.9	+06:27:49	1.506±0.003	21.20	20.69	20.13	$\Delta\theta(\text{C-A})=21.1$	pd(C-A)=178	$\Delta V(\text{C-A})= 250$
QQQ J1432-0106:									
– QQQ1432A	14:32:29.2	–01:06:16	2.076	17.15	16.32	15.88	$\Delta\theta(\text{A-B})= 5.1$	pd(A-B)= 42	...
– QQQ1432B	14:32:28.9	–01:06:13	2.076	20.42	20.00	19.27	$\Delta\theta(\text{B-C})= 3.6$	pd(B-C)= 30	...
– QQQ1432C	14:32:29.2	–01:06:12	~2.08	...	21.66	21.17	$\Delta\theta(\text{C-A})= 4.3$	pd(C-A)= 36	...

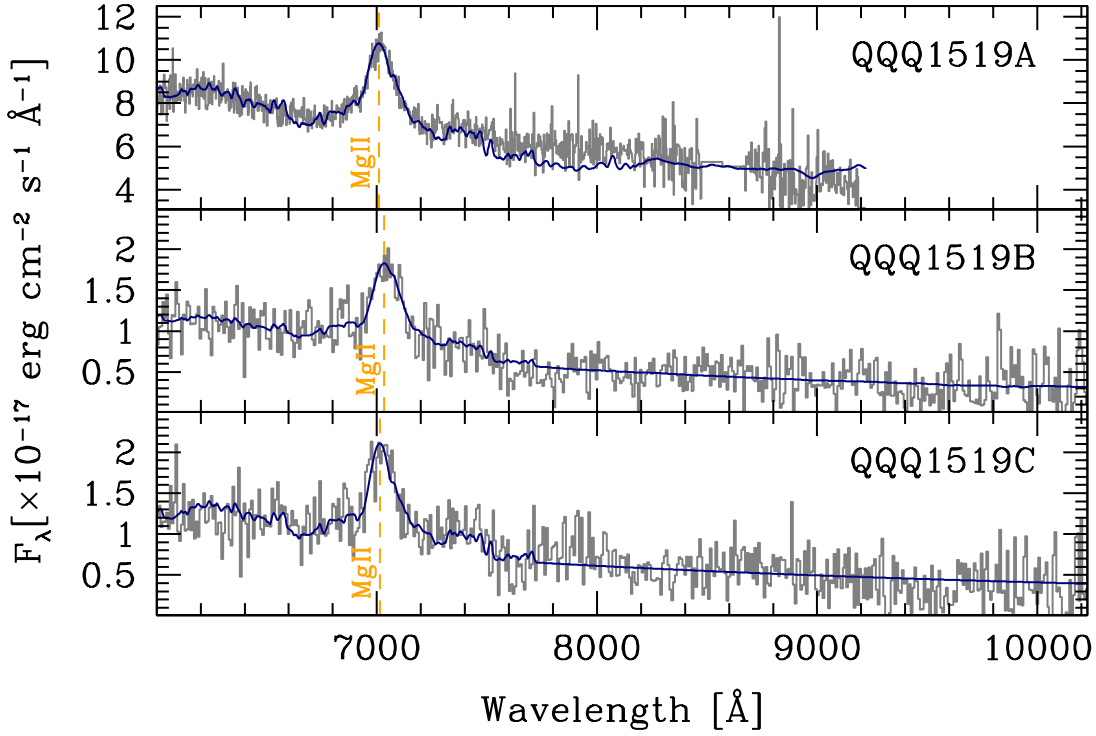


Figure 6.1: Spectra of the three quasars of QQQ J1519+0627 (grey), binned by 2 pixel. The results of the fitting procedure on Mg II and Fe II lines are plotted in blue (see text for details). The positions of the Mg II peaks are marked with orange dashed lines.

6.2 Observations and data reduction

6.2.1 Long-slit spectroscopy

Spectra of QQQ1519B and QQQ1519C were gathered with the ESO Faint Object Spectrograph and Camera 2 (EFOSC2; Buzzoni et al. 1984) mounted on the New Technology Telescope (NTT) in La Silla (Chile). We performed long-slit spectroscopy on February 17, 2012, using a slit width of 1'' and setting the Position Angle to -49.7° , so that both quasars were observed simultaneously. Grism #16 was used in order to continuously cover the wavelength range 6015 Å–10320 Å with a spectral resolution $\lambda/\Delta\lambda \sim 550$ as measured on the night sky emission lines. Five frames of 900 s were acquired, for a total exposure time of 75 min on source. Standard IRAF tools were used in the data reduction (bias subtraction, flat-fielding, wavelength and flux calibration, spectra extraction, see Section 2.2). As flux calibrator we observed the spectrophotometric standard star Hiltner 600. Typical residuals in the wavelength calibration are ~ 1 Å.

For the fit of the quasar spectra we followed the same procedure we have successfully applied for the study of projected quasar pairs and that we have introduced in Section 2.2. The two NTT spectra and the one from SDSS are shown in Figure 6.1. A bright emission line, identified as Mg II, is observed in all the spectra at ~ 7000 Å. The line identification is supported by the lack of other bright emission lines in the observed spectra, and by a

6 One (new) physical triplet of quasars

tentative detection of the iron multiplets around the line (see our fit results in Figure 6.1). These pieces of evidence firmly pin down the redshifts of the quasars to 1.504 ± 0.001 , 1.513 ± 0.003 and 1.506 ± 0.003 for A, B and C respectively, where uncertainties are given by the positional accuracy of the Mg II line centroids.

6.2.2 Broad band photometry

We gathered NIR broad band images of the QQQ J1519+0627 field using Omega2000 (Kovács et al. 2004) at the 3.5 m telescope in Calar Alto (Spain). Observations were performed on March 8, 2012 as Director Discretionary Time. We observed a region of $15' \times 15'$ around the system in z, J, and H bands, i.e., sampling the rest-frame u, g, and r at $z = 1.51$. We adapted usual jittering observing strategies in order to effectively subtract night sky emission. We collected 180×15 s frames in z (total integration time: 45 min), 18×100 s frames in J (total integration time: 30 min), and 36×50 s frames in H (total integration time: 30 min). Images were processed with our package of NIR image processing based on standard IRAF tasks. We compute the astrometric solution using the `astrometry.net` software¹ (Lang et al. 2010). Photometric calibration is achieved by comparing the photometry of field stars observed in our images with the fluxes reported in the SDSS (z-band) and 2MASS (J- and H-band) catalogues, using the following filter transformations:

$$z_{\Omega 2k} = z_{\text{SDSS}} - 0.05 (i - z)_{\text{SDSS}} \quad (6.1)$$

$$J_{\Omega 2k} = J_{2\text{MASS,AB}} + 0.11 (J - H)_{2\text{MASS,AB}} \quad (6.2)$$

$$H_{\Omega 2k} = H_{2\text{MASS,AB}} - 0.02 (J - H)_{2\text{MASS,AB}} \quad (6.3)$$

Equations 6.1–6.3 are derived by computing the spectral magnitudes of template O- to M-type stars.

The seeing during the observations was $2''$ (as measured on the final images), and the 5σ limit magnitudes (computed from the rms of sky counts over a seeing area) are 23.90, 23.38 and 22.25 in z, J and H respectively. We use `SExtractor` (Bertin & Arnouts 1996) in order to identify and catalogue the sources in our images. Within the limit fluxes of our observations, we are able to study the environment of the quasar system down to $M^*(z) + 1$, where $M^*(z)$ is the rest-frame B-band characteristic luminosity of galaxies at redshift z as derived from the fit of the galaxy luminosity function (Ilbert et al. 2005). Due to limit imposed by the seeing, we can not use the morphological information to distangle between Galactic and extra-Galactic objects, we thus rely upon different colour-colour diagrams, also including sources from the SDSS photometric database (see Figure 6.2). We classified a source as *star* if it is not resolved (i.e., FWHM \lesssim seeing in all the considered images), and it lies within the locus of main sequence stars estimated through the prediction of the `Trilegal` software (Girardi et al. 2005), and from the distribution of the SDSS spectroscopically confirmed stars detected also in

¹<http://astrometry.net/>

2MASS (Skrutskie et al. 2006). Our colours cuts are summarised here:

$$\begin{cases} -0.58 + 0.61(u - g) < (g - r) < 0.06 + 0.61(u - g) \\ -0.32 + 0.86(z - J) < (J - H) < 0.05 + 0.86(z - J) & \text{if } (z - J) \leq 0.3 \\ -0.11 + 0.04(z - J) < (J - H) < 0.29 + 0.04(z - J) & \text{if } (z - J) > 0.3 \end{cases} \quad (6.4)$$

Note that these cuts are a simplified version of those adopted by Richards et al. (2002) on the SDSS photometric database. We also check the consistency of the sources not classified as stars with the reference colours of Elliptical, Sc galaxies and quasars obtained from the templates of Mannucci et al. (2001) and of Francis et al. (1991). In summary in the $15' \times 15'$ region explored we detect 2048 sources, 807 of which are classified as star on the basis of their colours. This yields a number density of ~ 3.5 stars per arcmin² that roughly correspond to the prediction of the *Trilegal* software in this region of the sky (~ 3.1 arcmin⁻²). The average surface density of extragalactic sources is 3.7 ± 0.2 arcmin⁻², that is consistent (within the uncertainties) with the 4.0 ± 0.2 arcmin⁻² observed in the Great Observatories Origins Deep Survey (GOODS, Giavalisco et al. 2004) once we consider our z-band sensitivity limits.

6.3 The origin of the triplet

In this Section we investigate possible origin of QQQ J1519+0627. In particular we test if the three quasars are indeed a multiple lensed image of the same object and if this system could be due to a simple chance superposition.

6.3.1 Gravitational lens

We note that small differences are reported in the colours and in the spectra of the three quasars (e.g., the Mg II lines peak at slightly different redshifts). This already disfavour the lensing scenario. However, due to the intrinsic similarity of quasar spectra (e.g., Kochanek et al. 1999; Mortlock et al. 1999) and to the limited signal-to-noise ratio of the NTT and SDSS data, we will focus our analysis mostly on the images. We test the lens hypothesis for QQQ J1519+0627 in two possible configurations: in case (i) QQQ1519B and QQQ1519C are images of the same, gravitationally lensed quasar while QQQ1519A is a different quasar at similar redshift; while in case (ii) we consider that also QQQ1519A is an image of the same quasar.

Case (i)

In this case we model the potential well of the lensing object with a singular isothermal sphere (SIS). Multiple images of similar brightness are obtained only along the Einstein ring, the radius of which is parametrised as θ_E (e.g., Narayan & Schneider 1990; Schneider et al. 2006; Chierigato et al. 2007):

$$\theta_E = 4\pi \left(\frac{\sigma}{c}\right)^2 \frac{D_{LS}}{D_S} \quad (6.5)$$

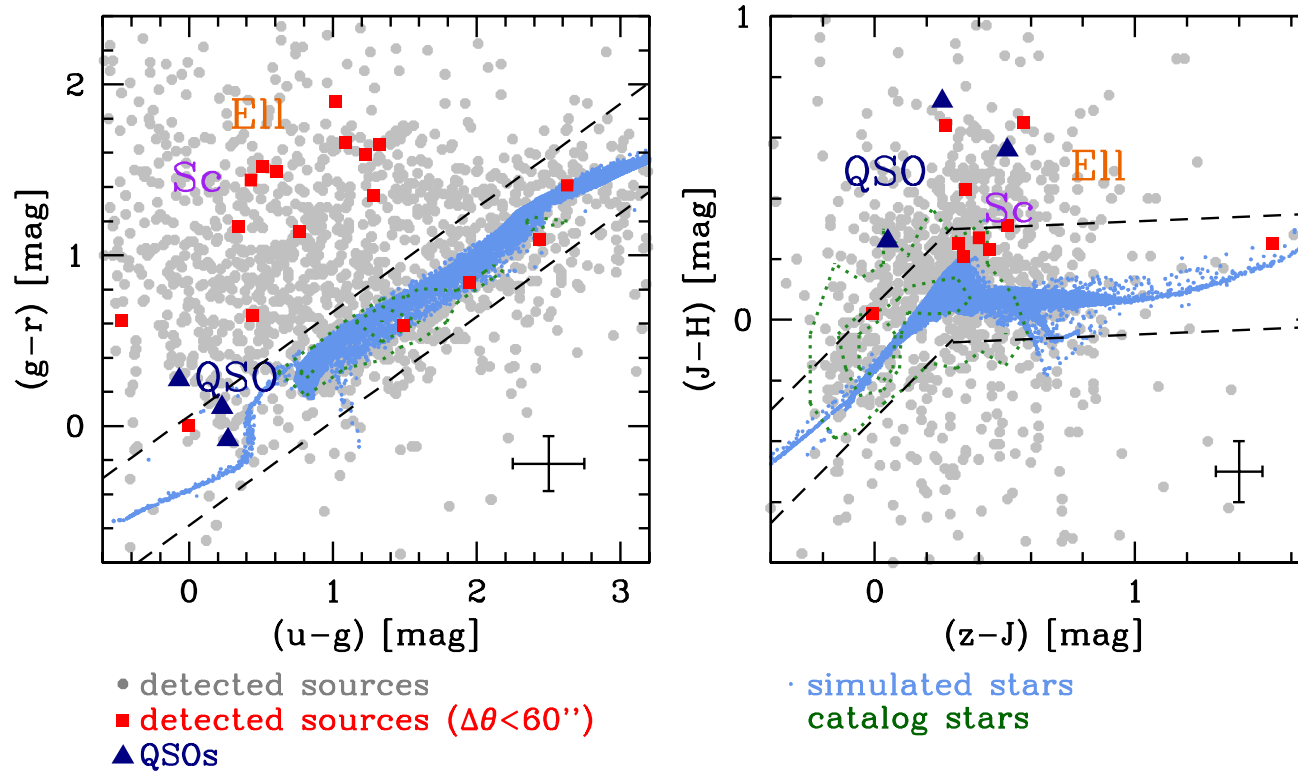


Figure 6.2: Colour-colour diagrams of the sources detected in the explored images (grey points). Objects within $60''$ from the QQQ J1519+0627 baricenter are highlighted in red. The blue triangles indicate the colours of the three quasars of the system. Note that the number of detected sources changes, according to the different depth of each band. For comparison we show the expected loci of Ellipticals and Sc galaxies at $z = 1$ and of quasars at $z = 1.5$ from the template of Mannucci et al. (2001) and Francis et al. (1991). The light blue points are the star colours simulated with the `Trilegal` software (Girardi et al. 2005), and dark green contours indicate the distribution of the spectroscopically confirmed stars detected in the SDSS and 2MASS in a region of $5^\circ \times 5^\circ$ around the triplet, and in the GOODS survey (Giavalisco et al. 2004). Black dashed lines show the colour cuts we imposed to separate stars and extragalactic objects (see text for details). The crosses in the bottom-right of the figures represent typical error bars on the colours.

Here σ is the velocity dispersion of the SIS, c is the speed of light, D_{LS} and D_S are the angular diameter distances between the source and the lens, and between the source and the observer, respectively. The minimum value of θ_E allowed in this system corresponds to half of the separation in the sky between QQQ1519B and C, i.e., $1''.85$. This implies that, for a given redshift of the lens, we can infer a lower limit for σ . If we adopt the working assumption that $\sigma = \sigma_*$ (the velocity dispersion of stars in the galaxy), we can use the Faber–Jackson relation (Faber & Jackson 1976) to convert the lower limit on σ into a luminosity limit for the lens galaxy. We use the updated version of the Faber–Jackson relation reported by Nigoche-Netro et al. (2010),

$$\log \frac{\sigma_*}{\text{km s}^{-1}} = (-1.208 \pm 0.205) - (0.157 \pm 0.009) M_r \quad (6.6)$$

where M_r is the rest–frame r–band absolute magnitude. We convert the observed z–band into M_r using the filter and k –corrections computed basing on the elliptical galaxy template by Mannucci et al. (2001). Figure 6.3 shows that a galaxy brighter than $z=19.6$ at redshift $z \sim 1.2$ is necessary to explain the observed geometry of the system in terms of strong gravitational lensing. The presence of such a galaxy is ruled out by our Omega2000 images (see Figure 6.4).

Case (ii)

This case is more extreme since wide separation lens systems are rare. In their search for lensed quasars with angular separation less than $\Delta\theta \lesssim 20''$, Inada et al. (2008) find in the SDSS only 3 out of 22 systems with $\Delta\theta > 3''$. Hennawi et al. (2007) estimated that in the SDSS quasar sample there should be only a few systems ($\lesssim 4$) multiply lensed by galaxy clusters with separations $> 20''$. Moreover, triple imaged quasars are not commonly observed (to our knowledge the only case is the triple radio source MG2016+112 presented by Lawrence et al. 1984).

The two largest separation quasar lenses known so far, SDSS J1029+2623 ($\Delta\theta = 22''.5$, $z = 2.197$ Inada et al. 2006) and SDSS J1004+4112 ($\Delta\theta = 14''.6$, $z = 1.734$ Inada et al. 2003), have separation similar to the ones reported here. In both these cases massive galaxy clusters act as lens (Inada et al. 2006; Oguri et al. 2004). As a zeroth order test, we estimate the velocity dispersion required to explain the separation of the images assuming again a SIS profile for the lens. As in case (i) we consider a limit for the Einstein radius $\theta_E \sim 10''$ that corresponds to $\sigma \sim 600$ km/s at $z \sim 0$ and $\sigma \sim 1200$ km/s at $z \sim 1$. In our image the presence of such clusters should be apparent, but in fact the surface density of galaxies within $60''$ from QQQ J1519+0627 (in z–band $4.1 \pm 1.1 \text{ arcmin}^{-2}$) is consistent with those detected in the whole frame ($3.7 \pm 0.2 \text{ arcmin}^{-2}$, see Section 6.2 and Figure 6.4. For instance, we consider the case that in our field was present XMMU J100750.5+125818: a galaxy cluster located at redshift $z \sim 1.08$ with a line–of–sight velocity dispersion of ~ 600 km/s (Schwope et al. 2010). If the cluster was centred on QQQ J1519+0627 in the first $60''$ there should be at least 10 galaxies in excess to the background. This is in contrast to what observed in the z–band where we detect only 12 galaxies instead of 22. We note that this estimate is conservative since we considered as reference only the (few) spectroscopically confirmed cluster members of XMMU J100750.5+125818, while the cluster should be more popu-

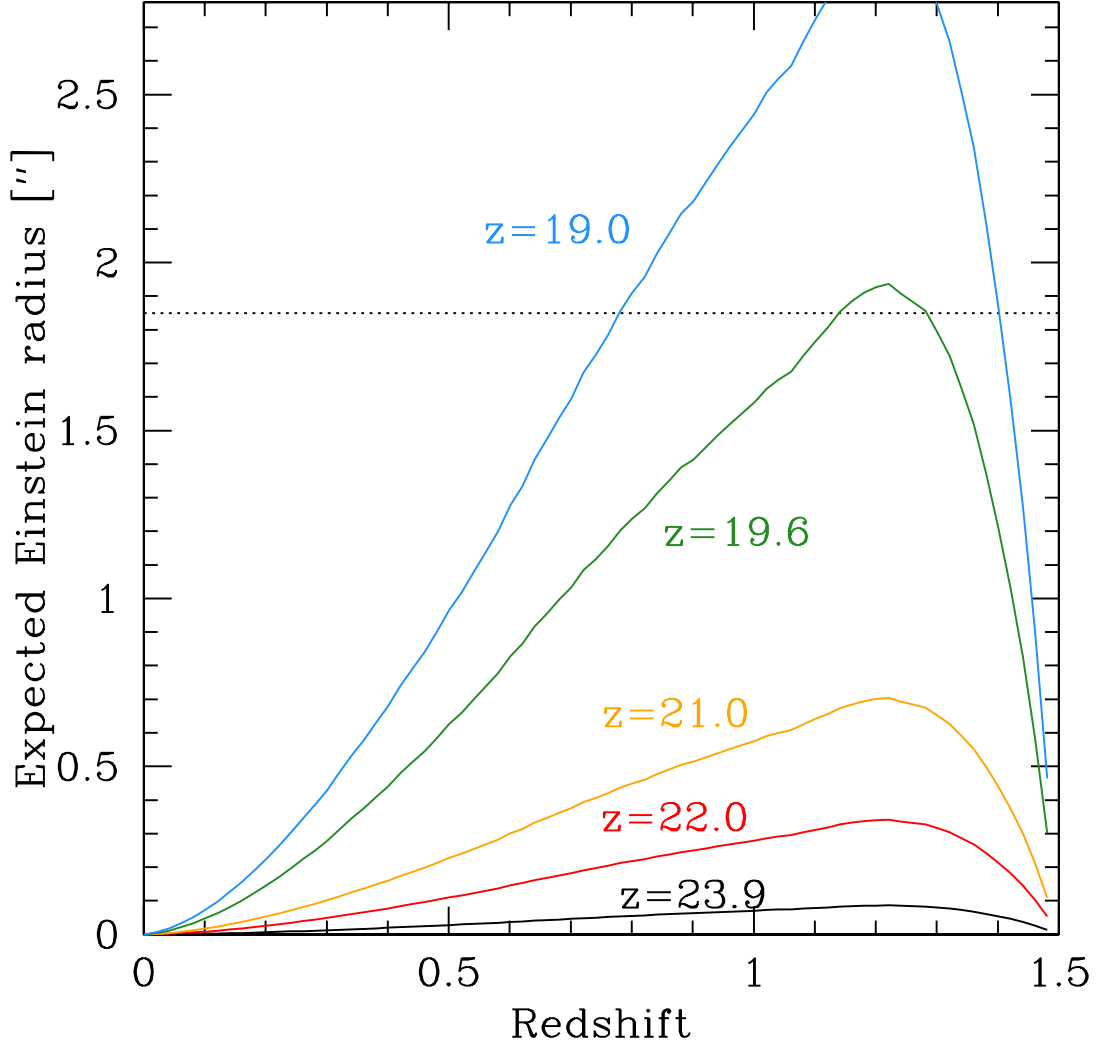


Figure 6.3: Expected Einstein ring radius for a lensing galaxy with various (observed) z -band magnitudes, as a function of redshift. The elliptical galaxy template by Mannucci et al. (2001) is used in order to compute k - and filter-corrections. We assume that the potential well of the lensing galaxy is well described by a SIS model with $\sigma = \sigma_*$, where σ_* is the stellar velocity dispersion as set by the Faber–Jackson relation (see text for details). The horizontal line shows the half-separation between QQQ1519A and B. No galaxy brighter than $z \sim 19.6$ is observed close to the two quasars, despite the depth of our images. This rules out the strong-lens scenario for these two quasars.

lated.

From the analysis of photometric data, we thus conclude that QQQ J1519+0627 is not a case of gravitational lens.

6.3.2 Chance superposition

QQQ J1519+0627 is the second triplet of quasars at similar redshift known, after QQQ J1432-0106 (Djorgovski et al. 2007). Here we estimate the expected number of quasar triplets in our sample that are originated by chance superposition of otherwise (physically) disconnected quasars. We start from the samples of spectroscopically confirmed quasars by Schneider et al. (2010) and the sample of photometrically-selected quasar candidates by Richards et al. (2009, both based on SDSS data) and we rely upon a procedure similar to the redshift permutation method (e.g., Osmer 1981; Zhdanov & Surdej 2001) that we have considered in the study of quasar pairs (see Section 5.3 and Farina et al. 2011). We assume that the quasars have the same position in the sky as in the original samples but a random redshift is assigned through a Monte Carlo simulation that takes into account the redshift distribution of our complete sample (~ 940000 objects). We find that ~ 0.05 quasar triplets with $\Delta V < 2000$ km/s and projected separations < 200 kpc are expected. We stress again that this method gives an upper limit for the number of chance triple quasars since in the computation most of the correlation was destroyed, but we kept the angular correlation among the quasars as in the original sample.

We thus conclude that the three quasars of QQQ J1519+0627 are physically connected and not due to a random superposition.

6.4 The galactic environment of the triplet

In the hypothesis that the system is virialised, the velocity differences among QQQ1519A, QQQ1519B and QQQ1519C (estimated from the broad Mg II emission line redshifts, see Section 5.2 for the reliability of these measures) imply a dynamical mass of $\sim 10^{13} M_{\odot}$, i.e. the system would lie inside a massive structure. In order to test this scenario, we search for galaxies at redshift ~ 1.5 in the proximity of the system. In Figure 6.5 we show the observed colour-magnitude diagram of the sources in our field. We compare the photometry of these sources with the apparent magnitude and colours of a $M^*(z)$ galaxy, where $M^*(z)$ is the characteristic luminosity (in absolute magnitudes) of galaxies at a given redshift z in the rest-frame B-band, as computed by Ilbert et al. (2005). For filter and k -correction, we refer to the elliptical galaxy template by Mannucci et al. (2001). We do not find evidence of a strong overdensity of sources with colours consistent with those of a red sequence at $z \sim 1.5$. This suggests that QQQ J1519+0627 is not located in a rich galaxy cluster or that the red sequence is not yet formed. The physical structure, where the three quasars reside, may be caught in the act of formation (similarly to what reported in e.g.: Decarli et al. 2009b, 2010a; Farina et al. 2011).

6 One (new) physical triplet of quasars

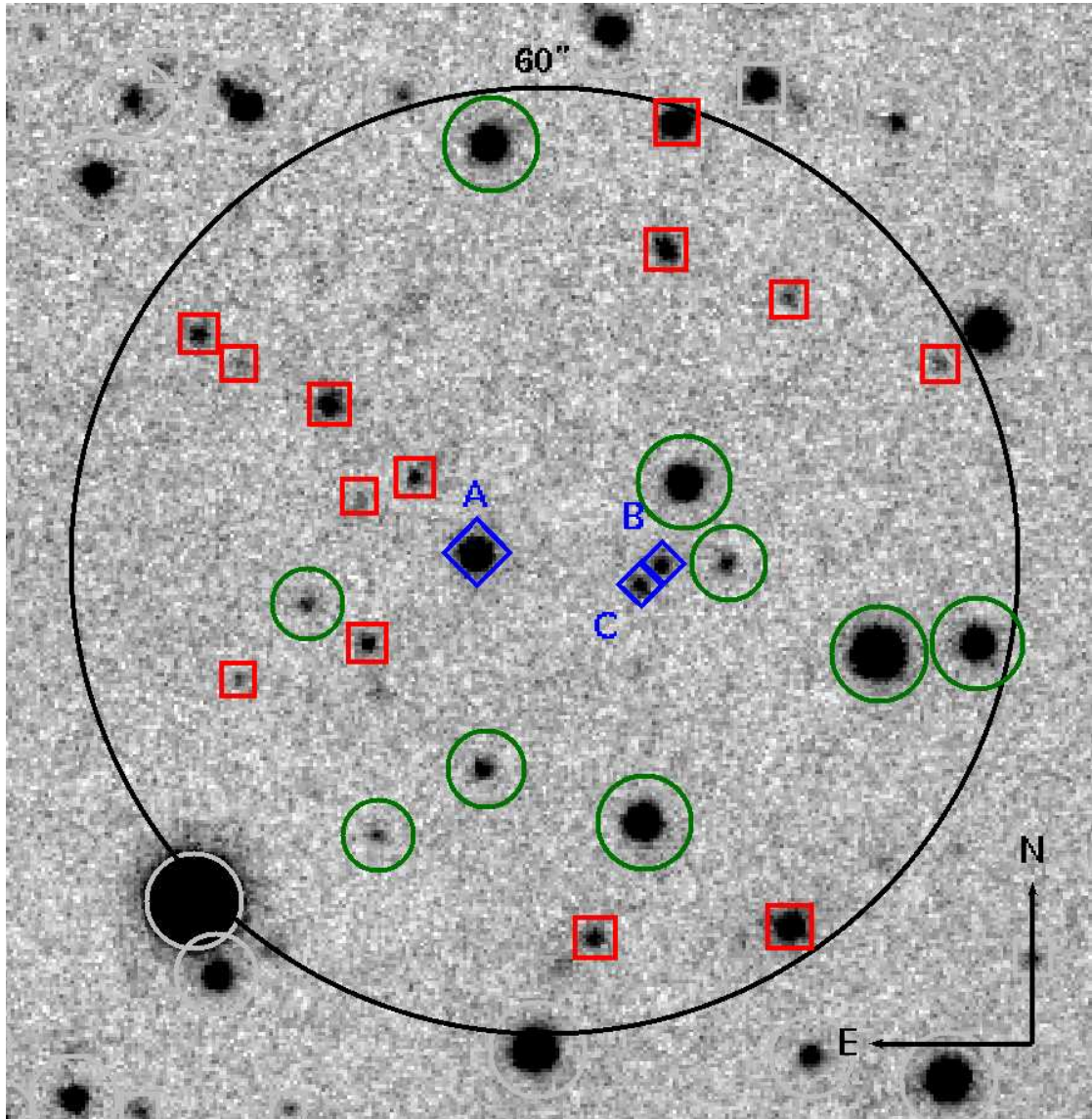


Figure 6.4: Image of the $60''$ around the triplet QQQ J1519+0627 as imaged in z-band at the Calar Alto Observatory. Blue diamonds are the three quasars. The 13 sources identified as galaxies are shown as red squares, while the 9 stars as green circles. The surface densities of Galactic and extragalactic sources in this area is consistent with the detections in the rest of the image.

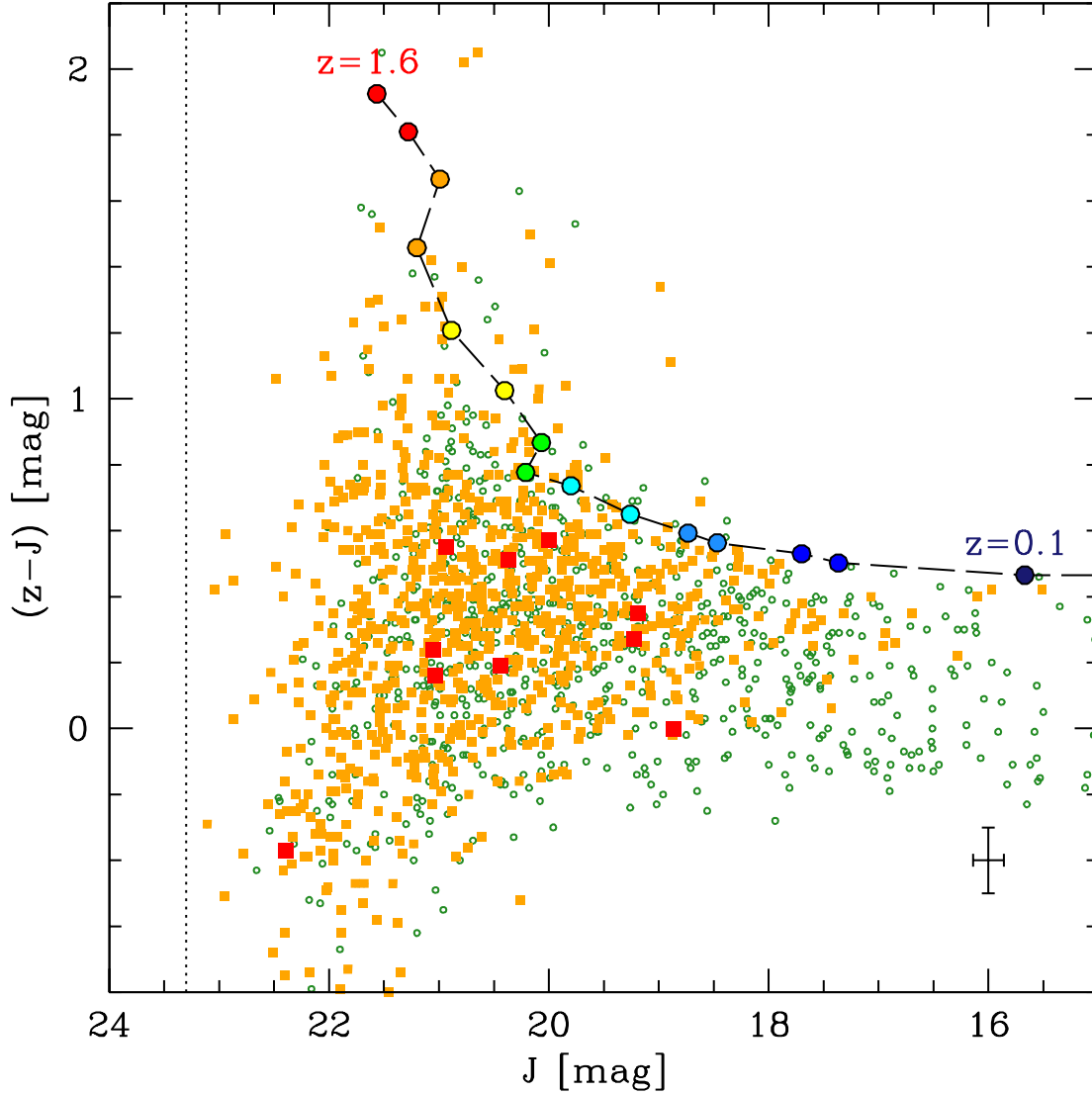


Figure 6.5: Observed colour–magnitude diagram for the objects detected by `SExtractor` in the field of QQQ J1519+0627 (green circles). Sources selected as galaxies (see text for details) are shown in orange, and those that lie within $60''$ from the triplet are highlighted with red squares. The vertical dotted line marks the 5σ detection limit (note that `SExtractor` is on average more conservative than the statistical limit magnitude). Typical error bars are shown as a cross in the bottom–right of the figure. The dashed line shows the location of an $M^*(z)$ galaxy at various redshifts, as derived from Ilbert et al. (2005), and assuming the elliptical galaxy template by Mannucci et al. (2001) for k -corrections. We do not find any evidence of an overdensity of galaxies with colours consistent with a red sequence at $z \sim 1.5$, thus suggesting that the environment of QQQ J1519+0627 is not a rich cluster.

6.5 Conclusions

In this Chapter we have presented the discovery of a triplet of quasars with angular separations between $3''.7$ and $23''.5$ at a similar redshift of $z \sim 1.5$. The three sources have relative velocities within ~ 1000 km/s as derived from our measurements of the Mg II broad emission line and of the surrounding Fe II multiplets in the observed optical spectra. From the analysis of u, g, r, i, z, J, and H broad band images we have concluded that this system consist of three distinct sources rather than being a multiply imaged lensed quasar. This would be the second physical triple quasar system discovered so far after QQQ J1432-0106 (Djorgovski et al. 2007). We have estimated that the probability that these systems are due to chance superposition are negligible. No clear galaxy overdensity is reported at photometric redshift consistent with the one of the triplet. We therefore have proposed that the three quasars are part of an ongoing common physical structure formation.

The projected separation of QQQ1519A from the other two members of the system is greater than the typical distances between interacting systems (~ 50 kpc, Hennawi et al. 2006b; Foreman et al. 2009). This implies that the observed nuclear activity of QQQ1519A was probably not triggered during an interaction involving the three systems at the same time. On the other hand, due to the smaller separation observed between QQQ1519B and C, the ignition of nuclear activity by galactic interactions may be a viable scenario for these quasars. More conclusive constraints on the dynamics of this peculiar system and on the properties of its environment will be obtained from future higher signal-to-noise ratio spectroscopic data in the NIR band (in order to measure the systemic velocities from [O III] lines, see Section 5.2) and deeper photometric images.

7 Conclusions and Future Perspective

In this Thesis we presented the analysis of projected and physical quasar pairs in order to investigate the presence of the cool gas and of the dark matter that surround quasars.

In the first part we have found that quasars possess a large envelope of gas similar to that of non-active galaxies. We showed that the anti-correlation between the strength of the absorption and the impact parameter is improved once the stellar mass of the galaxies is taken into account. This suggests that the detected absorptions are due to an inflows of cool enriched gas onto the quasar host galaxies. However, a fully consistent interpretation of these results require further efforts in refining the picture sketched here. In particular, some key points are yet to be clarified:

- i) Which is the extent of the cool gas halos of quasar? We will address with this issue thanks to the new OSIRIS-GTC spectra of 33 quasar pairs that span projected separations as large as 200 kpc.
- ii) What happen in the region closer to the quasars? If the inflow model for the origin of the absorbing gas is correct, in the proximity of the quasar an increase of the strength of the absorptions is expected. To study of this regions requires a sample of extremely close projected quasar pairs. However, the number of such systems drops rapidly down with the angular separation, and this effect is enhanced by the fiber collision limit that affects spectroscopic surveys. The combination of photometric and spectroscopic quasar catalogues should mitigate the effects of the fiber, and thus should allow to construct a large sample of quasars with separations less than $pd \lesssim 50$ kpc.
- iii) Which is the origin of the cool gas? Luminous quasars are expected to be embedded in rich environment (e.g., Martini & Weinberg 2001; Haiman & Hui 2001; Hall & Green 1998; Djorgovski 1998, 1999), and thus the detected absorption could be simply due to intervening galaxies. The strongest features could be also due to star formation driven outflows of gas, in this scenario a correlation between the colour/star formation rate of the host galaxies and the rest frame equivalent width of the absorbers is expected (see e.g., Zibetti et al. 2007). However the detection of the hosts and the study of the galactic environment of high redshift quasars are not trivial, since the light from the host galaxy is typically outshone by the nuclear component. Previous studies led by our group (e.g., Kotilainen et al. 1998; Falomo et al. 2001, 2004, 2005; Hyvönen et al. 2007; Decarli et al. 2009c) have shown that a large collecting area, optimal seeing conditions and good resolutions are mandatory in this kind of studies. Future broad band IR observations of the field of the foreground quasars performed with large telescopes, such as ESO-VLT or GTC, will allows to put more stringent constraints on the mechanisms that give rise to the detected absorption systems.

7 Conclusions and Future Perspective

In the second part the Thesis we studied the properties of 6 low redshift quasars pairs ($z \leq 0.8$) and of one newly discovered triplet at $z \sim 1.5$. It is worth noting that the separations between the considered quasars are larger than the typical scales of interacting systems (~ 50 kpc, see e.g., Hennawi et al. 2006b; Foreman et al. 2009). Thus the nuclear activity was not probably due to the mutual interactions of the two (or three) quasars at the same time.

Using a simple statistical method we have estimated that these systems are most probably physically associated and that their dynamical masses are larger than those expected from the host galaxies. Possible explanations for this excess are that quasars are harboured by massive dark matter halos (e.g., Myers et al. 2007a,b; Richardson et al. 2012) or by group/cluster of galaxies (e.g., Boris et al. 2007). This last hypothesis, however, is rejected by the analysis of broad band optical and near infrared images, that reveal a poor environment for all these systems, with the exception of one pairs.

In order to strengthen the evidences of this surplus of mass, we need a larger sample of physically connected quasars that allow the identification of [O III] strong emission lines and thus an accurate study of their dynamics. Possible candidates will come from the catalogues of already known quasar pairs (e.g., Hennawi et al. 2006b; Kayo & Oguri 2012) or from photometric quasar catalogues (e.g., Richards et al. 2009). We expect to find most of this systems at high redshift, where the peak of the quasar activity occur (e.g., Fontanot et al. 2007), thus in order to infer the systemic velocity difference of the quasars from the [O III] narrow lines and to explore the galactic environment of the selected systems we have to move in the IR bands. Optimal instrument for these kind of studies are the broad band imager HAWK-I and the medium resolution spectrograph X-SHOOTER mounted on the ESO-VLT telescopes.

A On the catalogues of quasars

In this Appendix we introduce the three catalogues scrutinised to find close quasar systems. The general properties of the two catalogues based on the SDSS survey are presented in Section A.1, and those of the Véron-Cetty & Véron (2010) one in Section A.2.

A.1 The SDSS catalogues

The SDSS uses a dedicated 2.5 m telescope located at the Apache Point Observatory to obtain images of more than a quarter of the sky ($\sim 11\,663\text{ deg}^2$ in the 7th Data Release, Abazajian et al. 2009). Observations are performed with a wide-field imager with $24\,2048 \times 2048$ CCDs with a pixel scale of $0''.396$ per pixel in 5 broad bands: u, g, r, i, and z (Fukugita et al. 1996; Gunn et al. 1998), centred at 3551 \AA , 4686 \AA , 6166 \AA , 7480 \AA , and 8932 \AA , respectively. The exposure time for each filter is $\sim 54\text{ s}$, that allows to reach a 5σ detection limit for point sources with $1''$ seeing in the u, g, r, i, and z filters of 22.0 mag, 22.2 mag, 22.2 mag, 21.3 mag, and 20.5 mag, respectively.

From this imaging data, spectroscopic targets are selected with various algorithms, mostly based on their location in the multidimensional SDSS colour space. The following samples are targeted: main galaxy sample (Strauss et al. 2002); Luminous Red Galaxies (LRG, Eisenstein et al. 2001); quasars (Richards et al. 2002); stars (point sources with colours typical of stars); objects near ROSAT All-Sky Survey (Voges et al. 1999, 2000) sources (Anderson et al. 2003); serendipity targets (sources with unusual colours or matches with the Very Large Array FIRST survey, Becker et al. 1995).

The selected objects are observed with two double spectrographs that cover the wavelength range 3800 \AA – 9200 \AA with a resolution of 1800–2200 depending on the wavelength. Each spectrograph accepts 320 fibres with a diameter of $3''$ in the sky, this allows to simultaneously observe 640 objects in a circular field of view of $1^\circ.49$ in radius. The exposure time for each plate is 45 minutes, typically splitted into into three parts for cosmic-ray rejection (York et al. 2000; Castander et al. 2001; Stoughton et al. 2002). It is worth noting that due to the finite size of optical-fibres two objects could not be observed if they lie within a separation of $< 55''$ (see below for details). However a fraction ($\sim 30\%$) of the spectroscopic survey area is covered by overlapping plates. These regions are observed more than one time, so these are not affected by the fiber collision limitation.

A.1.1 The spectroscopic quasar catalogue

The Schneider et al. (2010) quasar catalogue based on the 7th Data Release of the SDSS contains $\sim 100\,000$ spectroscopically confirmed quasars that were selected mostly on the basis of their high luminosity (i.e., $M_i < -22.0$) and of the width of their emission lines (i.e., at least one line have to be larger than $\text{FWHM} = 1000\text{ km/s}$). The selected quasars

A On the catalogues of quasars

are in the redshift range $0.07 \lesssim z \lesssim 5.46$ and the i-band magnitudes span from ~ 14.9 (limit imposed to avoid CCD saturation) to ~ 22.4 (see Figure A.1).

The spectra have a typical signal-to-noise ratio of $S/N \sim 15$ per 69 km/s pixel. The SDSS resolution of ~ 2000 allows to resolve spectral features with a FWHM $> 150 \text{ km/s}$ at the central wavelength. The redshifts of the quasars are estimate with the Tonry & Davis (1979) cross-correlation technique and the quasar template from Vanden Berk et al. (2001) and with the comparison of the observed-frame and the rest-frame wavelength emission line location. It is worth noting that the catalogue redshift could differ from the systemic redshift of more than $\sim 500 \text{ km/s}$ (Hewett & Wild 2010). Thus the observation of forbidden emission lines or of host galaxy absorptions are mandatory to investigate the dynamics gravitationally bounded quasar pairs (see for instance Chapter 5 and Farina et al. 2011).

The finite dimension of the support of the SDSS spectroscopic fibres constraints the sources observed in the same plate to be separated by more than $55''$. However in the region that are covered by more than one plate, it is possible to observe closer objects. In the following we give a rough estimate of the number of the quasar pairs lost in the Schneider et al. (2010) catalogue due to the collision limit.

The fiber collision limits

The fiber collision limit does not allow to SDSS to spectroscopically observe two quasars in a pair with angular separation $\Delta\theta < 55''$, unless they lie in overlapping plates (Blanton et al. 2003). In order to assess its relevance on the search of close pairs we select all the objects in the Schneider et al. (2010) catalogue that have angular separation between $3''$ and $250''$ (see Figure A.2). The effect of the fiber collision limit is apparent. At angular separation smaller than $55''$ the number of systems found decrease of a factor $f_Q \sim 0.55$.

It is worth noting that the number of systems lost due to the fiber collision limit at a fixed projected separation is redshift dependent. If one seek for pairs with $pd < pd_{\text{lim}}$, the fraction of the search area surrounding a quasar affected by the the fiber collision (f_A) at redshift $z = z_{\text{QSO}}$, is:

$$f_A(z_{\text{QSO}}) = \begin{cases} pd_{\text{FC}}^2(z_{\text{QSO}})/pd_{\text{lim}}^2 & \text{if } pd_{\text{FC}}(z_{\text{QSO}}) \leq pd_{\text{lim}}, \\ 1 & \text{if } pd_{\text{FC}}(z_{\text{QSO}}) > pd_{\text{lim}} \end{cases} \quad (\text{A.1})$$

where $pd_{\text{FC}}(z)$ is the projected distance that correspond to the fiber limit of $55''$ at redshift z . The ratio between the number of pairs found in the catalogue (N_{Found}) and the number of which expected if the survey was not affected by the fiber collision ($N_{\text{Exp.}}$), is thus given by:

$$f_{\text{FC}} = \frac{N_{\text{Found}}}{N_{\text{Exp.}}} = 1 + f_A(f_Q - 1). \quad (\text{A.2})$$

For instance, in the Schneider et al. (2010) catalogue at $z < 0.8$ there are 6 pairs with $pd < 500 \text{ kpc}$ and $\Delta V < 500 \text{ km/s}$ (see Chapter 5 and Farina et al. 2011), and ~ 3 more are expected in absence of the fiber collision limit (see Figure A.2).

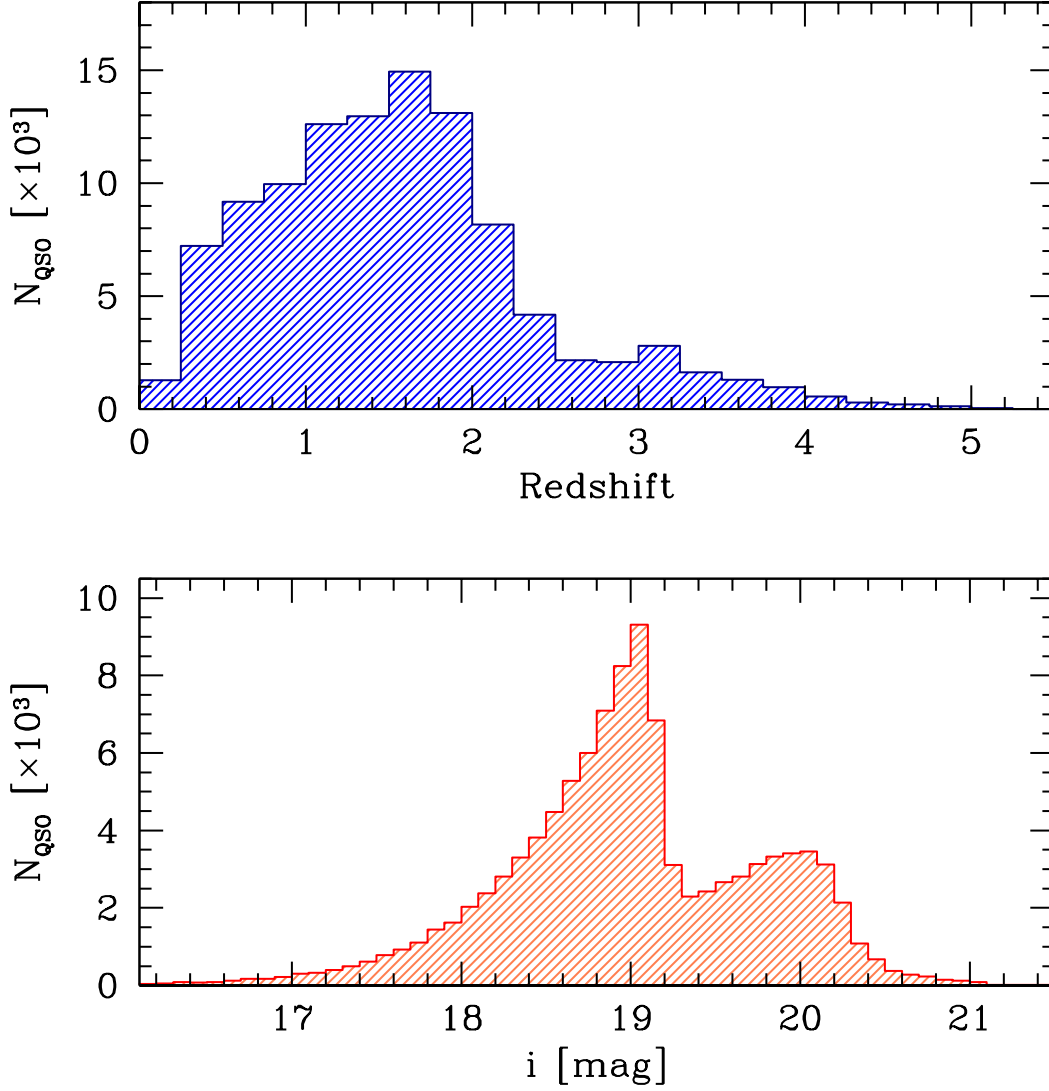


Figure A.1: Properties of the quasars in the (Schneider et al. 2010) catalogue. In the *Top Panel* we show the redshift distribution. At $z \sim 2.7$ and $z \sim 3.5$ it is apparent the reduced efficiency of the algorithm that select the photometric candidates that will be spectroscopically observed (see, Richards et al. 2002). This selection algorithm influence also the i -band magnitude distribution (*Bottom Panel*). The sharp drop at $i \sim 19.1$ is due to the magnitude limit imposed to the candidates whose colours indicate a probable redshift less than ~ 3 .

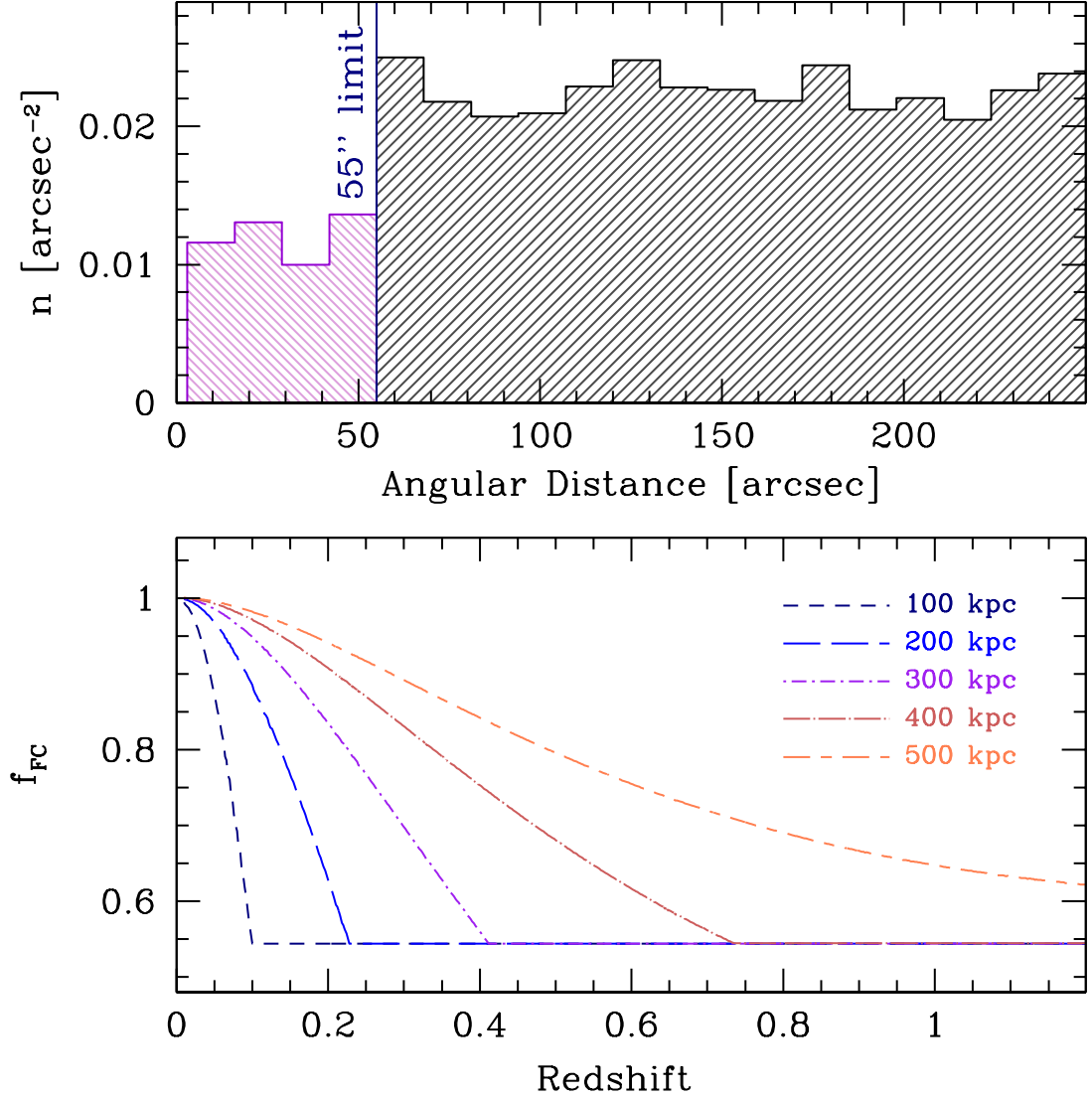


Figure A.2: Effect of the fiber collision limit in the Schneider et al. (2010) catalogue. *Top Panel:* the distribution of the angular separations of the systems with $3'' < \Delta\theta < 250''$. *Bottom Panel:* for different projected separation explored and as a function of redshift, the Figure shows the fraction between the number of pairs found in the catalogue and the expectation in absence of fiber collision limit (f_{FC} , see text for details).

A.1.2 Quasars photometric selection

Richards et al. (2009) present a photometric quasar catalogue that contains more than 1 000 000 point sources with a limiting magnitude $i = 21.3$ from the 6th data release of the SDSS (Adelman-McCarthy et al. 2008). As for the spectroscopic catalogue, a limiting i -band magnitude of $i > 14.5$ in order to avoid CCD saturation.

The quasar candidates are selected through the Kernel Density Estimation (KDE) algorithm. Briefly, to each position in the SDSS colour-colour space is assigned an expected density of stars and quasars estimated from a spectroscopically confirmed control sample of $\sim 75\,000$ quasars and $\sim 450\,000$ stars. From these density probability to be a quasars is associated to a given photometric objects. The efficiency of this procedure is estimated to be $\sim 80\%$. The catalogue completeness to type 1 quasars is expected to be $\sim 70\%$ with most of the missing objects occurring at $z \lesssim 0.7$ (where white dwarfs are a source of contamination) and at $2.5 \lesssim z \lesssim 3.0$ (where quasars and stars are similar in the SDSS colour-colour space).

All the quasar candidates in the catalogue are provided of a photometric redshift determined minimising the difference of the colours of each object with the median colours of quasars as a function of redshift (Weinstein et al. 2004). The typical accuracy of this procedure is $|\Delta z| < 0.3$, with an increase at redshifts $1 < z < 2$ where more comparison data exists. The photometric redshift and i -band distributions of the candidates quasars are shown in Figure A.3.

A.2 The Véron-Cetty and Véron catalogue

The 13th edition of the Véron-Cetty & Véron (2010) catalogue is a compilation of (almost) all the quasars with measured redshift and absolute magnitude brighter than $M_B = -22.25$ known prior to July 1st, 2009. The general properties of this catalogue are shown in Figure A.4. It contains more than 130 000 quasars mainly originating from the 2QZ Catalogue (Croom et al. 2001, 2004) and from the SDSS (Adelman-McCarthy et al. 2007, 2008; Abazajian et al. 2009). Due to the fiber collision limits ($55''$ for SDSS, $30''$ for 2QZ) these survey often fails to find close separation pairs (see §A.1.1). However, this problem is diluted in the region where the two survey overlap and thus the Véron-Cetty & Véron (2010) catalogue contains more close separation systems than the single 2QZ and SDSS surveys. After cleaning for the known gravitational lens, there are 120 quasars with projected separation $pd \leq 100$ kpc. 54 of which have line-of-sight velocity difference $\Delta V \leq 2000$ km/s. For comparison, the Schneider et al. (2010) catalogue contains only 19 pairs with $pd \leq 100$ kpc 7 of which with $\Delta V \leq 2000$ km/s. As well as the effect of the SDSS–2QZ overlapping region, the number of close systems is increased thanks to surveys focussed on the discovery of quasar pairs (e.g., Hennawi et al. 2006b, 2010; Myers et al. 2008) and to rejected gravitational lens systems (e.g., Inada et al. 2008).

It is worth noting that, however, due to the heterogeneous origin of the quasars in the catalogue, some objects have an erroneous classification or are duplicate of the same object (see for instance, Decarli et al. 2009a; Cupani et al. 2011; Flesch 2012).

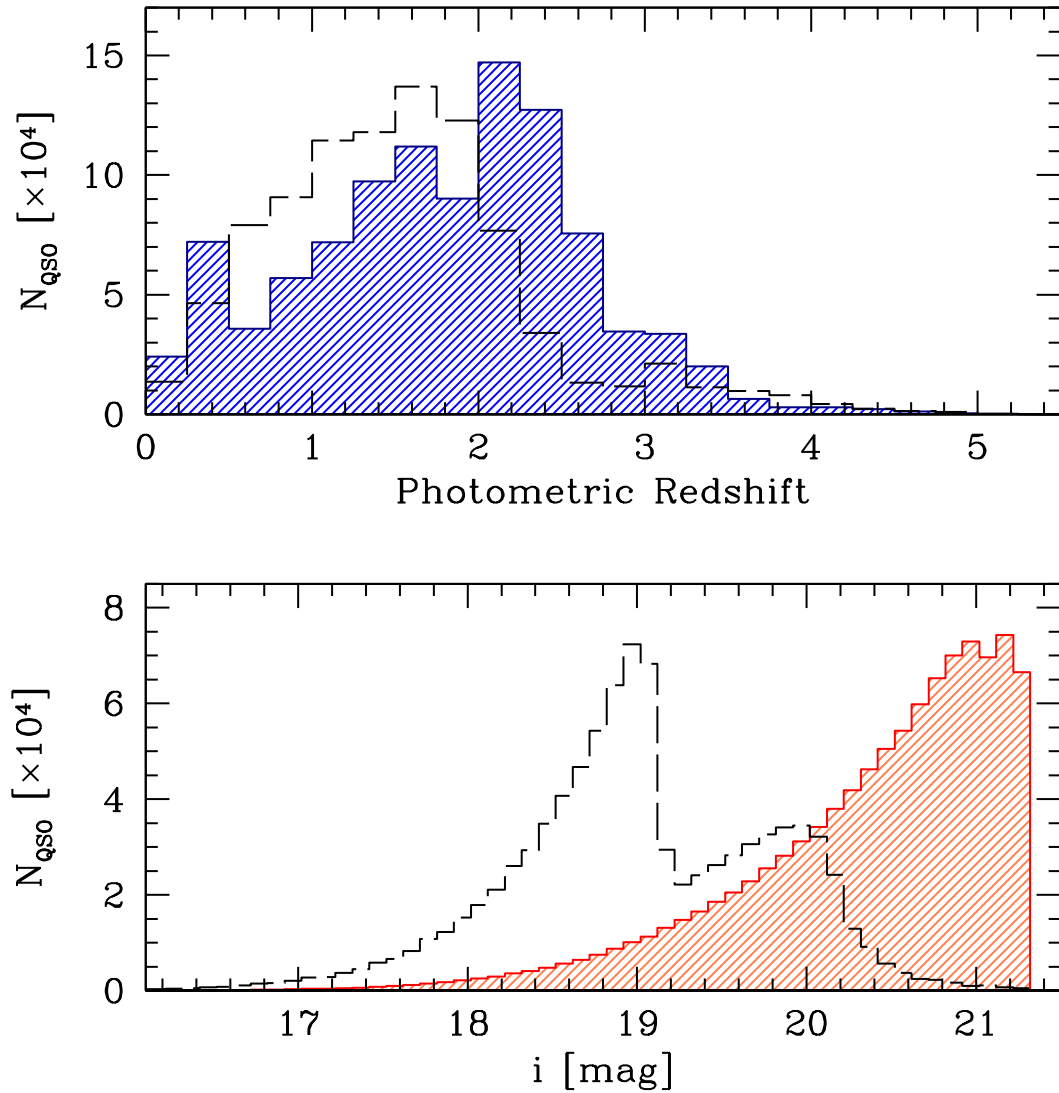


Figure A.3: Distribution of photometric selected quasars in the sample of (Richards et al. 2009). For the sake of comparison the dashed lines show the distribution of spectroscopically confirmed quasars normalised to 10^3 . *Top Panel:* Redshift; *Bottom Panel:* i-band magnitude.

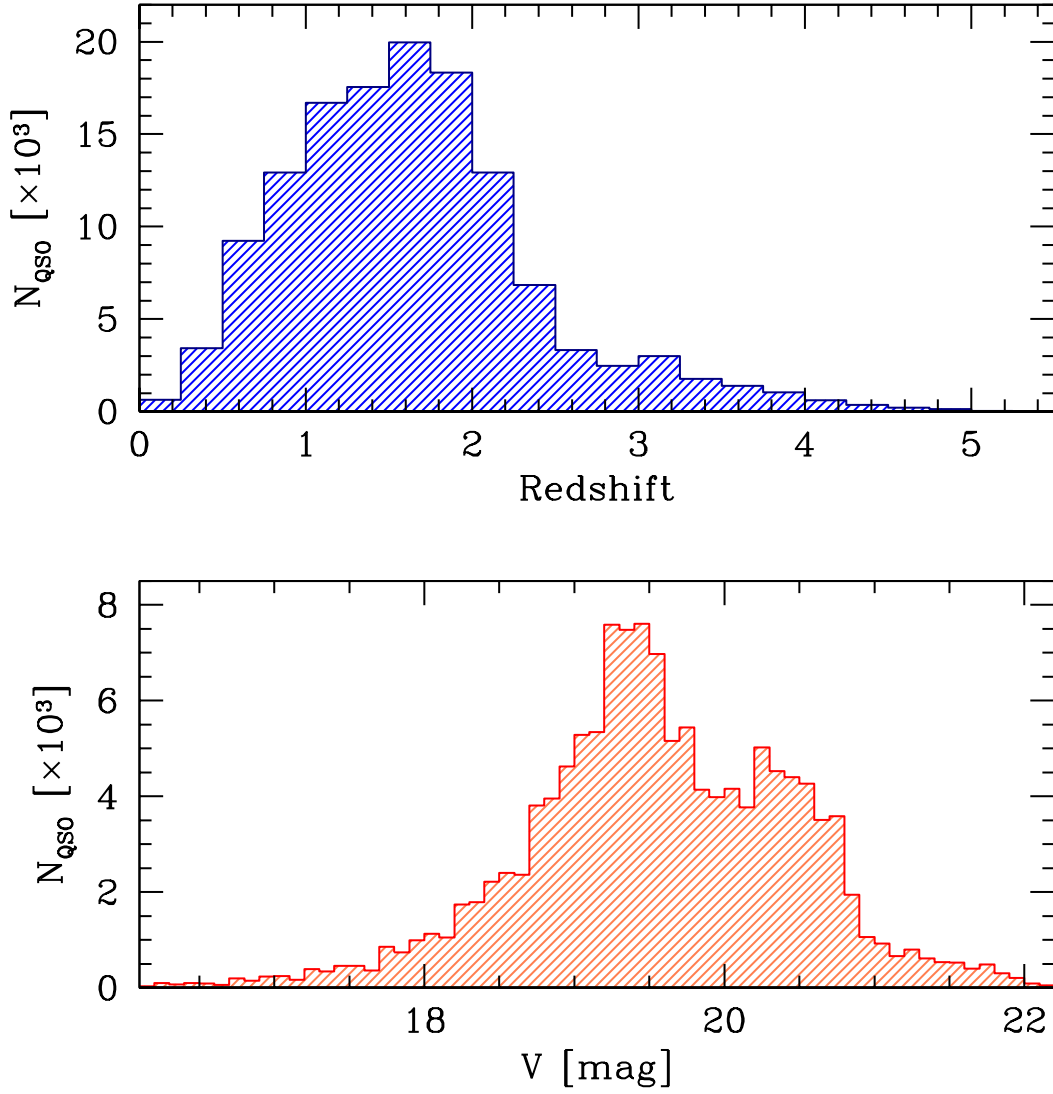


Figure A.4: Distribution of the quasars listed in the (Véron-Cetty & Véron 2010) catalogue. *Top Panel:* Redshift; *Bottom Panel:* V-band magnitude.

A On the catalogues of quasars

B Notes on individual projected quasar pairs

This Appendix contains notes on the projected quasars pairs that we have presented in Chapter 2.

QQ04: The two quasars of the pair are very close in redshift thus the association of the absorption feature to the foreground or to the background quasar are uncertain. QQ04F shows two C IV absorption systems superimposed to the broad emission line. A stronger one at redshift $z_{\text{abs}} \sim 2.1120$ and a fainter blueshifted one at $z_{\text{abs}} \sim 2.1350$. The two component of the stronger absorption system are partially blended, and thus fitted simultaneously with the sum of two Gauss functions. Moreover, other absorptions lines are present at $\lambda = 4822.7 \text{ \AA}$ and at $\lambda = 4845.8 \text{ \AA}$, whose identification is uncertain as they are superimposed on the stronger absorption system.

Due to the velocity range that we have considered to associate the absorption features to the QSO_F (see Section 2.3), we have assumed that the stronger feature is due to the quasar halo, while the weaker one (with $\Delta V \sim 3000 \text{ km/s}$ from the former) to a simple chance superposition. However, the uncertainties in the redshift determination based on C IV broad emission line are large, mostly due to the presence of the strong absorption features (see e.g., Hewett & Wild 2010). This does not allow to exclude the possibility that the weaker absorption system is connected to the QSO_F halo and that the stronger one is due to a gas outflow. QQ04B shows a broad absorption lines in the blue wing of the C IV emission lines. These P–Cygni like profile, are usually interpreted as radiatively driven winds associated to strong outflows from quasars (e.g., Scargle et al. 1970; Turnshek 1984). In the spectra of QQ04B, two more C IV absorption features are present at redshift $z_{\text{abs}} = 2.0302$ and $z_{\text{abs}} = 2.0443$, suggesting a very rich environment for this pair or an interaction between the quasars (see Table B.1).

QQ05: In the spectra of QQ05B we detect Fe II($\lambda 2586$) and Fe II($\lambda 2600$) lines at the same redshift of the Mg II doublet associated to the QSO_F ($EW_r(\lambda 2586) = (0.12 \pm 0.04) \text{ \AA}$ and $EW_r(\lambda 2600) = (0.39 \pm 0.04) \text{ \AA}$).

QQ07: Associated to the Mg II absorption feature at redshift $z_{\text{abs}} = 1.3355$ (see Table B.1) we detect Fe II($\lambda 2586$) and Fe II($\lambda 2600$) lines with $EW_r(\lambda 2586) = (0.61 \pm 0.07) \text{ \AA}$ and $EW_r(\lambda 2600) = (0.70 \pm 0.04) \text{ \AA}$. A Fe II($\lambda 2382$) line is present at the same redshift of the Mg II doublet at $z_{\text{abs}} = 1.5186$ ($EW_r(\lambda 2382) = (0.23 \pm 0.04) \text{ \AA}$, see Table B.1).

QQ10: Two C IV doublets are superimposed to the C IV broad emission of QSO_B. Their redshifts are $z_{\text{abs}} = 2.5127$ and $z_{\text{abs}} = 2.5167$, corresponding to a velocity difference of $\sim 500 \text{ km/s}$ (see Table B.1).

B Notes on individual projected quasar pairs

Table B.1: Properties of Mg II and CIV absorption features not associated to QSO_F detected on the quasar spectra. (01) our identification label of the quasar, (02,04) observed wavelength, (03,05) rest frame equivalent width, (06) doublet ratio, and (07) redshift of the absorption.

Mg II						
ID	$\lambda 2796$		$\lambda 2803$		DR	z_{abs}
	λ_{abs} [Å]	EW_r [Å]	λ_{abs} [Å]	EW_r [Å]		
(01)	(02)	(03)	(04)	(05)	(06)	(07)
QQ01F	5954.7	0.86±0.15	5970.3	0.45±0.14	1.91±0.68	1.1294±0.0001
QQ07B	6378.1	0.46±0.06	6395.0	0.43±0.03	1.07±0.16	1.2810±0.0002
QQ07B	6531.0	1.10±0.04	6547.9	1.09±0.06	1.01±0.07	1.3355±0.0001
QQ07B	7042.9	0.58±0.06	7061.0	0.46±0.04	1.26±0.17	1.5186±0.0002
QQ08B	6958.9	1.02±0.10	6975.6	0.51±0.11	2.00±0.47	1.4882±0.0008

C IV						
ID	$\lambda 1548$		$\lambda 1551$		DR	z_{abs}
	λ_{abs} [Å]	EW_r [Å]	λ_{abs} [Å]	EW_r [Å]		
(01)	(02)	(03)	(04)	(05)	(06)	(07)
QQ04B	4691.5	0.54±0.03	4699.1	0.37±0.02	1.46±0.11	2.0302±0.0002
QQ04B	4713.4	0.27±0.02	4721.0	0.22±0.05	1.23±0.29	2.0443±0.0003
QQ10B	5438.4	0.22±0.03	5447.4	0.16±0.06	1.38±0.55	2.5127±0.0002
QQ10B	5444.7	0.19±0.06	5453.6	0.19±0.04	1.00±0.38	2.5167±0.0002
QQ13B	5142.3	0.14±0.03	5151.1	0.07±0.03	2.00±0.96 [†]	2.3215±0.0001
QQ13B	5151.1	0.40±0.03	5159.7	0.20±0.03	2.00±0.34 [†]	2.3272±0.0001

[†] Assumed value for DR (see text for details)

QQ13: This pair was already investigated by Decarli et al. (2009a), who have noticed a non resolved Mg II absorption feature associated to the foreground quasar. Moreover they observe QSO13F in Ks band to detect the host galaxy. This allows to give a independent estimate of the host galaxy mass ($M_{\text{host}} = 5 \times 10^{11} M_{\odot}$) that is consistent with the value estimated indirectly from the M_{BH} .

In the spectra of QSO_B we identify two CIV doublet at redshifts discordant with that of the quasar ($z_{\text{abs}} \sim 2.3215$ and $z_{\text{abs}} \sim 2.3272$). Due to their redshift difference the component of the doublets are superimposed, we thus infer the EW_r assuming that the lines are not saturated and thus a theoretical doublet ratio value of DR= 2 (see Table B.1).

C List of publications

- **Farina E. P.**, Montuori C., Decarli M., & Fumagalli M., 2012, MNRAS, submitted: *Caught in the act: discovery of a physical quasar triplet.*

We present the discovery of a triplet of quasars at $z \sim 1.51$. The whole system is well accommodated within $25''$ (i.e., 200 kpc in projected distance). The velocity differences among the three objects (as measured through the broad Mg II emission line) are < 1000 km/s, implying physical association of the quasars. Broad band NIR images of the field do not reveal evidence of galaxies or galaxy clusters that could act as a gravitational lens, ruling out the possibility that two or all the three quasars are multiple images of a single, strongly lensed source. QQQ J1519+0627 is the second physical triplet of quasars known up to date. We estimate that these systems are extremely rare in terms of simple accidental superposition, suggesting a possible common origin for the quasar ignition.

Based on observations collected at the La Silla Observatory with the New Technology Telescope (NTT) of the European Southern Observatory (ESO) and at the Calar Alto Observatory with the 3.5m telescope of the Centro Astrónmico Hispano Alemán (CAHA).

- **Farina E. P.**, Falomo R., Decarli M., Treves A., & Kotilainen J. K., 2012, accepted for publication in MNRAS: *On the cool gaseous haloes of quasars.*

We present optical spectroscopy of projected quasar pairs to investigate the Mg II and the C IV absorption features imprinted on the spectrum of the background object by the gaseous halo surrounding the foreground quasar. We observed 13 projected pairs in the redshift range $0.7 \lesssim z_F \lesssim 2.2$ spanning projected separations between 60 kpc and 120 kpc. In the spectra of the background quasars, we identify Mg II intervening absorption systems associated to the foreground quasars in 7 out of 10 pairs, and 1 absorption out of 3 is found for C IV. The distribution of the equivalent width as a function of the impact parameter shows that, unlike the case of normal galaxies, some strong absorption systems ($EW_r > 1 \text{ \AA}$) are present also beyond a projected radius of ~ 70 kpc. If we take into account the mass of the galaxies as an additional parameter that influence the extent of the gaseous haloes, the distribution of the absorptions connected to the quasars is consistent to that of galaxies. In the spectra of the foreground quasars we do not detect any Mg II absorption lines originated by the gas surrounding the quasar itself, but in 2 cases these features are present for C IV. The comparison between the absorptions observed in the transverse direction and those along the line of sight allows us to comment on the distribution of the absorbing gas and on the emission properties of the quasars.

Based on observations undertaken at the European Southern Observatory (ESO) Very Large Telescope (VLT) under Programmes 085.B-0210(A) and 086.B-0028(A).

C List of publications

- Fumagalli M., Furniss A., O’Meara J. M., Prochaska J. X., Williams D. A., & **Farina E. P.**, 2012, *A&A*, 545, A68: *On the redshift of the blazar PKS 0447-439.*

PKS 0447-439 is one of the BL Lacertae objects that have been detected at very high energy. There has been a recent report of a lower limit of $z \gtrsim 1.246$ for the redshift of this blazar, challenging the current paradigm in which very high-energy γ -rays cannot freely propagate in the $z \gtrsim 1$ universe. In this research note, we present a new MagE/Magellan spectrum of PKS 0447-439 with exquisite signal-to-noise ($S/N > 150$ at 6500 \AA). Our analysis confirms the presence of the previously-reported absorption line at 6280 \AA , which we identify, however, with a known telluric absorption, invalidating the claim that this blazar lies at $z > 1$. Since no other extragalactic spectral features are detected, we cannot establish a redshift based on our spectrum.

This paper includes data gathered with the 6.5 m Magellan Telescopes located at Las Campanas Observatory, Chile.

- **Farina E. P.**, Decarli R., Falomo R., Treves A., & Raiteri C. M., 2012, *MNRAS*, 424, 393: *The optical spectrum of PKS 1222+216 and its black hole mass.*

We investigate the optical spectral properties of the blazar PKS 1222+216 during a period of ~ 3 years. While the continuum is highly variable (i.e., from $\lambda L_\lambda(5100 \text{ \AA}) \sim 3.5 \times 10^{45} \text{ erg/s}$ up to $\sim 15.0 \times 10^{45} \text{ erg/s}$) the broad line emission is practically constant. This supports a scenario in which the broad line region is not affected by jet continuum variations. We thus infer the thermal component of the continuum from the line luminosity and we show that it is comparable with the continuum level observed during the phases of minimum optical activity. The mass of the black hole is estimated through the virial method from the FWHM of Mg II, H β , and H α broad lines and from the thermal continuum luminosity. This yields a consistent black hole mass value of $\sim 6 \times 10^8 M_\odot$.

- **Farina E. P.**, Falomo R., & Treves A., 2011, *MNRAS*, 415, 3163: *A study of six low-redshift quasar pairs.*

The dynamical properties of six SDSS quasar pairs at $z \leq 0.8$ are investigated. The pairs have proper transverse separation $pd \leq 500 \text{ kpc}$, and velocity difference along the line of sight $\Delta V \leq 500 \text{ km/s}$. If they are bound systems their dynamical mass can be evaluated and compared with that of host galaxies. Evidence is found of an excess of the former mass with respect to the latter. This suggests that these quasar pairs are hosted by galaxies with massive dark halos or that they reside in a group/cluster of galaxies.

Bibliography

- Abazajian K.N., Adelman-McCarthy J.K., Agüeros M.A., et al., Jun. 2009, ApJS, 182, 543
- Adelman-McCarthy J.K., Agüeros M.A., Allam S.S., et al., Oct. 2007, ApJS, 172, 634
- Adelman-McCarthy J.K., Agüeros M.A., Allam S.S., et al., Apr. 2008, ApJS, 175, 297
- Anderson S.F., Voges W., Margon B., et al., Nov. 2003, AJ, 126, 2209
- Antonucci R., 1993, ARA&A, 31, 473
- Appenzeller I., Fricke K., Fürtig W., et al., Dec. 1998, The Messenger, 94, 1
- Bahcall J.N., Salpeter E.E., Nov. 1965, ApJ, 142, 1677
- Bahcall J.N., Salpeter E.E., May 1966, ApJ, 144, 847
- Bahcall J.N., Spitzer L. Jr., May 1969, ApJ, 156, L63
- Barlow T.A., Sargent W.L.W., Jan. 1997, AJ, 113, 136
- Barton E.J., Cooke J., Dec. 2009, AJ, 138, 1817
- Bechtold J., Ellingson E., Sep. 1992, ApJ, 396, 20
- Becker R.H., White R.L., Helfand D.J., Sep. 1995, ApJ, 450, 559
- Bennert N., Canalizo G., Jungwiert B., et al., Apr. 2008, ApJ, 677, 846
- Bennert V.N., Treu T., Woo J.H., et al., Jan. 2010, ApJ, 708, 1507
- Bergeron J., Boissé P., Mar. 1991, A&A, 243, 344
- Bergeron J., Boissé P., Ménard B., Jan. 2011, A&A, 525, A51
- Bertin E., Arnouts S., Jun. 1996, A&AS, 117, 393
- Blanton M.R., Lin H., Lupton R.H., et al., Apr. 2003, AJ, 125, 2276
- Boksenberg A., Sargent W.L.W., Feb. 1978, ApJ, 220, 42
- Bonning E.W., Shields G.A., Salviander S., Sep. 2007, ApJ, 666, L13
- Boris N.V., Sodré L. Jr., Cypriano E.S., et al., Sep. 2007, ApJ, 666, 747
- Boroson T., Aug. 2005, AJ, 130, 381

Bouché N., Murphy M.T., Péroux C., Csabai I., Wild V., Sep. 2006, MNRAS, 371, 495

Bowen D.V., Chelouche D., Jan. 2011, ApJ, 727, 47

Bowen D.V., Hennawi J.F., Ménard B., et al., Jul. 2006, ApJ, 645, L105

Burbidge E.M., Lynds C.R., Burbidge G.R., Apr. 1966, ApJ, 144, 447

Buzzoni B., Delabre B., Dekker H., et al., Dec. 1984, The Messenger, 38, 9

Callegari S., Kazantzidis S., Mayer L., et al., Mar. 2011, ApJ, 729, 85

Canalizo G., Bennert N., Jungwiert B., et al., Nov. 2007, ApJ, 669, 801

Castander F.J., Nichol R.C., Merrelli A., et al., May 2001, AJ, 121, 2331

Cepa J., Aguiar-Gonzalez M., Bland-Hawthorn J., et al., Mar. 2003, In: Iye M., Moorwood A.F.M. (eds.) Society of Photo-Optical Instrumentation Engineers (SPIE) Conference Series, vol. 4841 of Society of Photo-Optical Instrumentation Engineers (SPIE) Conference Series, 1739–1749

Charlton J.C., Churchill C.W., Jul. 1996, ApJ, 465, 631

Chelouche D., Ménard B., Bowen D.V., Gnat O., Aug. 2008, ApJ, 683, 55

Chen H.W., Lanzetta K.M., Webb J.K., Jul. 2001, ApJ, 556, 158

Chen H.W., Helsby J.E., Gauthier J.R., et al., May 2010a, ApJ, 714, 1521

Chen H.W., Wild V., Tinker J.L., et al., Dec. 2010b, ApJ, 724, L176

Chierigato M., Miranda M., Jetzer P., Nov. 2007, A&A, 474, 777

Churchill C.W., Vogt S.S., Aug. 2001, AJ, 122, 679

Churchill C.W., Rigby J.R., Charlton J.C., Vogt S.S., Jan. 1999, ApJS, 120, 51

Churchill C.W., Mellon R.R., Charlton J.C., et al., Sep. 2000, ApJS, 130, 91

Churchill C.W., Vogt S.S., Charlton J.C., Jan. 2003, AJ, 125, 98

Churchill C.W., Kacprzak G.G., Steidel C.C., Mar. 2005, In: Williams P., Shu C.G., Menard B. (eds.) IAU Colloq. 199: Probing Galaxies through Quasar Absorption Lines, 24–41

Cortese L., Gavazzi G., Boselli A., et al., Jul. 2006, A&A, 453, 847

Crenshaw D.M., Kraemer S.B., George I.M., 2003, ARA&A, 41, 117

Croom S.M., Smith R.J., Boyle B.J., et al., Apr. 2001, MNRAS, 322, L29

Croom S.M., Smith R.J., Boyle B.J., et al., Apr. 2004, MNRAS, 349, 1397

Croom S.M., Richards G.T., Shanks T., et al., Nov. 2009, MNRAS, 399, 1755

Crotts A.P.S., Jan. 1989, *ApJ*, 336, 550

Cupani G., Cristiani S., D'Odorico V., Milvang-Jensen B., Krogager J.K., May 2011, *A&A*, 529, A99

Curran S.J., Webb J.K., Murphy M.T., et al., 2002, *PASA*, 19, 455

De Rosa G., Decarli R., Walter F., et al., Oct. 2011, *ApJ*, 739, 56

Decarli R., Labita M., Treves A., Falomo R., Jul. 2008, *MNRAS*, 387, 1237

Decarli R., Falomo R., Kotilainen J., et al., Mar. 2009a, *The Open Astronomy Journal*, 2, 23

Decarli R., Reynolds M.T., Dotti M., Jul. 2009b, *MNRAS*, 397, 458

Decarli R., Treves A., Falomo R., Jun. 2009c, *MNRAS*, 396, L31

Decarli R., Falomo R., Treves A., Barattini M., Feb. 2010a, *A&A*, 511, A27

Decarli R., Falomo R., Treves A., et al., Mar. 2010b, *MNRAS*, 402, 2441

Decarli R., Falomo R., Treves A., et al., Mar. 2010c, *MNRAS*, 402, 2453

Decarli R., Dotti M., Treves A., May 2011, *MNRAS*, 413, 39

Decarli R., Falomo R., Kotilainen J.K., et al., 2012, *Advances in Astronomy*, 2012

Di Matteo T., Springel V., Hernquist L., Feb. 2005, *Nature*, 433, 604

Disney M.J., Boyce P.J., Blades J.C., et al., Jul. 1995, *Nature*, 376, 150

Djorgovski S., 1991, In: Crampton D. (ed.) *The Space Distribution of Quasars*, vol. 21 of *Astronomical Society of the Pacific Conference Series*, 349–353

Djorgovski S.G., May 1998, *ArXiv:astro-ph/9805159*

Djorgovski S.G., 1999, In: Bunker A.J., van Breugel W.J.M. (eds.) *The Hy-Redshift Universe: Galaxy Formation and Evolution at High Redshift*, vol. 193 of *Astronomical Society of the Pacific Conference Series*, 397

Djorgovski S.G., Courbin F., Meylan G., et al., Jun. 2007, *ApJ*, 662, L1

Dobrzycki A., Bechtold J., Aug. 1991, *ApJ*, 377, L69

Dunlop J.S., Peacock J.A., Nov. 1990, *MNRAS*, 247, 19

Dunlop J.S., McLure R.J., Kukula M.J., et al., Apr. 2003, *MNRAS*, 340, 1095

Efstathiou G., Rees M.J., Feb. 1988, *MNRAS*, 230, 5P

Eisenstein D.J., Annis J., Gunn J.E., et al., Nov. 2001, *AJ*, 122, 2267

Elvis M., Dec. 2000, *ApJ*, 545, 63

Faber S.M., Jackson R.E., Mar. 1976, *ApJ*, 204, 668

Falomo R., Kotilainen J., Treves A., Jan. 2001, *ApJ*, 547, 124

Falomo R., Kotilainen J.K., Pagani C., Scarpa R., Treves A., Apr. 2004, *ApJ*, 604, 495

Falomo R., Kotilainen J.K., Scarpa R., Treves A., May 2005, *A&A*, 434, 469

Falomo R., Kotilainen J.K., Scarpa R., Treves A., Uslenghi M., Nov. 2006, *New Astronomy Review*, 50, 732

Falomo R., Treves A., Kotilainen J.K., Scarpa R., Uslenghi M., Feb. 2008, *ApJ*, 673, 694

Farina E.P., Falomo R., Treves A., Aug. 2011, *MNRAS*, 415, 3163

Farina E.P., Decarli R., Falomo R., Treves A., Raiteri C.M., Jul. 2012a, *MNRAS*, 424, 393

Farina E.P., Falomo R., Decarli R., Treves A., Kotilainen J.K., Nov. 2012b, accepted for publication in *MNRAS*, ArXiv e-prints 1211.3433

Farina E.P., Montuori C., Decarli R., Fumagalli M., 2012c, *MNRAS*, submitted

Ferrarese L., Merritt D., Aug. 2000, *ApJ*, 539, L9

Flesch E., Jun. 2012, ArXiv e-prints 1206.1144

Floyd D.J.E., Kukula M.J., Dunlop J.S., et al., Nov. 2004, *MNRAS*, 355, 196

Floyd D.J.E., Dunlop J.S., Kukula M.J., et al., Aug. 2012, ArXiv e-prints 1208.4143

Foltz C.B., Weymann R.J., Peterson B.M., et al., Aug. 1986, *ApJ*, 307, 504

Fontanot F., Cristiani S., Monaco P., et al., Jan. 2007, *A&A*, 461, 39

Foreman G., Volonteri M., Dotti M., Mar. 2009, *ApJ*, 693, 1554

Francis P.J., Hewett P.C., Foltz C.B., et al., Jun. 1991, *ApJ*, 373, 465

Fukugita M., Ichikawa T., Gunn J.E., et al., Apr. 1996, *AJ*, 111, 1748

Fukugita M., Nakamura O., Schneider D.P., Doi M., Kashikawa N., Mar. 2004, *ApJ*, 603, L65

Fumagalli M., Prochaska J.X., Kasen D., et al., Dec. 2011, *MNRAS*, 418, 1796

Fumagalli M., Furniss A., O'Meara J.M., et al., Sep. 2012, *A&A*, 545, A68

Gallerani S., Ferrara A., Fan X., Choudhury T.R., May 2008, *MNRAS*, 386, 359

Gaskell C.M., Dec. 1982, *ApJ*, 263, 79

Gauthier J.R., Chen H.W., Tinker J.L., Sep. 2009, *ApJ*, 702, 50

Gebhardt K., Bender R., Bower G., et al., Aug. 2000, ApJ, 539, L13

Giavalisco M., Ferguson H.C., Koekemoer A.M., et al., Jan. 2004, ApJ, 600, L93

Girardi L., Groenewegen M.A.T., Hatziminaoglou E., da Costa L., Jun. 2005, A&A, 436, 895

Girardi M., Biviano A., Giuricin G., Mardirossian F., Mezzetti M., Jan. 1995, ApJ, 438, 527

Girardi M., Borgani S., Giuricin G., Mardirossian F., Mezzetti M., Oct. 1998a, ApJ, 506, 45

Girardi M., Giuricin G., Mardirossian F., Mezzetti M., Boschin W., Sep. 1998b, ApJ, 505, 74

Graham A.W., Driver S.P., Jan. 2007, ApJ, 655, 77

Green P.J., Myers A.D., Barkhouse W.A., et al., Feb. 2010, ApJ, 710, 1578

Green P.J., Myers A.D., Barkhouse W.A., et al., Dec. 2011, ApJ, 743, 81

Greenstein J.L., Schmidt M., Jul. 1964, ApJ, 140, 1

Gunn J.E., Carr M., Rockosi C., et al., Dec. 1998, AJ, 116, 3040

Haiman Z., Hui L., Jan. 2001, ApJ, 547, 27

Hall P.B., Green R.F., Nov. 1998, ApJ, 507, 558

Hamann F., Barlow T.A., Beaver E.A., et al., Apr. 1995, ApJ, 443, 606

Heckman T.M., Armus L., Miley G.K., Dec. 1990, ApJS, 74, 833

Heckman T.M., Miley G.K., Lehnert M.D., van Breugel W., Mar. 1991, ApJ, 370, 78

Heisler J., Tremaine S., Bahcall J.N., Nov. 1985, ApJ, 298, 8

Hennawi J.F., Prochaska J.X., Burles S., et al., Nov. 2006a, ApJ, 651, 61

Hennawi J.F., Strauss M.A., Oguri M., et al., Jan. 2006b, AJ, 131, 1

Hennawi J.F., Dalal N., Bode P., Ostriker J.P., Jan. 2007, ApJ, 654, 714

Hennawi J.F., Myers A.D., Shen Y., et al., Aug. 2010, ApJ, 719, 1672

Hernquist L., Aug. 1989, Nature, 340, 687

Hewett P.C., Foltz C.B., Apr. 2003, AJ, 125, 1784

Hewett P.C., Wild V., Jul. 2010, MNRAS, 405, 2302

Hewett P.C., Foltz C.B., Chaffee F.H., Apr. 1995, AJ, 109, 1498

- Hopkins P.F., Hernquist L., Cox T.J., et al., Sep. 2005, *ApJ*, 630, 705
- Hopkins P.F., Hernquist L., Cox T.J., et al., Mar. 2006, *ApJS*, 163, 1
- Hopkins P.F., Hernquist L., Cox T.J., Kereš D., Apr. 2008, *ApJS*, 175, 356
- Hutchings J.B., Scholz P., Bianchi L., Mar. 2009, *AJ*, 137, 3533
- Hyvönen T., Kotilainen J.K., Örndahl E., Falomo R., Uslenghi M., Feb. 2007, *A&A*, 462, 525
- Ilbert O., Tresse L., Zucca E., et al., Sep. 2005, *A&A*, 439, 863
- Inada N., Oguri M., Pindor B., et al., Dec. 2003, *Nature*, 426, 810
- Inada N., Oguri M., Morokuma T., et al., Dec. 2006, *ApJ*, 653, L97
- Inada N., Oguri M., Becker R.H., et al., Feb. 2008, *AJ*, 135, 496
- Kacprzak G.G., Churchill C.W., Steidel C.C., Murphy M.T., Mar. 2008, *AJ*, 135, 922
- Kacprzak G.G., Churchill C.W., Evans J.L., Murphy M.T., Steidel C.C., Oct. 2011, *MNRAS*, 416, 3118
- Kacprzak G.G., Churchill C.W., Nielsen N.M., May 2012, *ArXiv e-prints* 1205.0245
- Kaspi S., Smith P.S., Netzer H., et al., Apr. 2000, *ApJ*, 533, 631
- Kauffmann G., Haehnelt M., Jan. 2000, *MNRAS*, 311, 576
- Kayo I., Oguri M., Aug. 2012, *MNRAS*, 424, 1363
- Keeney B.A., Stocke J.T., Danforth C.W., Carilli C.L., Feb. 2011, *AJ*, 141, 66
- Kirkman D., Tytler D., Dec. 2008, *MNRAS*, 391, 1457
- Knapen J.H., Jan. 2005, *Ap&SS*, 295, 85
- Kochanek C.S., Falco E.E., Muñoz J.A., Jan. 1999, *ApJ*, 510, 590
- Kormendy J., Richstone D., 1995, *ARA&A*, 33, 581
- Kotilainen J.K., Falomo R., Scarpa R., Apr. 1998, *A&A*, 332, 503
- Kotilainen J.K., Falomo R., Treves A., Uslenghi M., Nov. 2006, *New Astronomy Review*, 50, 772
- Kotilainen J.K., Falomo R., Decarli R., et al., Oct. 2009, *ApJ*, 703, 1663
- Kovács Z., Mall U., Bizenberger P., Baumeister H., Röser H.J., Sep. 2004, In: Garnett J.D., Beletic J.W. (eds.) *Society of Photo-Optical Instrumentation Engineers (SPIE) Conference Series*, vol. 5499 of *Society of Photo-Optical Instrumentation Engineers (SPIE) Conference Series*, 432–441

Lang D., Hogg D.W., Mierle K., Blanton M., Roweis S., May 2010, *AJ*, 139, 1782

Lanzetta K.M., Turnshek D.A., Wolfe A.M., Nov. 1987, *ApJ*, 322, 739

Lapi A., Shankar F., Mao J., et al., Oct. 2006, *ApJ*, 650, 42

Lawrence C.R., Schneider D.P., Schmidt M., et al., Jan. 1984, *Science*, 223, 46

Limber D.N., Mathews W.G., Sep. 1960, *ApJ*, 132, 286

Liske J., Williger G.M., Dec. 2001, *MNRAS*, 328, 653

Liu X., Shen Y., Strauss M.A., Jul. 2011, *ApJ*, 736, L7

Lundgren B.F., Brunner R.J., York D.G., et al., Jun. 2009, *ApJ*, 698, 819

Lynden-Bell D., Aug. 1969, *Nature*, 223, 690

Madau P., Pozzetti L., Dickinson M., May 1998, *ApJ*, 498, 106

Magorrian J., Tremaine S., Richstone D., et al., Jun. 1998, *AJ*, 115, 2285

Maiolino R., Gallerani S., Neri R., et al., Sep. 2012, *MNRAS*, 425, L66

Mannucci F., Basile F., Poggianti B.M., et al., Sep. 2001, *MNRAS*, 326, 745

Marconi A., Hunt L.K., May 2003, *ApJ*, 589, L21

Martin C.L., Shapley A.E., Coil A.L., et al., Jun. 2012, *ArXiv e-prints* 1206.5552

Martini P., Weinberg D.H., Jan. 2001, *ApJ*, 547, 12

McLure R.J., Jarvis M.J., Targett T.A., Dunlop J.S., Best P.N., May 2006, *MNRAS*, 368, 1395

Ménard B., Chelouche D., Mar. 2009, *MNRAS*, 393, 808

Ménard B., Wild V., Nestor D., et al., Oct. 2011, *MNRAS*, 417, 801

Merritt D., 1988, In: Dickey J.M. (ed.) *The Minnesota lectures on Clusters of Galaxies and Large-Scale Structure*, vol. 5 of *Astronomical Society of the Pacific Conference Series*, 175–196

Merritt D., Storch-Bergmann T., Robinson A., et al., Apr. 2006, *MNRAS*, 367, 1746

Misawa T., Charlton J.C., Eracleous M., et al., Jul. 2007, *ApJS*, 171, 1

More S., van den Bosch F.C., Cacciato M., et al., Jan. 2011, *MNRAS*, 410, 210

Mortlock D.J., Webster R.L., Francis P.J., Nov. 1999, *MNRAS*, 309, 836

Mortlock D.J., Warren S.J., Venemans B.P., et al., Jun. 2011, *Nature*, 474, 616

Myers A.D., Brunner R.J., Nichol R.C., et al., Mar. 2007a, *ApJ*, 658, 85

Myers A.D., Brunner R.J., Richards G.T., et al., Mar. 2007b, ApJ, 658, 99
Myers A.D., Richards G.T., Brunner R.J., et al., May 2008, ApJ, 678, 635
Narayan R., Schneider P., Mar. 1990, MNRAS, 243, 192
Nelson C.H., Dec. 2000, ApJ, 544, L91
Nelson C.H., Whittle M., Jul. 1996, ApJ, 465, 96
Nestor D.B., Turnshek D.A., Rao S.M., Aug. 2005, ApJ, 628, 637
Nestor D.B., Johnson B.D., Wild V., et al., Apr. 2011, MNRAS, 412, 1559
Nigoche-Netro A., Aguerri J.A.L., Lagos P., et al., Jun. 2010, A&A, 516, A96
Oguri M., Inada N., Keeton C.R., et al., Apr. 2004, ApJ, 605, 78
Oke J.B., Feb. 1974, ApJS, 27, 21
Osmer P.S., Aug. 1981, ApJ, 247, 762
Pâris I., Petitjean P., Aubourg E., et al., Oct. 2012, ArXiv e-prints 1210.5166
Peebles P.J.E., 1980, The large-scale structure of the universe
Peng C.Y., Dec. 2007, ApJ, 671, 1098
Peng C.Y., Impey C.D., Ho L.C., Barton E.J., Rix H.W., Mar. 2006a, ApJ, 640, 114
Peng C.Y., Impey C.D., Rix H.W., et al., Oct. 2006b, ApJ, 649, 616
Petitjean P., Bergeron J., May 1990, A&A, 231, 309
Popesso P., Biviano A., Böhringer H., Romaniello M., Voges W., Apr. 2005, A&A, 433, 431
Portinari L., Kotilainen J., Falomo R., Decarli R., Feb. 2012, MNRAS, 420, 732
Postman M., Lauer T.R., Szapudi I., Oegerle W., Oct. 1998, ApJ, 506, 33
Press W.H., Schechter P., Feb. 1974, ApJ, 187, 425
Prochaska J.X., Hennawi J.F., Jan. 2009, ApJ, 690, 1558
Prochter G.E., Prochaska J.X., Burles S.M., Mar. 2006, ApJ, 639, 766
Quashnock J.M., Stein M.L., Apr. 1999, ApJ, 515, 506
Quashnock J.M., vanden Berk D.E., Jun. 1998, ApJ, 500, 28
Rao S.M., Turnshek D.A., Nestor D.B., Jan. 2006, ApJ, 636, 610
Reichard T.A., Richards G.T., Schneider D.P., et al., Apr. 2003, AJ, 125, 1711

Richards G.T., York D.G., Yanny B., et al., Mar. 1999, ApJ, 513, 576

Richards G.T., Fan X., Newberg H.J., et al., Jun. 2002, AJ, 123, 2945

Richards G.T., Lacy M., Storrie-Lombardi L.J., et al., Oct. 2006, ApJS, 166, 470

Richards G.T., Myers A.D., Gray A.G., et al., Jan. 2009, ApJS, 180, 67

Richardson J., Zheng Z., Chatterjee S., Nagai D., Shen Y., Aug. 2012, ApJ, 755, 30

Richstone D., Ajhar E.A., Bender R., et al., Oct. 1998, Nature, 395, A14

Rigby J.R., Charlton J.C., Churchill C.W., Feb. 2002, ApJ, 565, 743

Rodriguez Hidalgo P., Hamann F., Eracleous M., et al., Mar. 2012, ArXiv e-prints 1203.3830

Rubin K.H.R., Weiner B.J., Koo D.C., et al., Aug. 2010, ApJ, 719, 1503

Rubin K.H.R., Prochaska J.X., Koo D.C., Phillips A.C., Mar. 2012, ApJ, 747, L26

Ryabinkov A.I., Kaminker A.D., Varshalovich D.A., Dec. 2003, A&A, 412, 707

Salpeter E.E., Aug. 1964, ApJ, 140, 796

Salviander S., Shields G.A., Oct. 2012, ArXiv e-prints 1210.7263

Sancisi R., Fraternali F., Oosterloo T., van der Hulst T., Jun. 2008, A&A Rev., 15, 189

Sandage A., May 1965, ApJ, 141, 1560

Sanmartin D., Storchi-Bergmann T., Brotherton M.S., Oct. 2012, ArXiv e-prints 1210.1208

Sargent W.L.W., Boksenberg A., Steidel C.C., Dec. 1988, ApJS, 68, 539

Sbarufatti B., Treves A., Falomo R., et al., Feb. 2005, AJ, 129, 559

Scargle J.D., Caroff L.J., Noerdlinger P.D., Aug. 1970, ApJ, 161, L115

Schawinski K., Urry M., Treister E., et al., Dec. 2011, ApJ, 743, L37

Schechter P., Jan. 1976, ApJ, 203, 297

Schirber M., Miralda-Escudé J., McDonald P., Jul. 2004, ApJ, 610, 105

Schlegel D.J., Finkbeiner D.P., Davis M., Jun. 1998, ApJ, 500, 525

Schmidt M., Mar. 1963, Nature, 197, 1040

Schneider D.P., Hartig G.F., Jannuzi B.T., et al., Jul. 1993, ApJS, 87, 45

Schneider D.P., Richards G.T., Hall P.B., et al., Jun. 2010, AJ, 139, 2360

Schneider P., Kochanek C., Wambsganss J., Meylan G., 2006, Gravitational Lensing, Strong, Weak and Micro, Saas-Fee advanced course 33, Swiss Society for Astrophysics and Astronomy Lecture notes [April 8 to 12, 2003, in Les Diablerets], Springer, URL <http://link.springer.com/book/10.1007/978-3-540-30310-7/>

Schwope A.D., Lamer G., de Hoon A., et al., Apr. 2010, A&A, 513, L10

Serber W., Bahcall N., Ménard B., Richards G., May 2006, ApJ, 643, 68

Shaver P.A., Robertson J.G., May 1983, ApJ, 268, L57

Shaver P.A., Robertson J.G., Jan. 1985, MNRAS, 212, 15P

Shaver P.A., Boksenberg A., Robertson J.G., Oct. 1982, ApJ, 261, L7

Shen Y., Loeb A., Dec. 2010, ApJ, 725, 249

Shen Y., Ménard B., Apr. 2012, ApJ, 748, 131

Shen Y., Hennawi J.F., Shankar F., et al., Aug. 2010, ApJ, 719, 1693

Shen Y., Richards G.T., Strauss M.A., et al., Jun. 2011, ApJS, 194, 45

Silk J., Rees M.J., Mar. 1998, A&A, 331, L1

Skrutskie M.F., Cutri R.M., Stiening R., et al., Feb. 2006, AJ, 131, 1163

Söchting I.K., Clowes R.G., Campusano L.E., Apr. 2002, MNRAS, 331, 569

Söchting I.K., Clowes R.G., Campusano L.E., Feb. 2004, MNRAS, 347, 1241

Springel V., Hernquist L., Mar. 2005, ApJ, 622, L9

Srianand R., Khare P., Aug. 1993, ApJ, 413, 486

Srianand R., Khare P., Jun. 1994, ApJ, 428, 82

Steidel C.C., Sargent W.L.W., May 1992, ApJS, 80, 1

Steidel C.C., Dickinson M., Persson S.E., Dec. 1994, ApJ, 437, L75

Stockton A.N., Lynds C.R., Apr. 1966, ApJ, 144, 451

Stoughton C., Lupton R.H., Bernardi M., et al., Jan. 2002, AJ, 123, 485

Strauss M.A., Weinberg D.H., Lupton R.H., et al., Sep. 2002, AJ, 124, 1810

Sulentic J.W., Rosado M., Dultzin-Hacyan D., et al., Dec. 2001, AJ, 122, 2993

The L.S., White S.D.M., Dec. 1986, AJ, 92, 1248

Tinker J.L., Chen H.W., Jun. 2008, ApJ, 679, 1218

Tonry J., Davis M., Oct. 1979, AJ, 84, 1511

Toomre A., Toomre J., Dec. 1972, *ApJ*, 178, 623

Tremonti C.A., Moustakas J., Diamond-Stanic A.M., Jul. 2007, *ApJ*, 663, L77

Tripp T.M., Bowen D.V., Mar. 2005, In: Williams P., Shu C.G., Menard B. (eds.) IAU Colloq. 199: Probing Galaxies through Quasar Absorption Lines, 5–23

Trump J.R., Hall P.B., Reichard T.A., et al., Jul. 2006, *ApJS*, 165, 1

Turnshek D.A., May 1984, *ApJ*, 280, 51

Tytler D., Fan X.M., Mar. 1992, *ApJS*, 79, 1

Tytler D., Gleed M., Melis C., et al., Feb. 2009, *MNRAS*, 392, 1539

Vanden Berk D., Khare P., York D.G., et al., May 2008, *ApJ*, 679, 239

Vanden Berk D.E., Richards G.T., Bauer A., et al., Aug. 2001, *AJ*, 122, 549

Véron-Cetty M.P., Véron P., Jul. 2010, *A&A*, 518, A10

Vestergaard M., Dec. 2003, *ApJ*, 599, 116

Vestergaard M., Osmer P.S., Jul. 2009, *ApJ*, 699, 800

Vestergaard M., Peterson B.M., Apr. 2006, *ApJ*, 641, 689

Vestergaard M., Wilkes B.J., May 2001, *ApJS*, 134, 1

Voges W., Aschenbach B., Boller T., et al., Sep. 1999, *A&A*, 349, 389

Voges W., Aschenbach B., Boller T., et al., May 2000, *IAU Circ.*, 7432, 3

Weiner B.J., Coil A.L., Prochaska J.X., et al., Feb. 2009, *ApJ*, 692, 187

Weinstein M.A., Richards G.T., Schneider D.P., et al., Dec. 2004, *ApJS*, 155, 243

Weymann R.J., Williams R.E., Peterson B.M., Turnshek D.A., Nov. 1979, *ApJ*, 234, 33

Weymann R.J., Carswell R.F., Smith M.G., 1981, *ARA&A*, 19, 41

Weymann R.J., Morris S.L., Foltz C.B., Hewett P.C., May 1991, *ApJ*, 373, 23

White S.D.M., Rees M.J., May 1978, *MNRAS*, 183, 341

Wild V., Kauffmann G., White S., et al., Jul. 2008, *MNRAS*, 388, 227

Wold M., Lacy M., Lilje P.B., Serjeant S., May 2001, *MNRAS*, 323, 231

Wolf C., Meisenheimer K., Rix H.W., et al., Apr. 2003, *A&A*, 401, 73

Worseck G., Wisotzki L., May 2006, *A&A*, 450, 495

York D.G., Adelman J., Anderson J.E. Jr., et al., Sep. 2000, *AJ*, 120, 1579

Young P., Sargent W.L.W., Boksenberg A., Apr. 1982, ApJS, 48, 455

Zel'dovich Y.B., Novikov I.D., 1964, Dokl. Akad. Nauk SSSR

Zhdanov V.I., Surdej J., Jun. 2001, A&A, 372, 1

Zibetti S., Ménard B., Nestor D.B., et al., Mar. 2007, ApJ, 658, 161

Zwaan M.A., van der Hulst J.M., Briggs F.H., Verheijen M.A.W., Ryan-Weber E.V.,
Dec. 2005, MNRAS, 364, 1467

Acknowledgement

Formal

EPF acknowledge helpful discussions with A. Treves, R. Falomo, R. Decarli, C. Montuori, M. Fumagalli, F. Haardt, J. Kotilainen, R. Scarpa, and C. M. Raiteri.

For this work EPF was supported by Società Carlo Gavazzi S.p.A. and by Thales Alenia Space Italia SpA.

This Thesis was based on the following observations: (i) spectra from ESO/VLT Telescope in Paranal; (ii) spectra from ESO/NTT Telescope in La Silla; (iii) imaging from CAHA/3.5m Telescope; and (iv) data from the Sloan Digital Sky Survey. Funding for the SDSS and SDSS-II has been provided by the Alfred P. Sloan Foundation, the Participating Institutions, the National Science Foundation, the U.S. Department of Energy, the National Aeronautics and Space Administration, the Japanese Monbukagakusho, the Max Planck Society, and the Higher Education Funding Council for England. The SDSS Web Site is <http://www.sdss.org/>. SDSS-III is managed by the Astrophysical Research Consortium for the Participating Institutions of the SDSS-III Collaboration including the University of Arizona, the Brazilian Participation Group, Brookhaven National Laboratory, University of Cambridge, University of Florida, the French Participation Group, the German Participation Group, the Instituto de Astrofísica de Canarias, the Michigan State/Notre Dame/JINA Participation Group, Johns Hopkins University, Lawrence Berkeley National Laboratory, Max Planck Institute for Astrophysics, New Mexico State University, New York University, Ohio State University, Pennsylvania State University, University of Portsmouth, Princeton University, the Spanish Participation Group, University of Tokyo, University of Utah, Vanderbilt University, University of Virginia, University of Washington, and Yale University. We thank the Calar Alto staff for the generous allocation of DDT time and the prompt execution of our programme.

This research has made use of the NASA/IPAC Extragalactic Database (NED) which is operated by the Jet Propulsion Laboratory, California Institute of Technology, under contract with the National Aeronautics and Space Administration.

This research has made use of the VizieR catalogue access tool, CDS, Strasbourg, France.

Relaxed

Sono particolarmente grato al mio supervisore, Aldo Treves, che mi ha supportato (sopportato) durante questi anni, e per avermi sempre spinto a farmi domande su cosa stessi combinando. Ringrazio inoltre Renato Falomo per avermi insegnato la cura quasi maniacale nell'analisi dei dati e avermi forgiato nello spirito dell'astronomo.

In grosso grazie va anche a Roberto (Roris efficienza pura) Decarli. Non si possono

contare il numero di birre che ti devo per il supporto tecnico, scientifico, smonghista e per non avermi mandato a cagare tutte le volte che ti facevo domande idiote e imbarazzanti. La variegata popolazione dell'ufficio astrofisici (quasi estinta nell'ultimo anno ma che ora sembrerebbe rinascere, in bocca al lupo alle future reclute!) che mi ha accompagnato durante il dottorato. MMMAura, Jakob di twilight, Berni (la miglior compagna di ufficio che si possa immaginare), Cavadini, Nicola, il picco mondiale di spankwire e i *je pe'*, Franni e la laurea in astrofisica honoris causa, Maria Angela, Marco, Angiul, il suo cartonato e i cadaveri del lago, Roris, Francesco e le sue storie, Martina, Ruben il sapiente, Dotti, Carmen e la pizza che mi deve, Luca e i caffè alle tre di notte, Giorgio ormai milanese per adozione, Stefanino, Alvin, 2.0, Angela, il Ripa, e chiunque altro sia mai entrato per dire due puttanate in compagnia (leggi, Andre, Vale, ecc.)..

Franni!! non ci sono parole, ma grazie per non avermi picchiato in questi ultimi mesi!! Un saluto anche a Michi, Silvia e Ale! Dalla Bicocca al mondo, ma sempre tra gli Amici piu' cari!

Gli Amici di sempre (smettetela subito di sposarvi!) Cappe, Gian, Titti, Marco♡Diana, Re, BBiella, Gio (a marzo sei prenotato)!

Il comandi `ctrl-shift-c` e `ctrl-shift-v` avranno sempre e comunque il mio incondizionato supporto.

Seba, Sbroisi e Alberga, per l'amicizia, le puttanate, e tutte le serate che sono iniziate con: *Ti ricordi quella volta che...* e il successivo sconcerto dei presenti.

Mamma e Papa', e' bello sapere di poter sempre contare sul vostro appoggio.

Marco, che e' piccolo, ma ha gia' dimostrato di avere le palle quadre per diventare qualcuno, la mia sorellona e la zia Dana.

Grazie Carmen per avermi iscritto al Dottorato e avermi sempre ricordato tutte le scadenze burocratiche e non.

Le molte cose che hanno reso unici questi anni: il Max gonfiabile, il porno illegalmente importato dalla Cina, la Bora (che continua ad andare, alla faccia dell'ingegneria meccanica), il Tommy, la vuvuzela, il basket, le alghe nella macchinetta del caffè, i copybara, le pistole, le apparizioni di Luca in orari e stati improbabili, plutone (o nettuno), le porte quantistiche, i succhini ai lati nelle macchinette, la moretti da 66, *vercingetorige*, Roger, le merendelle, i T-rex, Vecchiato, i nomi indiani, la collezione di bottiglie, il carrello della spesa,.. e tutto quanto ha reso l'ufficio astrofisici meno ufficio possibile.

Bene, detto questo.. that's all folks..



Only the stupids cite themselves.

E. P. Farina

